Autonomous measurement of seawater total alkalinity as an enhancement of ocean carbon observations: From performance characterization to long-term field deployment

Dissertation

zur Erlangung des

Doktorgrades

der Mathematisch-Naturwissenschaftlichen Fakultät
der Christian-Albrechts-Universität zu Kiel

vorgelegt von

Katharina Seelmann

Kiel, 2020

Erster Gutachter: Prof. Dr. Arne Körtzinger
Zweite Gutachterin: PD Dr. Christa A. Marandino
Tag der mündlichen Prüfung: 02.09.2020
Zum Druck genehmigt: 02.09.2020

Gez. Prof. Dr. Frank Kempken, Dekan

„Science isn't about why! It's about why not! “
Cave Johnson, Portal 2

„Did I ever tell you what the definition of insanity is? Insanity is doing the exact same thing...over and over again...expecting it to change... That. Is. Crazy.“
Vaas Montenegro, Farcry 3

„We all make choices, but in the end our choices make us! “
Andrew Ryan, BioShock

Eidesstattliche Erklärung

Hiermit erkläre ich, Katharina Seelmann, dass ich diese Dissertation, abgesehen durch die Beratung meines Betreuers, selbstständig verfasst und alle wörtlichen, sowie inhaltlichen Zitate als solche markiert habe.

Die Arbeit wurde unter Einhaltung der Regeln guter wissenschaftlicher Praxis der Deutschen Forschungsgemeinschaft verfasst.

Sie hat weder ganz, noch in Teilen, einer anderen Stelle im Rahmen eines Prüfungsverfahrens vorgelegen und ist weder veröffentlicht, noch zur Veröffentlichung eingereicht.

Außerdem erkläre ich, dass mir kein akademischer Grad entzogen wurde.

Kiel, 19.06.2020

Katharina Seelmann

Abstract

Since around the mid of the 18th century, the global atmospheric carbon dioxide (CO_2) concentration has significantly increased due to anthropogenic activities. For 2018, around 11.5 $GtC\,yr^{-1}$ were emitted by fossil fuel combustion and cement production, and land use changes. A sink for the atmospheric CO_2 is the ocean, which has taken up around 2.6 $GtC\,yr^{-1}$ in 2018. The relative good understanding of the current global mean oceanic uptake of anthropogenic CO_2 is contrasted by a lack of knowledge how the natural carbon cycle will respond regionally to changes introduced by anthropogenic CO_2 emissions, like global warming, ocean acidification or ocean deoxygenation. In view of the central role of the oceanic CO_2 sink and its vulnerability to these changes, extensive ocean carbon observations are necessary. Over several years, the Ships of Opportunity (SOOP) network provides high-quality CO_2 partial pressure ($p(CO_2)$) data of the surface ocean, and, therefore, forms the backbone of the global observation system for the oceanic CO_2 sink. However, to get full insight into the marine CO_2 system, at least two of the four measurable carbonate variables are required, which are $p(CO_2)$, total alkalinity (A_T), dissolved inorganic carbon (C_T) and pH. The so far common workaround is the prediction of A_T by using established temperature-salinity based parameterizations. However, compared with direct measurements, this procedure leads to higher uncertainties and spatiotemporal biases. Therefore, autonomous SOOP-based A_T measurements are of great interest and, in the end, should enhance ocean carbon observations. In order to achieve this enhancement, this thesis goals to provide an example of a successful implementation of a novel autonomous analyzer for seawater A_T, the CONTROS HydroFIA® TA (-4H-JENA engineering GmbH, Germany), on a Carbon-SOOP station operating in the subpolar North Atlantic (together with fundamental guidelines and recommendations leading to high-quality A_T data).

The first part of this thesis dealt with an extensive performance characterization of the analyzer in the laboratory and in field in order to verify if the A_T data meet fundamental quality requirements. The field measurements were conducted during two major research cruises across the South Atlantic, and from the eastern North Atlantic to the eastern Subtropical Atlantic, respectively. Both in the laboratory and in field the analyzer featured high-quality requirements, which are accepted within the oceanographic community. We additionally found a linear offset drift is the typical behavior of the system, which can be corrected for by regular

reference measurements. Based on the experiences from this study, we provided recommendations for automated long-term deployments.

The second part of this thesis dealt with the influences of impurities in the indicator dye bromocresol green (BCG) on the measurements with the CONTROS HydroFIA® TA. We developed a high-performance liquid chromatography (HPLC) purification method for BCG and analyzed dyes from four different vendors, which showed different impurity types and quantities. Laboratory measurements with the CONTROS HydroFIA® TA using both unpurified and purified BCG revealed direct influences of the impurity types and quantities on e.g. the analyzer's drift behavior and the measurement quality. However, to gain optimal A_T measurements, an indicator purification is not necessarily required as long as the purchased dye has a purity grade of at least 98 % (quantified with the developed method described in this thesis). Concluding, high-quality A_T measurements do not need pure but the purest BCG dye that is purchasable.

The last part of this thesis dealt with the final implementation of the analyzer on the North Atlantic SOOP line. We described the installation in detail and addressed major issues encountered with autonomous measurements using this analyzer, e.g. automated cleaning and stabilization routines, and waste handling. Furthermore, during long-term deployments, large-volume reference seawater containers are essential for regular reference measurements, and, therefore drift correction. For that, we tested several containers with respect to their suitability to store seawater over a long time period with without significant A_T changes. Only one gas-sampling bag made of polyvinylidene fluoride (PVDF) satisfied the stability requirements. Finally, the performance of the entire installed system was characterized by an intercomparison with discrete samples during the first two campaigns. The overall measurement uncertainty fulfilled requirements for autonomous A_T measurements on SOOP lines and, therefore, verified that high-quality A_T measurements in unattended mode on SOOP stations with high spatiotemporal coverage are totally possible.

But were these autonomous A_T data, measured like it is described in this thesis, an enhancement of ocean carbon observations? A comparison of the SOOP-based A_T data set with predicted A_T values using an established and often used temperature-salinity parameterization revealed fundamental limitations of such predictions. By predicting A_T spatial, temporal and seasonal biases were introduced into the resulting marine carbonate chemistry calculations, which may lead to misinterpretations. Direct A_T measurements with high spatiotemporal coverage described in this study overcame these limitations, and, in conclusion, enhanced ocean carbon observations.

Zusammenfassung

Seit ungefähr der Mitte des 18. Jahrhunderts ist die atmosphärische Konzentration an Kohlenstoffdioxid (CO_2) aufgrund von anthropogenen Aktivitäten signifikant angestiegen. Im Jahr 2018 wurden rund 11,8 $GtC\,yr^{-1}$ durch Verbrennung fossiler Brennstoffe und Zementproduktion sowie Landnutzungsänderungen emittiert. Eine Senke für das atmosphärische CO_2 ist der Ozean, der im Jahr 2018 rund 2,6 $GtC\,yr^{-1}$ aufgenommen hat. Im Gegensatz zum relativ gutem Verständnis der aktuellen globalen mittleren ozeanischen Aufnahme von anthropogenem CO_2, ist wenig über regionale Reaktionen des natürlichen Kohlenstoffkreislaufes auf Veränderungen bekannt, welche durch das anthropogene CO_2 hervorgerufen werden, wie zum Beispiel globale Erwärmung, Ozeanversauerung oder Ozean-Deoxygenierung. Angesichts der zentrale Rolle der ozeanischen CO_2-Senke und seiner Anfälligkeit gegenüber diesen Veränderungen, sind weitreichende Beobachtungen des marinen CO_2 Systems unerlässlich. Über mehrere Jahre hinweg stellt das „Ships of Opportunity" (SOOP) Programm qualitativ hochwertige CO_2-Partialdruck ($p(CO_2)$) Daten der Ozeanoberfläche zur Verfügung, und bildet damit das Fundament des weltweiten Ozeanbeobachtungssystems für die marine CO_2-Senke. Allerdings sind für einen vollständigen Einblick in das marine CO_2-System mindestens zwei der vier messbaren Carbonat-Variablen notwendig, welche wären: $p(CO_2)$, die Gesamtalkalinität (A_T), der gelöste anorganische Kohlenstoff (C_T) und pH. Die derzeit noch gängige Lösung ist die Schätzung von A_T mit etablierten Temperatur-Salinitäts-Parametrisierungen. Im Vergleich mit direkten Messungen führt diese Herangehensweise allerdings zu erhöhten Unsicherheiten und räumlich-temporalen Verzerrungen. Aus diesem Grund sind autonome SOOP-basierte A_T-Messungen von großem Interesse und sollten schlussendlich die marinen Kohlenstoffbeobachtungen verbessern. Um diese Verbesserungen zu erreichen, zielt diese Dissertation darauf ab, ein Beispiel für die erfolgreiche Implementierung eines neuartigen autonomen Messsystems für Seewasser-A_T, das CONTROS HydroFIA® TA (-4H-JENA engineering GmbH, Deutschland), auf einer Kohlenstoff-SOOP Station, welche im subpolaren Nordatlantik operiert, zu liefern (zusammen mit Richtlinien und Empfehlungen, welche zu qualitativ hochwertigen A_T-Daten führen).

Der erste Teil dieser Arbeit beschäftigte sich mit einer ausführlichen Charakterisierung des Systems sowohl im Labor als auch im Feld abzielend auf die Einhaltung von grundlegenden Qualitätsanforderungen. Die Messungen im Feld wurden während zwei großen Forschungsseefahrten entlang des Südatlantiks bzw. vom östlichen

Nordatlantik zum östlichen subtropischen Atlantik durchgeführt. Sowohl unter Labor- als auch unter Feldbedingungen erfüllte der Analysator die hohen Anforderungen, welche in der ozeanografischen Gemeinschaft anerkannt sind. Wir fanden außerdem heraus, dass ein linearer Offset-Drift zum typischen Messverhalten des Systems zählt, welcher durch regelmäßige Referenzmessungen korrigiert werden kann. Basierend auf den Erfahrungen dieser Studie, stellten wir Empfehlungen für autonome Langzeiteinsätze des Systems zur Verfügung.

Der zweite Teil dieser Arbeit beschäftigte sich mit den Einflüssen von Verunreinigungen im Farbstoff Bromokresolgrün (BKG) auf die Messungen des CONTROS HydroFIA® TA's. Wir entwickelten eine Hochleistungsflüssigkeitschromatographie (englisch: high-performance liquid chromatography, HPLC) Methode zur Aufreinigung des BKG's und analysierten Farbstoffe von vier verschiedenen Anbietern, welche unterschiedliche Arten und Mengen an Verunreinigungen aufwiesen. Labormessungen mit dem CONTROS HydroFIA® TA, welche mit sowohl nicht-aufgereinigtem als auch aufgereinigtem BKG durchgeführt wurden, zeigten einen direkten Einfluss der Verunreinigungen auf z.B. das Driftverhalten des Systems und die Qualität der Messungen. Allerdings ist für optimale A_{T}-Messungen keine Farbstoffaufreinigung notwendig, solange das gekaufte BKG einen Reinheitsgrad von mindestens 98 % aufweist (quantifiziert mit der in dieser Arbeit entwickelten Methode). Schlussendlich benötigen qualitativ hochwertige A_{T}-Messungen nicht reinen, aber den reinsten BKG-Farbstoff, welcher käuflich erwerbbar ist.

Der letzte Teil dieser Arbeit beschäftigte sich mit der finalen Implementierung des Analysators auf der Nordatlantik-SOOP-Linie. Wir beschrieben detailliert die Installation und berücksichtigten Probleme, welche während autonomen Messungen des Systems festgestellt wurden, z.B. automatisierte Reinigungs- und Stabilitätsroutinen und die Handhabung des Abfalls. Außerdem sind während Langzeiteinsätzen hoch-volumige Behälter für Referenzseewasser essentiell, um die regelmäßigen Referenzmessungen und die damit verbundene Driftkorrektur durchführen zu können. Dafür testeten wir verschiedenste Behälter in Bezug auf ihre Eignung, Seewasser über längere Zeit ohne signifikante A_{T}-Veränderungen zu lagern. Nur ein Gasbeprobungsbeutel hergestellt aus Polyvinylidenfluorid (PVDF) konnte die Stabilitätsanforderungen erfüllen. Zum Schluss wurde die Performance des gesamten installierten Systems durch Vergleichsmessungen mit diskreten Proben während der ersten beiden Kampagnen charakterisiert. Die Gesamtmessunsicherheit erfüllte die Anforderungen, welche an autonome A_{T}-Messungen auf SOOP-Linien gestellt werden, und bestätigte somit, dass qualitativ hochwertige A_{T}-Messungen auf SOOP-Stationen mit hoher räumlich-temporaler Abdeckung unter unbeaufsichtigten autonomen Bedingungen möglich sind.

Aber sind diese autonomen A_{T}-Daten, welche so gemessen wurden, wie es diese Arbeit beschreibt, eine Verbesserung der marinen Kohlenstoffbeobachtungen? Ein Vergleich der SOOP-basierten A_{T}-Datensets mit A_{T}-Daten, welche durch eine etablierte und oft genutzte Temperatur-Salinitäts-Parametrisierung abgeschätzt wurden, enthüllte grundlegende Limitierungen dieser Abschätzung. Wenn A_{T}-Werte abgeschätzt werden, werden räumliche, temporale und saisonale Ver-

zerrungen in die resultierenden marinen Carbonatchemie-Berechnungen induziert, welches zu Missinterpretationen führen könnte. Direkte A_{T}-Messungen mit hoher räumlich-temporaler Abdeckung, wie sie in dieser Dissertation beschrieben sind, überwinden diese Limitierungen, und verbessern somit schlussendlich die marinen Kohlenstoffbeobachtungen.

Manuscript overview

This dissertation is based on the following manuscripts:

1. *Seelmann, K.*, S. Aßmann, A. Körtzinger. **2019**. Characterization of a novel autonomous analyzer for seawater total alkalinity: Results from laboratory and field tests. Limnol Oceanogr Methods, 17: 515-532. doi: 10.1002/lom3.10329

   My contribution: I designed the study together with SA and AK, participated in the field studies, performed the laboratory and field measurements, visualized the results, analyzed the results together with SA and AK, wrote the first draft of the manuscript, and wrote the final manuscript with contributions from SA and AK.

2. *Seelmann, K.*, M. Gledhill, S. Aßmann, A. Körtzinger. **2020**. Impact of impurities in bromocresol green indicator dye on spectrophotometric total alkalinity measurements. Ocean Sci. doi: 10.5194/os-16-535-2020

   My contribution: I designed the study together with MG, SA and AK, performed the indicator purification and the total alkalinity measurements in the laboratory, visualized the results, analyzed the results together with MG, SA and AK, wrote the first draft of the manuscript, and wrote the final manuscript with contributions from MG, SA and AK.

3. *Seelmann, K.*, T. Steinhoff, S. Aßmann, A. Körtzinger. **2020**. Enhance ocean carbon observations: Successful implementation of a novel autonomous analyzer on a Ship of Opportunity. Manuscript submitted to: Frontiers in Marine Science.

   My contribution: I designed the study together with TS, SA and AK, installed the systems on the ship together with TS and AK, participated in cruises on the ship, performed the laboratory and field measurements, visualized the results, analyzed the results together with TS, SA and AK, wrote the first draft of the manuscript, and wrote the final manuscript with contributions of TS, SA and AK.

Danksagung

Zuallererst bedanke ich mich bei meinem Betreuer und Doktorvater, Prof. Dr. Arne Körtzinger, nicht nur für die Möglichkeit dieses sehr spannende Thema zu bearbeiten, sondern auch für das in mich gesetzte Vertrauen und vor allem für die wissenschaftliche und auch emotionale Unterstützung. Danke, dass deine Tür immer für mich offen stand, auch, wenn sie eigentlich immer offen steht. ;-)

Weiterhin bedanke ich mich bei Steffen, der nicht nur ein wichtiger Teil meines ISOS-Komitees und gewinnbringender Co-Autor meiner Publikationen war, sondern auch bei Fragen und Problemen rund um „Der Gerät" immer sofort zur Stelle war.

Ein weiteres „Danke schön" geht an PD Dr. Christa A. Marandino, insbesondere für ihre Bereitschaft, das zweite Gutachten dieser Arbeit zu übernehmen, aber auch für ihre bereichernde Teilnahme an meinen ISOS Meetings, nicht nur wissenschaftlich, sondern auch menschlich.

Zudem danke ich Tobi, insbesondere für die sowohl lustigen als auch manchmal eher niederschmetternden Sail-Momente. Irgendwie haben wir das doch alles hinbekommen, auch wenn ich handwerklich oder beim Schleppen keine große Hilfe war. ;-)

Darüber hinaus möchte ich der gesamten, restlichen (C)O_2 Arbeitsgruppe (Anna, Björn, Melf, tobi) für ihre wissenschaftlichen Kommentare und Ratschläge, aber auch für die immer lustigen Zusammenkünfte danken. Es war mir eine Ehre, mit euch zusammen zu arbeiten. Insbesondere danke ich Anna und tobi für die unvergessliche gemeinsame Zeit auf der M133 als die „Chemical Group". Weiterhin geht ein besonderes „Danke schön" an meinen Büro-Sitznachbarn Melf für die immer sehr lustigen und meistens nicht so ernsten „Diskussionen".

Ein besonderer Dank geht an Annette, Pratirupa und Sonja aus meinem Büro alias der „High-productivity Area near the Kiel Fjord" (und natürlich auch an die Ehemaligen: Melina, Sinikka, Steffen und Tim) dafür, dass sie immer zum schnacken bereit waren, sei es beruflich oder auch privat.

Der restlichen Chemischen Ozeanographie danke ich für die wundervollen Jahre der Zusammenarbeit. Ich war jeden Tag so gern auf Arbeit! :-D Ein besonderer Dank geht dabei an Hermann für seine Bereitschaft, in meinem Disputations-Komitee mitzuwirken.

Den Mitarbeitern der -4H-JENA engineering GmbH (ehemals Kongsberg Maritime Contros GmbH) in Kiel, insbesondere Nadja, danke ich für die tollen Jahre der Zusammenarbeit an „Der Gerät".

Weiterhin bedanke ich mich bei Jens und Daniela für die sowohl finanzielle, als auch wissenschaftliche Unterstützung aus „Digital Earth”. Ich hoffe, ich konnte euren Erwartungen gerecht werden.

Ich möchte mich insbesondere noch bei den Kapitänen und Crews der Schiffe (RV *Meteor*, RV *Maria S. Merian* und MV *Atlantic Sail*), auf denen ich zu Gast sein durfte, für ihre tatkräftige Unterstützung bedanken. Ohne euch wären die Feldversuche niemals möglich gewesen.

Ein ganz, ganz großes „Danke schön” geht an dieser Stelle an meine Familie, insbesondere an meinen Fels-in-der-Brandung Philip, an meine Eltern Ingrid und Klaus, und an meine Schwiegermutti Silvia. Danke, dass ihr immer hinter mir standet und stets für mich da wart und immer noch seid. Ohne euch wäre das alles niemals möglich gewesen.

Außerdem möchte ich mich noch bei meinen gesamten Freunden bedanken, insbesondere bei Christian. Unsere virtuellen Zocker-Stunden am Wochenende waren und sind ein perfekter Ausgleich.

Diese Arbeit wurde finanziell durch das europäische H2020 Projekt „AtlantOS” und das „Digital Earth” Projekt aus dem Impuls- und Vernetzungsfond der Helmholtz-Gemeinschaft unterstützt.

Ein letzter, ganz besonderer Dank geht an meine Katze Nicky, die mich beim Schreiben dieser Arbeit im Home Office immer tatkräftig unterstützt hat, wie man im unteren Bild sehr gut erkennt. ;-)

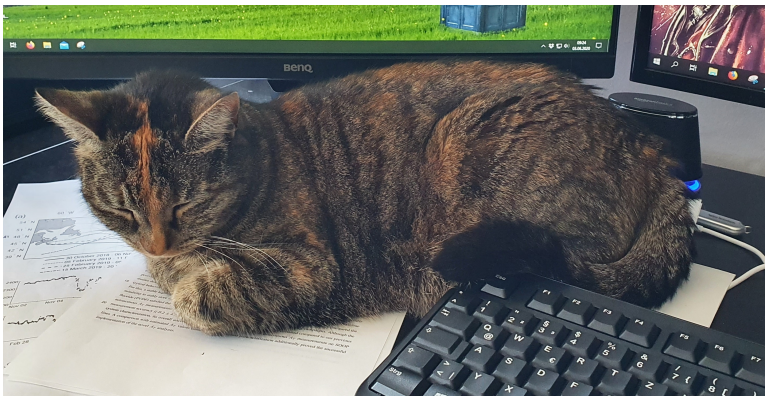

Contents

List of Figures

List of Tables

Chapter 1

Introduction

1.1 The global carbon cycle

Since the beginning of the Industrial Era (around the mid of the 18th century), the global atmospheric carbon dioxide (CO_2) concentration has increased from about 277 parts per million (ppm) in 1750 (Joos and Spahni 2008) up to 412.02 ± 0.1 ppm in December 2019 (Dlugokencky and Tans 2020). Hence, atmospheric CO_2 increased by over 45 % since the beginning of industrialization. Figure 1.1 shows the monthly mean CO_2 concentration from 1960 to 2018.

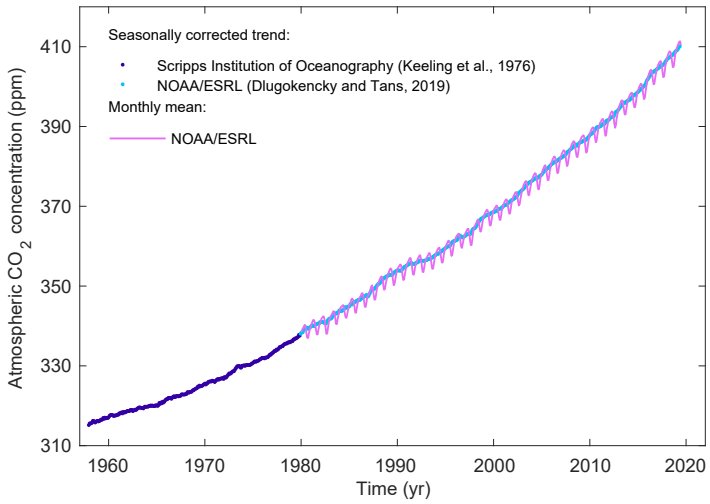

Figure 1.1: Monthly mean CO_2 concentrations from 1958 to 2018. The data from NOAA ESRL (Dlugokencky and Tans 2020) are based on averaged direct atmospheric CO_2 measurements from multiple stations in the marine boundary layer (Masarie and Tans 1995). The monthly data from 1958 to 1979 are based on averaged direct CO_2 measurements from the Mauna Loa, Hawaii and South Pole stations (Scripps Institution of Oceanography) (Keeling et al. 1976). Source: Friedlingstein et al. (2019)

The main causes for the observed increase in CO_2 are anthropogenic emissions. Between 1750 and 2018, such emissions to the atmosphere were 675 ± 80 gigatonnes carbon (GtC; 1 GtC = 10^{15} gC) with 440 ± 20 GtC from fossil fuel combustion and cement production, and 235 ± 75 GtC from land use changes. Approximately half of these emissions remained in the atmosphere (275 ± 5 GtC since 1750).

The second half was taken up by sinks and therefore, stored in natural reservoirs. Between 1750 and 2018, the ocean has taken up 170 ± 20 GtC, and 220 ± 50 GtC was stored in vegetation biomass and soils (not affected by land use changes) (Friedlingstein et al. 2019). These data were published by the "Global Carbon Project", which synthesizes all available observation data related to the carbon cycle that have undergone and passed thorough quality control and annually publishes the prestigious "Global Carbon Budget" with quantified anthropogenic CO_2 emissions and their redistribution among the atmosphere, ocean, and terrestrial biosphere (Friedlingstein et al. 2019). Figure 1.2 shows a schematic illustration of the global carbon cycle, mainly focusing on its overall perturbation caused by anthropogenic activities, with the stored amount of carbon in each natural reservoir (in GtC) and the fluxes between the sources and sinks (in gigatonnes carbon per year, $\mathrm{GtC\,yr^{-1}}$) between 2009 and 2018 (Friedlingstein et al. 2019). Figure 1.3 illustrates the increase of the anthropogenic emission quantities from fossil fuels, industry and land use change over time, and the increase of carbon taken up by the ocean, land and atmosphere over time. It emphasizes the huge amount of carbon emitted by fossil fuel burning and other industry over the industrial years, especially since 1950, where the emissions largely increase in comparison to the previous decades. For 2018, the total anthropogenic emissions were calculated with 11.5 ± 0.9 $\mathrm{GtC\,yr^{-1}}$ with 10.0 ± 0.5 $\mathrm{GtC\,yr^{-1}}$ from fossil CO_2 emissions and 1.5 ± 0.7 $\mathrm{GtC\,yr^{-1}}$ from land use changes. In comparison, between 1960 and 1969, the annual total anthropogenic emissions were estimated with 4.5 ± 0.5 $\mathrm{GtC\,yr^{-1}}$ (3.0 ± 0.2 $\mathrm{GtC\,yr^{-1}}$ for fossil CO_2 emissions and 1.4 ± 0.7 $\mathrm{GtC\,yr^{-1}}$ from land use changes) (Friedlingstein et al. 2019). These values show that the burning of fossil fuels (and other industry) is the main cause for the increase in atmospheric CO_2 since 1960, as the emissions from land use changes were approximately stable.

Simultaneous to the increase in carbon emissions, the amount of carbon taken up by the ocean, land and atmosphere rises. In 2018, the atmosphere has taken up 5.1 ± 0.2 $\mathrm{GtC\,yr^{-1}}$, the ocean 2.6 ± 0.6 $\mathrm{GtC\,yr^{-1}}$, and the land 3.5 ± 0.7 $\mathrm{GtC\,yr^{-1}}$. Between 1960 and 1969, the growth rate in atmospheric CO_2 was 1.8 ± 0.07 $\mathrm{GtC\,yr^{-1}}$, in oceanic CO_2 1.0 ± 0.6 $\mathrm{GtC\,yr^{-1}}$, and in terrestrial CO_2 1.3 ± 0.4 $\mathrm{GtC\,yr^{-1}}$ (Friedlingstein et al. 2019).

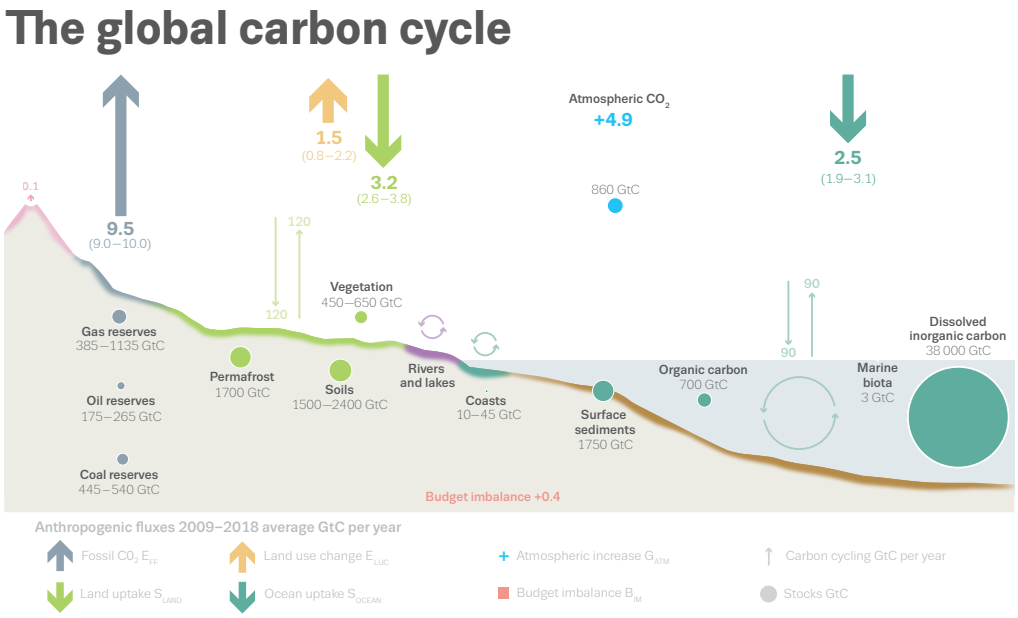

Figure 1.2: Schematic illustration of the global carbon cycle, averaged globally for 2009 - 2018, mainly focusing on anthropogenic effects. Source: Friedlingstein et al. (2019).

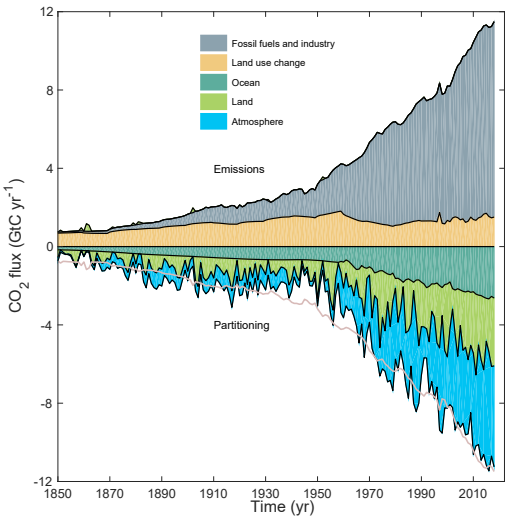

Figure 1.3: The global carbon budget as a function of time for anthropogenic emissions and their sinks. Source: Friedlingstein et al. (2019)

1.2 The marine carbon cycle

The major part of the oceanic carbon (approximately 37,100 petagrams carbon, PgC, 1 PgC = 10^{15} gC) is stored in the intermediate and deep sea, whereby the surface ocean is a relative small carbon reservoir (900 PgC) (Ciais et al. 2013). Hence, only about 2.4 % of carbon taken up by the ocean remains in the surface layer. Therefore, regarding the carbon cycle, the surface ocean acts as a connector between the deep ocean and the atmosphere. Figure 1.4 shows a schematic illustration of the marine carbon distribution between the surface ocean, intermediate and deep sea, and the ocean floor surface sediments with their respective carbon amounts. Furthermore, additional oceanic carbon stocks are shown like the dissolved organic carbon (700 PgC) and the marine biota (3 PgC).

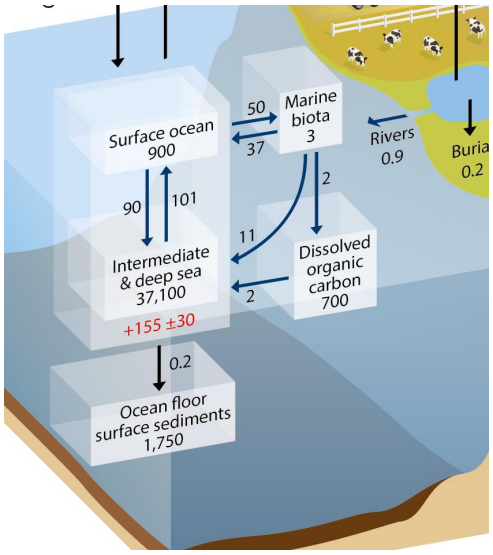

Figure 1.4: Schematic illustration of the marine carbon distribution, where black numbers represent preindustrial conditions and red numbers account for the respective anthropogenic influences (averaged over the period of 2000 - 2009). Arrows represent the annual fluxes. Stocks are given in PgC, and fluxes are given in PgC yr^{-1}. Source: Ciais et al. (2013)

Atmospheric CO_2 is exchanged to the surface ocean via gas exchange. The main driver for this exchange is the CO_2 partial pressure ($p(CO_2)$) difference between the air and the sea. Is the oceanic $p(CO_2)$ smaller than the atmospheric, the surface ocean acts as a sink for CO_2, and vise versa. Figure 1.5 shows the global mean annual carbon air-sea flux estimated from the "Global Carbon Budget 2018" (Le Quéré et al. 2018) for the year 2017, where blue areas represent CO_2 sinks, and red areas CO_2 sources. Huge sinks for atmospheric CO_2 are the North and South Atlantic Ocean, the southern Indian Ocean and the Arctic Ocean. Oceanic CO_2 sources are mainly distributed in tropical areas, e.g. the tropical Pacific Ocean.

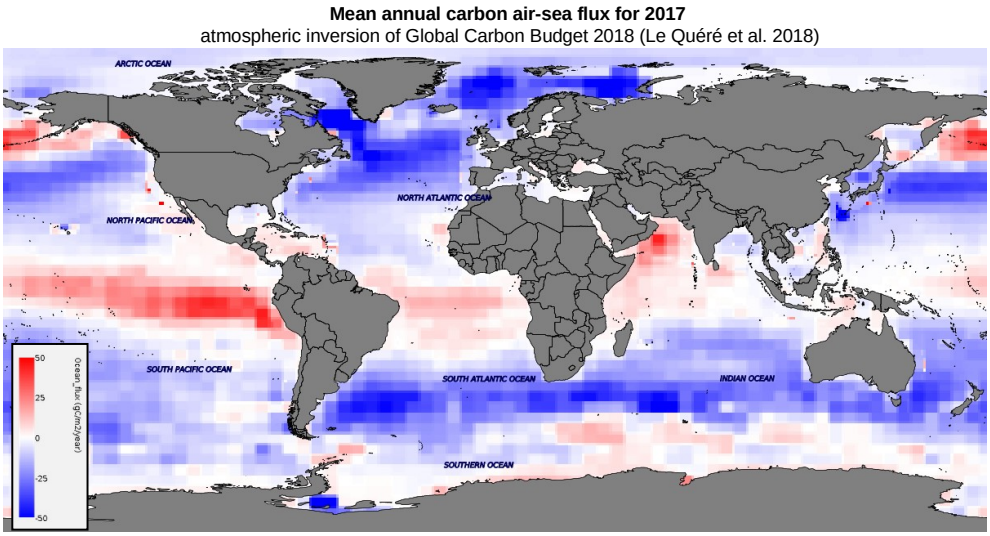

Figure 1.5: Mean annual carbon air-sea flux (in $\mathrm{gC\,m^{-2}\,yr^{-1}}$) estimated from the "Global Carbon Budget" (Le Quéré et al. 2018) for 2017. Blue color means carbon sink, and red color means carbon source. The figure was generated by the "Global Carbon Atlas" (Flux Maps tool, available at: `http://www.globalcarbonatlas.org/en/flux-maps`, last accessed: 12.03.2020)

The transportation of the dissolved carbon in the ocean (mainly available as dissolved inorganic carbon, C_T; see Sect. 1.3 for more details) follows physical and biochemical processes against a gradient. These mechanisms are the so called marine carbon pumps, which are divided into the physical carbon pump (or solubility pump), the organic carbon pump and the inorganic carbon pump. The last two are combined in the biological pump. Figure 1.6 illustrates these three pumps.

The physical carbon pump is driven by the thermohaline (thermo = temperature; haline = salinity) circulation, also known as Global Ocean Conveyor, which is caused by a combination of temperature and salinity driven currents in the deep sea, and wind driven currents on the surface: Cold, salty water is dense and sinks to the bottom of the ocean while warm water is less dense and remains on the surface. Due to the fact that the solubility of CO_2 in sea water increases with decreasing sea surface temperature, the atmospheric CO_2 dissolves in cold surface waters, e.g. in the North Atlantic. Afterwards it is transported to the intermediate and deep sea by deep water formation at high latitudes. Since deep water is formed under the same surface conditions that promote CO_2 solubility, it contains a higher concentration of C_T than might be expected from average surface concentrations. Hence, the CO_2 is pumped from the atmosphere into the ocean's interior. One consequence of this is that when deep water upwells in warmer, equatorial latitudes, e.g. in tropical areas, it strongly outgasses carbon dioxide to the atmosphere because of the reduced solubility of the gas.

The biological organic pump is driven by the primary production of marine organisms, like phytoplankton, in the marine surface layer. During this process, the oceanic C_T and dissolved nutrients are converted into organic matter through photosynthesis. It is mainly limited by the availability of light and nutrients such as phosphate, nitrate and silicic acid, and micronutrients, such as iron. After a period of time, the formed biomass dies and sinks, where it is remineralized by bacteria. This procedure releases CO_2 into deeper sea levels. However, just a minor amount ($\approx 0.2\ \mathrm{PgC\,yr^{-1}}$) of carbon bound by biomass reaches the deep sea and finally the seafloor (Denman et al. 2007).

The biological inorganic pump is driven by the formation of calcareous shells of certain oceanic microorganisms in the surface ocean. This calcification process consumes calcium and bicarbonate ions, and releases CO_2 into the seawater. The shelled microorganisms sink to deeper waters, where the calcite ($CaCO_3$) solubility increases with increasing pressure and decreasing temperature. At a certain depth, the so called lysocline, the solubility increases dramatically and the calcite dissolves by consuming dissolved CO_2.

The biological inorganic pump is the counterpart to the biological organic pump with regard on the CO_2 exchange between atmosphere and ocean surface. Whereas the primary production of the organic pump removes CO_2 from surface waters and therefore decreases $p(CO_2)$, which results into an oceanic absorption of atmospheric CO_2, the calcification progress of the inorganic pump releases CO_2 into the surface layer and therefore increases $p(CO_2)$ (see Fig. 1.6). Hence, the effect of the biological production (photosynthesis and calcification) in surface areas on the atmosphere

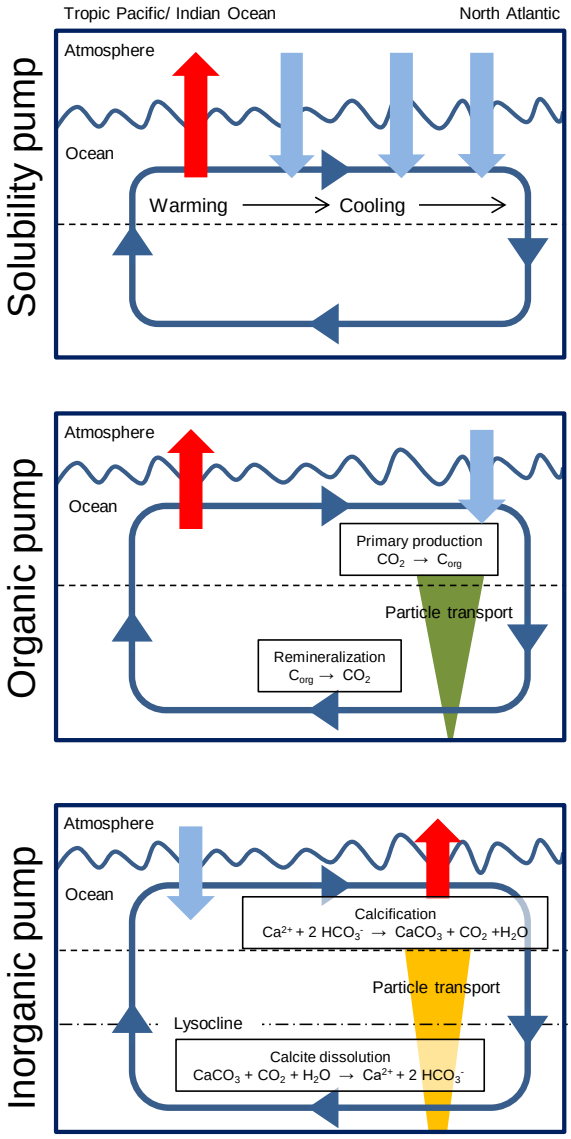

Figure 1.6: The three marine carbon pumps: The physical pump (or solubility pump), and the biological pump, which is divided into the organic and inorganic pump. The dashed black line in each illustration indicates the separation between surface and intermediate/ deep ocean (not to scale). Red arrows represent the release of CO_2 to the atmosphere, whereby light blue arrows represent the dissolution of CO_2. The size of the arrows is not related to the amount of carbon flux. The illustration was adapted from Körtzinger (2010).

depends on the relation between biomass and calcite in the transported material, the so called "rain ratio".

1.3 The marine carbonate chemistry

The marine carbonate chemistry or carbonate system describes, what happens with the absorbed atmospheric CO_2 in the ocean. It is of utmost importance in oceanography, because it is the main part (95 %) of the oceanic buffering capacity and, therefore, controls the acidity of seawater. Furthermore, it is an important controller for the global carbon cycle (Emerson and Hedges 2008).

Oceanic inorganic carbon appears in four different forms: 1) dissolved CO_2 gas, or aqueous CO_2, $CO_2(aq)$, 2) carbonic acid, H_2CO_3, 3) bicarbonate ion, HCO_3^-, and 4) carbonate ion, CO_3^{2-}. The last three forms result from the chemical reaction of CO_2 with water and are in chemical equilibrium on only short time scales (few minutes). Due to the fact, that only approximately 0.1 % of the neutral carbonate species exists as H_2CO_3 at equilibrium, $CO_2(aq)$ and H_2CO_3 are combined in CO_2^* and calculated as follows:

$$[CO_2^*] = [CO_2(aq)] + [H_2CO_3] \tag{1.1}$$

where squared parentheses represent concentrations of the respective species. The equilibria of the carbonate system can be expressed as follows:

$$CO_2(g) \overset{K_0}{\rightleftharpoons} CO_2^* \tag{1.2}$$

$$CO_2^* + H_2O \overset{K_1}{\rightleftharpoons} HCO_3^- + H^+ \tag{1.3}$$

$$HCO_3^- \overset{K_2}{\rightleftharpoons} CO_3^{2-} + H^+ \tag{1.4}$$

where $CO_2(g)$ is the atmospheric CO_2, K_0 is the so called Henry constant of CO_2 in seawater, and K_1 and K_2 are the first and second dissociation constant of H_2CO_3 in seawater. The constants are depend on temperature, salinity and pressure, and were described by several authors (e.g. Hansson 1973; Mehrbach et al. 1973; Goyet and Poisson 1989; Roy et al. 1993; Lueker et al. 2000; Mojica-Prieto and Millero 2002; Millero et al. 2006).

Figure 1.7 shows the logarithmic concentrations of the respective carbonate species in dependence of the pH (Heinze et al. 2015). At the pH of natural seawater ($\approx 8.2 \pm 0.3$, Raven et al. (2005)), the major form of inorganic carbon is HCO_3^- with ≈ 86.5 %, followed by CO_3^{2-} with $\approx 13\%$ and CO_2^* with ≈ 0.5 % (Zeebe and Wolf-Gladrow 2001). Although these species represent the marine carbonate system,

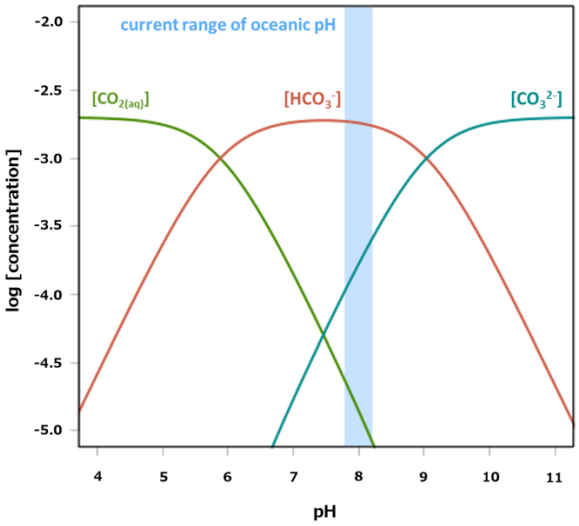

Figure 1.7: Logarithmic concentrations of carbonate species in seawater as a function of pH. Source: Heinze et al. (2015)

their concentrations can not be analyzed directly. For characterizing the marine carbonate system, four measurable variables were defined: C_T, pH, total alkalinity (A_T), and $p(CO_2)$. Due to their thermodynamic relationships, only two of these four variables are necessary for a full characterization (Millero 2007). Figure 1.8 shows, how the measurable variables are generally related to the marine carbonate system.

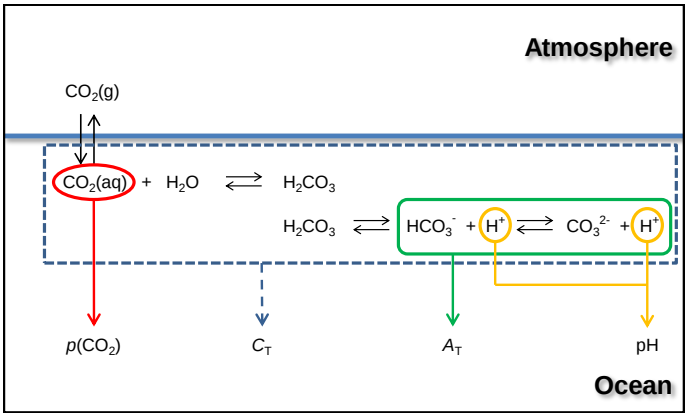

Figure 1.8: The marine carbonate system and its measurable variables

Total dissolved inorganic carbon C_T is the sum of the concentrations of the dissolved inorganic carbonate species and, therefore, represents the mass balance of the oceanic carbonate system. It is of total quantity, which means that C_T is

independent of temperature and pressure.

$$C_{\mathrm{T}} = [\mathrm{HCO_3^-}] + [\mathrm{CO_3^{2-}}] + [\mathrm{CO_2^*}] \tag{1.5}$$

pH The pH is generally defined as the negative common logarithm of the $\mathrm{H^+}$-ion concentration.

$$\mathrm{pH} = -\log_{10}[\mathrm{H^+}] \tag{1.6}$$

In the oceanographic community, three different stoichiometric concentration scales for $[\mathrm{H^+}]$ are applied: total scale ($[\mathrm{H^+}]_{\mathrm{T}}$), free scale ($[\mathrm{H^+}]_{\mathrm{F}}$), and seawater scale ($[\mathrm{H^+}]_{\mathrm{SWS}}$). These scales calculates the pH with different considerations of protonated species of sulphate and fluoride ions (see Equ. 1.7, 1.8 and 1.9). All three scales are convertible among each other.

$$\mathrm{pH_F} = -\log_{10}([\mathrm{H^+}]_{\mathrm{F}}) \tag{1.7}$$
$$\mathrm{pH_T} = -\log_{10}([\mathrm{H^+}]_{\mathrm{F}} + [\mathrm{HSO_4^-}]) \tag{1.8}$$
$$\mathrm{pH_{SWS}} = -\log_{10}([\mathrm{H^+}]_{\mathrm{F}} + [\mathrm{HSO_4^-}] + [\mathrm{HF}]) \tag{1.9}$$

Total alkalinity Dickson (1981) defined the A_{T} of a seawater sample as "the number of moles of hydrogen ion equivalent to the excess of proton acceptors (bases formed from weak acids with a dissociation constant $K \leq 10^{-4.5}$ at 25 °C and zero ionic strength) over proton donors (acids with $K \geq 10^{-4.5}$) in one kilogram of sample". Therefore, A_{T} is a measure of the oceanic buffer capacity.

$$\begin{aligned} A_{\mathrm{T}} = {} & [\mathrm{HCO_3^-}] + 2 \times [\mathrm{CO_3^{2-}}] + [\mathrm{B(OH)_4^-}] + [\mathrm{HPO_4^{2-}}] \\ & + 2 \times [\mathrm{PO_4^{3-}}] + [\mathrm{SiO(OH)_3^-}] + [\mathrm{NH_3}] + [\mathrm{HS^-}] + \cdots \\ & - [\mathrm{H^+}]_{\mathrm{F}} - [\mathrm{HSO_4^-}] - [\mathrm{HF}] - [\mathrm{H_3PO_4}] - \cdots \end{aligned} \tag{1.10}$$

The three dots in Equ. 1.10 represent negligible or unknown (e.g. organic) bases and acids. A_{T} is strongly related to the charge balance of seawater. Furthermore, like C_{T}, it is of total quantity, hence, independent of temperature and pressure. About 96 % of A_{T} is related to the carbonate species and is termed carbonate alkalinity, A_{C}, which represents a shortened form of A_{T}:

$$A_{\mathrm{C}} = [\mathrm{HCO_3^-}] + 2 \times [\mathrm{CO_3^{2-}}] \tag{1.11}$$

CO_2 partial pressure $p(CO_2)$ in air equilibrated with a seawater sample (at a specified temperature) is a measure of the degree of saturation of the sample with CO_2 gas. It is strongly depended from temperature by changing about 4.2 % per Kelvin (Dickson 2011). It can be calculated by the expression:

$$p(\mathrm{CO_2}) = \chi(\mathrm{CO_2}) \times p \tag{1.12}$$

where $\chi(CO_2)$ is the CO_2 mole fraction in the gas phase, and p is the total pressure. This calculation provides ideal behavior of the respective gas. However, CO_2 is not an ideal gas and, therefore, the more accurate fugacity, $f(CO_2)$, was introduced, which takes the non-ideal behavior into account. Weiss (1974) showed that the difference between $p(CO_2)$ and $f(CO_2)$ is not large. Consequently, $f(CO_2)$ is only needed for highly accurate observations.

The four measurable carbonate variables are differently influenced by the following processes: air-sea gas exchange, photosynthesis, respiration, calcification and calcite dissolution. Figure 1.9 illustrates these influences. At different depths in the ocean different processes and impacts are dominant.

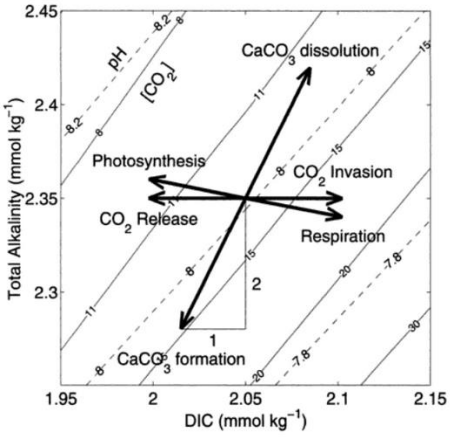

Figure 1.9: The carbonate system variables affected by different processes: air-sea gas exchange, photosynthesis, respiration, calcification and calcite dissolution. Dashed and solid contours indicates different values of pH and $[CO_2]$ as a function of C_{T} (here: DIC) and A_{T}. Arrows indicate the influences of each process on the carbonate variables. Source: Zeebe and Wolf-Gladrow (2001)

In upper layers of the ocean, CO_2 absorption from the atmosphere leads to an increase in C_T, $p(CO_2)$, and a decrease in pH, whereas A_T is not influenced, because the charge balance is not affected. CO_2 release from the ocean into the atmosphere leads to an opposite effect. Photosynthesis in the surface ocean leads to a decrease in C_T and an slightly increase in A_T due to the additional uptake of nutrients, whereas respiration has the opposite effect. Calcification (in upper layers) and calcite dissolution (in deeper layers) processes have the biggest impact on A_T and C_T, which is a result of the change in the mass and charge balance (see chemical reactions in Fig. 1.6). A_T and C_T decrease in a fixed ratio of 2:1. At the same time, $p(CO_2)$ increases and pH decreases during calcification processes, and vise versa during calcite dissolution processes.

1.4 Impacts of anthropogenic CO_2 on the marine carbonate system

In pre-industrial times, it is assumed that all CO_2 exchanges from the carbon pumps over the surface ocean are in balance ("steady-state") and compensate each other (Raven et al. 2005; Zeebe and Ridgwell 2011).

Since 1750, start of the Industrial Era, the atmospheric CO_2 concentration has constantly increased due to human activities. One consequence of this is an unbalanced physical carbon pump. The atmosphere over the North Atlantic, which acts as a sink of atmospheric CO_2, is additionally loaded with anthropogenic CO_2, whereas the marine CO_2 sources in equatorial regions are still under more pre-industrial conditions. These circumstances lead to higher oceanic CO_2 absorption. A direct consequence of these elevated marine $p(CO_2)$ values in the upper ocean is an equilibrium shift within the marine carbonate system towards bicarbonate and hydrogen ions. At the same time, $[CO_3^{2-}]$ decreases due the pH drop caused by the higher amounts of $[H^+]$. This pH drop in surface waters caused by anthropogenic CO_2 uptake is called "ocean acidification" and becomes more prominent over the last decades as another huge "CO_2 problem" (besides global warming) (e.g. Raven et al. 2005; Doney et al. 2009; Hennige et al. 2014). The oceanic surface pH declines from about 8.3 during the last glacial maximum, 8.18 just prior to the Industrial Era, and 8.10 at present (Billé et al. 2013). Projections based on models predict an oceanic surface pH of about 7.8 in year 2100 (Orr 2011), with pH reduces at a rate of about –0.0013 and -0.0024 pH units yr^{-1} (Rhein et al. 2013). Besides pH reduction, ocean acidification affects the ocean by 1) broad changes in seawater chemistry (e.g. changed chemical speciations and elemental stoichiometries (Hoffmann et al. 2012; Bijma et al. 2013)), and 2) reduced aragonite and calcite saturations due to the decline in $[CO_3^{2-}]$ and progressive dissolution of $CaCO_3$ (Orr et al. 2005; Veron et al. 2009; Bijma et al. 2013). The extent and direction of any changes in the biological carbon pump are still unclear and unpredictable (Passow and Carlson 2012). The named oceanic chemical changes directly affect the marine biology (e.g. reduced calcification rates of calcifying organisms such as reef-building corals,

which leads to reef erosion (Bijma et al. 2013; Hennige et al. 2014)).

Besides chemical changes, the marine carbonate system is also affected by physical changes. Due to global warming, which is a direct result of anthropogenic CO_2 emissions, the oceanic sea surface temperature (SST) rises. This leads to a decreasing CO_2 solubility in the upper ocean, and, therefore, a decreasing efficiency of the solubility pump. Model based estimates predict a 9-15 % reduced oceanic CO_2 uptake (equals about 45-70 GtC), and a solubility pump efficiency reduction of about 10 % at the end of the 21st century (Riebesell et al. 2009; Körtzinger 2010).

Concluding, anthropogenic CO_2 emissions and the oceanic CO_2 uptake have huge impacts on the ocean and oceanic life. Ocean acidification, global warming and other stressors like oceanic deoxygenation will change ocean physics, chemistry and ecosystems enormously over the next years and decades (Turley et al. 2016). The exact consequences for the future global life are hard to predict, but they will be fateful.

1.5 Global oceanic carbon observations

In view of the central role of the ocean's CO_2 sink and its vulnerability to global change, comprehensive observations and documentation of the changing marine carbonate cycle are of utmost importance. The relatively good understanding of the current global mean oceanic uptake of anthropogenic CO_2 is contrasted by a lack of knowledge how the natural carbonate cycle will respond regionally to global change. These observations require globally concerted observational effort that makes use of the existing observation networks. One of the most important networks regarding observations for the oceanic CO_2 sink is the Ship of Opportunity network (Carbon-SOOP), which is organized in the Surface Ocean CO_2 Network (SOCONET) (Wanninkhof et al. 2019). The "Surface Ocean CO_2 Atlas" (SOCAT) is the high relevant result of the observations obtained from Carbon-SOOP after quality control (Bakker et al. 2016). The recent release of SOCAT version 2019 features 25.7 million quality-controlled $p(CO_2)$ measurements from the period 1957-2019. Figure 1.10 shows all these $p(CO_2)$ measurements. However, there is one severe shortcoming with the current ocean Carbon-SOOP network: $p(CO_2)$ is mostly the only measured marine carbonate variable. This variable is required for net air-sea CO_2 flux calculations, but on its own it is not sufficient to get the full insight into the marine carbonate system. As mentioned in Sect. 1.3, two out of the four marine carbonate variables are necessary. A so far common workaround is the prediction of A_T from SST and sea surface salinity (SSS) using established parameterizations (Millero et al. 1998; Lee et al. 2006). Unfortunately, this procedure leads to additional uncertainties and is particularly prone to regional and seasonal bias.

An optimized solution for the latter problem is the direct measurement of a second carbonate variable on Carbon-SOOP stations. Such measurements are only

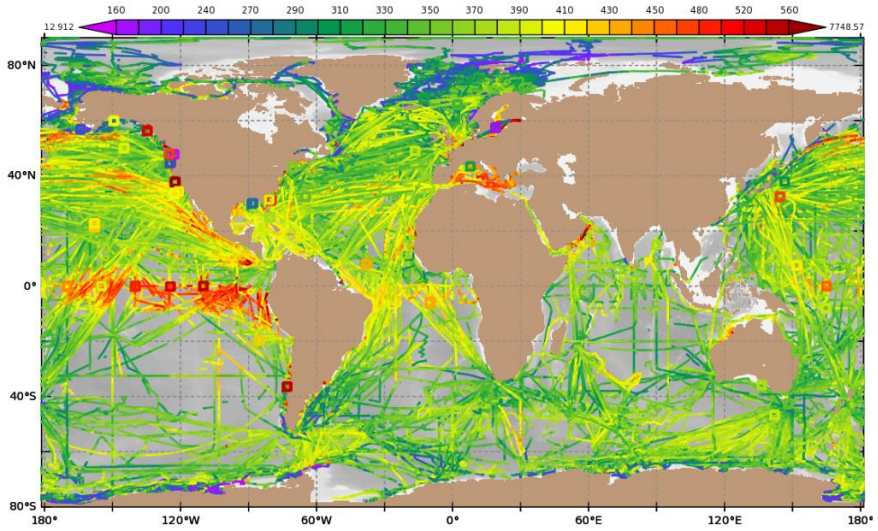

Figure 1.10: Global $p(CO_2)$ measurements in SOCAT version 2019 from the time period 1957-2019 (Bakker et al. 2016). This figure was generated by the interactive dataset viewer from SOCAT (available at: `https://ferret.pmel.noaa.gov/socat/las/UI.vm`, last accessed: 01.04.2020)

feasible as long as they can be conducted by autonomous systems (underway or *in situ*), that can be easily obtained by the community (e.g. commercially available). At the time of this study, C_T measurements are not feasible due to the fact that no autonomous measurement system is available. Of course, there are several published approaches measuring C_T autonomously (e.g. Liu et al. 2013; Fassbender et al. 2015; Call et al. 2017), but non of these become common within the oceanographic community (to our knowledge). In contrast, autonomous sensors and underway systems for A_T and pH are available and commonly used. Table 1.1 gives an overview over some exemplary chosen sensors and underway systems. Of course, the operators of Carbon-SOOP stations can choose by themselves, which variable they measure. But it must be taken into account that the combination $p(CO_2)$-pH leads to higher uncertainties in the resulting calculations of the carbonate chemistry then $p(CO_2)$-A_T (Dickson 2011). Extensive uncertainty calculations performed by Steinhoff and Skjelvan (2020) showed that calculated C_T and A_T values from $p(CO_2)$ and pH data do not fulfill the uncertainty requirements for SOOP-based measurements (ICOS Ocean Thematic Centre 2020), whereas calculated C_T and pH values from $p(CO_2)$ and A_T data meet these requirements.

Table 1.1: Exemplary chosen autonomous sensors and underway systems for A_T and pH measurements (not a complete list)

Variable	Underway	*In situ* sensor
A_T	CONTROS HydroFIA® TA (-4H-JENA engineering GmbH, Germany)	SAMI-Alk (Sunburst Sensors, USA)
pH	SP101-LB (SensorLab S.L., Spain)	SP200-SM (SensorLab S.L., Spain)
	CONTROS HyroFIA® pH (-4H-JENA engineering GmbH, Germany)	SeaFET V2 (Sea-Bird Electronics, USA)
	AFT-pH (Sunburst Sensors, USA)	SAMI-pH (Sunburst Sensors, USA)
		Durafet pH Sensor (Honeywell International Inc., USA)

References

Bakker, D. C. E., B. Pfeil, C. S. Landa, N. Metzl, K. M. O'Brien, and others. **2016**. A multi-decade record of high-quality fCO_2 data in version 3 of the Surface Ocean CO_2 Atlas (SOCAT). Earth System Science Data. 8: 383–413, doi: 10.5194/essd-8-383-2016

Bijma, J., H.-O. Pörtner, C. Yesson, and A. D. Rogers. **2013**. Climate change and the oceans – What does the future hold? Marine Pollution Bulletin. 74: 495–505, doi: 10.1016/j.marpolbul.2013.07.022

Billé, R., R. Kelly, A. Biastoch, E. Harrould-Kolieb, D. Herr, and others. **2013**. Taking Action Against Ocean Acidification: A Review of Management and Policy Options. Environmental Management. 52: 761–779, doi: 10.1007/s00267-013-0132-7

Call, M., K. G. Schulz, M. C. Carvalho, I. R. Santos, and D. T. Maher. **2017**. Technical note: Coupling infrared gas analysis and cavity ring down spectroscopy for autonomous, high-temporal-resolution measurements of DIC and δ 13 C–DIC. Biogeosciences. 14: 1305–1313, doi: 10.5194/bg-14-1305-2017

Ciais, P., C. Sabine, B. Govindasamy, L. Bopp, V. Brovkin, and others. eds.: Stocker, T., D. Qin, and G.-K. Platner. **2013**. Chapter 6: Carbon and Other Biogeochemical Cycles, in: Climate Change 2013: The Physical Science Basis. Cambridge University Press, Cambridge, United Kingdom and New York, NY, USA.

Denman, K., G. Brasseur, A. Chidthaisong, P. Ciais, P. Cox, and others. eds.: Solomon, S., D. Qin, M. Manning, Z. Chen, M. Marquis, and others. **2007**. Couplings Between Changes in the Climate System and Biogeochemistry, in: Climate Change 2007: The Physical Science Basis. Cambridge University Press, Cambridge, United Kingdom and New York, NY, USA.

Dickson, A. G. **1981**. An exact definition of total alkalinity and a procedure for the estimation of alkalinity and total inorganic carbon from titration data. Deep Sea Research Part A. Oceanographic Research Papers. 28: 609–623, doi: 10.1016/0198-0149(81)90121-7

Dickson, A. G. **2011**. The carbon dioxide system in seawater: equilibrium chemistry and measurements, in: Guide to best practices for ocean acidification research and data reporting. Office for Official Publications of the European Communities, Luxembourg.

Dlugokencky, E. and P. P. Tans. **2020**. Trends in atmospheric carbon dioxide. National Oceanic & Atmospheric Administration, Earth System Research

Laboratory (NOAA/ESRL). Available at: `https://www.esrl.noaa.gov/gmd/ccgg/trends/global.html`, last access: 11.03.2020.

Doney, S. C., V. J. Fabry, R. A. Feely, and J. A. Kleypas. **2009**. Ocean Acidification: The Other CO_2 Problem. Annual Review of Marine Science. 1: 169–192, doi: 10.1146/annurev.marine.010908.163834

Emerson, S. and J. Hedges. **2008**. Chemical oceanography and the marine carbon cycle. Cambridge University Press, Cambridge, United Kingdom and New York, NY, USA.

Fassbender, A. J., C. L. Sabine, N. Lawrence-Slavas, E. H. De Carlo, C. Meinig, and S. Maenner Jones. **2015**. Robust Sensor for Extended Autonomous Measurements of Surface Ocean Dissolved Inorganic Carbon. Environmental Science & Technology. 49: 3628–3635, doi: 10.1021/es5047183

Friedlingstein, P., M. W. Jones, M. O'Sullivan, R. M. Andrew, J. Hauck, and others. **2019**. Global Carbon Budget 2019. Earth System Science Data. 11: 1783–1838, doi: 10.5194/essd-11-1783-2019

Goyet, C. and A. Poisson. **1989**. New determination of carbonic acid dissociation constants in seawater as a function of temperature and salinity. Deep Sea Research Part A. Oceanographic Research Papers. 36: 1635–1654, doi: 10.1016/0198-0149(89)90064-2

Hansson, I. **1973**. A new set of acidity constants for carbonic acid and boric acid in sea water. Deep Sea Research and Oceanographic Abstracts. 20: 461–478, doi: 10.1016/0011-7471(73)90100-9

Heinze, C., S. Meyer, N. Goris, L. Anderson, R. Steinfeldt, N. Chang, C. Le Quéré, and D. C. E. Bakker. **2015**. The ocean carbon sink – impacts, vulnerabilities and challenges. Earth System Dynamics. 6: 327–358, doi: 10.5194/esd-6-327-2015

Hennige, S., J. M. Roberts, P. Williamson, and others. **2014**. An updated synthesis of the impacts of ocean acidification on marine biodiversity. CBD Technical Series. 75.

Hoffmann, L., E. Breitbarth, P. Boyd, and K. Hunter. **2012**. Influence of ocean warming and acidification on trace metal biogeochemistry. Marine Ecology Progress Series. 470: 191–205, doi: 10.3354/meps10082

ICOS Ocean Thematic Centre. **2020**. ICOS Ocean Station Labelling Step 2. doi: 10.18160/8SDC-K4FR

Joos, F. and R. Spahni. **2008**. Rates of change in natural and anthropogenic radiative forcing over the past 20,000 years. Proceedings of the National Academy of Sciences. 105: 1425–1430, doi: 10.1073/pnas.0707386105

Keeling, C. D., R. B. Bacastow, A. E. Bainbridge, C. A. Ekdahl, P. R. Guenther, L. S. Waterman, and J. F. S. Chin. **1976**. Atmospheric carbon dioxide variations at Mauna Loa Observatory, Hawaii. Tellus. 28: 538–551, doi: 10.1111/j.2153-3490.1976.tb00701.x

Körtzinger, A. **2010**. Der globale Kohlenstoffkreislauf im Anthropozän. Betrachtung aus meereschemischer Perspektive. Chemie in unserer Zeit. 44: 118–129, doi: 10.1002/ciuz.201000507

Le Quéré, C., R. M. Andrew, P. Friedlingstein, S. Sitch, J. Hauck, and others. **2018**. Global Carbon Budget 2018. Earth System Science Data. 10: 2141–2194, doi: 10.5194/essd-10-2141-2018

Lee, K., L. T. Tong, F. J. Millero, C. L. Sabine, A. G. Dickson, and others. **2006**. Global relationships of total alkalinity with salinity and temperature in surface waters of the world's oceans. Geophysical Research Letters. 33: L19605, doi: 10.1029/2006GL027207

Liu, X., R. H. Byrne, L. Adornato, K. K. Yates, E. Kaltenbacher, X. Ding, and B. Yang. **2013**. In Situ Spectrophotometric Measurement of Dissolved Inorganic Carbon in Seawater. Environmental Science & Technology. 47: 11106–11114, doi: 10.1021/es4014807

Lueker, T. J., A. G. Dickson, and C. D. Keeling. **2000**. Ocean pCO_2 calculated from dissolved inorganic carbon, alkalinity, and equations for K1 and K2: validation based on laboratory measurements of CO2 in gas and seawater at equilibrium. Marine Chemistry. 70: 105–119, doi: 10.1016/S0304-4203(00)00022-0

Masarie, K. A. and P. P. Tans. **1995**. Extension and integration of atmospheric carbon dioxide data into a globally consistent measurement record. Journal of Geophysical Research. 100: 11593, doi: 10.1029/95JD00859

Mehrbach, C., C. H. Culberson, J. E. Hawley, and R. M. Pytkowicx. **1973**. Measurement of the apparent dissociation constants of carbonic acid in seawater at atmospheric pressure. Limnology and Oceanography. 18: 897–907, doi: 10.4319/lo.1973.18.6.0897

Millero, F. J., K. Lee, and M. Roche. **1998**. Distribution of alkalinity in the surface waters of the major oceans. Marine Chemistry. 60: 111–130, doi: 10.1016/S0304-4203(97)00084-4

Millero, F. J., T. B. Graham, F. Huang, H. Bustos-Serrano, and D. Pierrot. **2006**. Dissociation constants of carbonic acid in seawater as a function of salinity and temperature. Marine Chemistry. 100: 80–94, doi: 10.1016/j.marchem.2005.12.001

Millero, F. J. **2007**. The Marine Inorganic Carbon Cycle. Chemical Reviews. 107: 308–341, doi: 10.1021/cr0503557

Mojica-Prieto, F. J. and F. J. Millero. **2002**. The values of pK1 + pK2 for the dissociation of carbonic acid in seawater. Geochimica et Cosmochimica Acta. 66: 2529–2540, doi: 10.1016/S0016-7037(02)00855-4

Orr, J., V. J. Fabry, O. Aumont, L. Bopp, S. C. Doney, and others. **2005**. Anthropogenic ocean acidification over the twenty-first century and its impact on calcifying organisms. Nature. 437: 681–686, doi: 10.1038/nature04095

Orr, J. **2011**. Recent and future changes in ocean carbonate chemistry, in: Ocean acidification. Oxford University Press Oxford.

Passow, U. and C. Carlson. **2012**. The biological pump in a high CO_2 world. Marine Ecology Progress Series. 470: 249–271, doi: 10.3354/meps09985

Raven, J., K. Caldeira, H. Elderfield, O. Hoegh-Guldberg, P. Liss, and others. **2005**. Ocean acidification due to increasing atmospheric carbon dioxide. The Royal Society, London, UK.

Rhein, M., S. Rintoul, S. Aoki, E. Campos, D. Chambers, and others. eds.: Stocker, T., D. Qin, G.-K. Plattner, M. Tignor, S. Allen, and others. **2013**. Chapter 3: Observations: Ocean, in: Climate Change 2013: The Physical Science Basis. Cambridge University Press, Cambridge, United Kingdom and New York, NY, USA.

Riebesell, U., A. Kortzinger, and A. Oschlies. **2009**. Sensitivities of marine carbon fluxes to ocean change. Proceedings of the National Academy of Sciences. 106: 20602–20609, doi: 10.1073/pnas.0813291106

Roy, R. N., L. N. Roy, K. M. Vogel, C. Porter-Moore, T. Pearson, C. E. Good, F. J. Millero, and D. M. Campbell. **1993**. The dissociation constants of carbonic acid in seawater at salinities 5 to 45 and temperatures 0 to 45° C. Marine Chemistry. 44: 249–267, doi: 10.1016/0304-4203(93)90207-5

Steinhoff, T. and I. Skjelvan. **2020**. Uncertainty analysis for calculations of the marine carbonate system for ICOS-Oceans stations. ICOS OTC. doi: 10.18160/VB7C-Z758

Turley, C., T. Keizer, P. Williamson, J. Gattuso, P. Ziveri, R. Munro, K. Boot, and M. Huelsenbeck. **2016**. Hot, Sour and Breathless–Ocean under Stress. Plymouth Marine Laboratory, UK Ocean Acidification Research Programme, European Project on Ocean Acidification, Mediterranean Sea Acidification in a Changing Climate project, Scripps Institution of Oceanography at UC San Diego, OCEANA.

Veron, J., O. Hoegh-Guldberg, T. Lenton, J. Lough, D. Obura, and others. **2009**. The coral reef crisis: The critical importance of<350ppm CO_2. Marine Pollution Bulletin. 58: 1428–1436, doi: 10.1016/j.marpolbul.2009.09.009

Wanninkhof, R., P. A. Pickers, A. M. Omar, A. Sutton, A. Murata, and others. **2019**. A Surface Ocean CO_2 Reference Network, SOCONET and Associated Marine Boundary Layer CO_2 Measurements. Frontiers in Marine Science. 6: doi: 10.3389/fmars.2019.00400

Weiss, R. **1974**. Carbon dioxide in water and seawater: the solubility of a non-ideal gas. Marine Chemistry. 2: 203–215, doi: 10.1016/0304-4203(74)90015-2

Zeebe, R. E. and D. Wolf-Gladrow. **2001**. CO_2 in seawater: equilibrium, kinetics, isotopes. Elsevier, Amsterdam, Netherlands.

Zeebe, R. E. and A. Ridgwell. **2011**. Past changes of ocean carbonate chemistry, in: Ocean acidification. Oxford University Press Oxford.

Chapter 2

Thesis objectives

Although there are many options for measuring a second carbonate variable, no or only very few Carbon-SOOP stations utilize them so far (to our knowledge). One possible reason could be that the implementation of such "new" systems is so far not established compared to autonomous $p(CO_2)$ measurements (Pierrot et al. 2009). Furthermore, such new implementations are complex and time consuming, and not all Carbon-SOOP station operators have the time, personnel or money to do that.

This thesis goals to provide an example of a successful implementation of a second carbonate variable on a Carbon-SOOP station together with guidelines and recommendations, which are mandatory for achieving high-quality data. This study was outlined in order to answer the following overarching research question:

Are autonomous, high-quality A_T measurements on a Carbon-SOOP station an enhancement of ocean carbon observations?

The implementation is conducted exemplary on a subpolar North Atlantic Carbon-SOOP line, which is operated by our working group since 2002. In the end, this research may become a blueprint for other Carbon-SOOP station operators leading into a better spatiotemporal coverage of surface ocean A_T, and a better understanding of the marine carbonate cycle.

Due to the fact that the existing $p(CO_2)$ installation on our SOOP line is based on the measurement of pumped seawater, the CONTROS HydroFIA® TA analyzer was chosen for autonomous A_T measurements as it was the only underway system available at the time of this study. Furthermore, its design and development is based on a previous dissertation carried out in our working group (Aßmann 2012).

This thesis is subdivided into the following three chapters, each of them addressing research questions, whose results are combined and discussed together in the conclusion chapter with regard to the main aim of the study.

1. **Can the CONTROS HydroFIA® TA provide high-quality A_T data under laboratory and field conditions, which meet fundamental quality requirements? (Chapter 4)**

The provision of high-quality A_T values especially in comparison with traditional measurement techniques is of utmost importance. This ensures reliability in the data and the resulting data products. The quality requirements for A_T measurements are precisely regulated within the oceanographic community, and stated in different guides. The most important one is the "Guide to best practices for ocean CO_2 measurements" (Dickson et al. 2007). Unfortunately, the performance characterization of the CONTROS HydroFIA® TA was only based on laboratory tests carried out by the manufacturer. Published quality test results from field deployments were completely missing. Consequently, the first part of this thesis deals with an intensive performance characterization of the analyzer in the laboratory and field. The field tests are based on data from two major research cruises in the South and North Atlantic Ocean.

This chapter is based on the following manuscript:

Seelmann, K., S. Aßmann, A. Körtzinger. **2019**. Characterization of a novel autonomous analyzer for seawater total alkalinity: Results from laboratory and field tests. Limnol Oceanogr Methods, 17: 515-532. doi: 10.1002/lom3.10329

2. **Do impurities in the used indicator dye bromocresol green (BCG) affect the measurements with the CONTROS HydroFIA® TA? Will the usage of purified BCG improve the measurement quality? (Chapter 5)**

   Yao et al. (2007) revealed that impurities in indicator dyes for seawater pH determination influence spectrophotometric measurements, and deteriorate them by an offset of up to 0.01 pH units. Indicator purification (e.g. Liu et al. 2011; Patsavas et al. 2013a; Nand and Ellwood 2018), or mathematical corrections for accurate pH measurements using unpurified indicator (Douglas and Byrne 2017) are effective ways to overcome these influences. At the time of this study, the influence of impurities in BCG indicator dye on spectrophotometric A_T determination was so far not investigated. Therefore, the second part of this thesis deals with the development of an high performance liquid chromatography (HPLC) purification method for BCG, and how the A_T measurements with the CONTROS HydroFIA® TA are influenced by indicator impurities in comparison to measurements with purified dye. For that, BCG dye from four different vendors are tested on their impurity types and quantities, and one of them is purified using the developed method.

   This chapter is based on the following manuscript:

   Seelmann, K., M. Gledhill, S. Aßmann, A. Körtzinger. **2020**. Impact of impurities in bromocresol green indicator dye on spectrophotometric total alkalinity measurements. Ocean Sci. doi: 10.5194/os-16-535-2020

3. **What needs to be considered for a successful implementation of the CONTROS HydroFIA® TA analyzer on a Ship of Opportunity in unattended measurement mode? Can the installed system provide high-quality A_T data meeting fundamental quality requirements? (Chapter 6)**

   Ships of Opportunity (SOOP) are the most important provider of oceanic $p(CO_2)$ data worldwide. These data are essential for CO_2 flux calculations. But to get full insight into the marine carbonate chemistry and its changes in times of global warming, ocean acidification and deoxygenation, a second carbonate variable is necessary. The third part of this thesis describes in detail, how the CONTROS HydroFIA® TA system is installed on the merchant vessel M/V *Atlantic Sail*, and what is necessary to get high-quality autonomous A_T measurements. For that, the measured A_T values are compared to discrete samples taken during the first two measurement campaigns, and predicted A_T values based on established parameterizations (e.g. Lee et al. 2006).

   This chapter is based on the following manuscript:

   Seelmann, K., T. Steinhoff, S. Aßmann, A. Körtzinger. **2020**. Enhance ocean carbon observations: Successful implementation of a novel autonomous analyzer on a Ship of Opportunity. Manuscript submitted to: Frontiers in Marine Science.

References

Aßmann, S. **2012**. Entwicklung und Qualifizierung autonomer Messsysteme für den pH-Wert und die Gesamtalkalinität von Meerwasser. Doctoral thesis. Available at: `https://macau.uni-kiel.de/receive/diss_mods_00010645`.

Dickson, A. G., C. L. Sabine, and J. R. Christian. **2007**. Guide to best practices for ocean CO_2 measurements. PICES Special Publications 3.

Douglas, N. K. and R. H. Byrne. **2017**. Achieving accurate spectrophotometric pH measurements using unpurified meta-cresol purple. Marine Chemistry. 190: 66–72, doi: 10.1016/j.marchem.2017.02.004

Lee, K., L. T. Tong, F. J. Millero, C. L. Sabine, A. G. Dickson, and others. **2006**. Global relationships of total alkalinity with salinity and temperature in surface waters of the world's oceans. Geophysical Research Letters. 33: L19605, doi: 10.1029/2006GL027207

Liu, X., M. C. Patsavas, and R. H. Byrne. **2011**. Purification and characterization of meta-cresol purple for spectrophotometric seawater pH measurements. Environ. Sci. Technol. 45: 4862–4868, doi: 10.1021/es200665d

Nand, V. and M. J. Ellwood. **2018**. A simple colorimetric method for determining seawater alkalinity using bromophenol blue. Limnology and Oceanography: Methods. 16: 401–410, doi: 10.1002/lom3.10253

Patsavas, M. C., R. H. Byrne, and X. Liu. **2013a**. Purification of meta-cresol purple and cresol red by flash chromatography: Procedures for ensuring accurate spectrophotometric seawater pH measurements. Marine Chemistry. 150: 19–24, doi: 10.1016/j.marchem.2013.01.004

Pierrot, D., C. Neill, K. Sullivan, R. Castle, R. Wanninkhof, and others. **2009**. Recommendations for autonomous underway pCO_2 measuring systems and data-reduction routines. Deep Sea Research Part II: Topical Studies in Oceanography. 56: 512–522, doi: 10.1016/j.dsr2.2008.12.005

Yao, W., X. Liu, and R. H. Byrne. **2007**. Impurities in indicators used for spectrophotometric seawater pH measurements: Assessment and remedies. Marine Chemistry. 107: 167–172, doi: 10.1016/j.marchem.2007.06.012

Chapter 3

Methods

3.1 General

The methods described in this chapter were used to answer the research questions of this dissertation. However, as the following chapters are based on published or for publication prepared manuscripts, they always contain sections for methodology descriptions. Consequently, if a method is explained in detail in some of the following chapters, there is a respective note and a reference to the certain section. This procedure avoids method explanation repetitions within the dissertation.

3.2 Analytical quantification of total alkalinity

3.2.1 Traditional method - Potentiometric open cell titration

The potentiometric open cell titration represents the most common technique for the quantification of A_T in a seawater sample. Its standard operating procedure (SOP) is described in the "Guide to Best Practices for Ocean CO_2 Measurements" by Dickson et al. (2007). It is based on the following principle: A known amount of a seawater sample is placed in an open titration cell, which is temperature controlled to 25 °C. There, it is titrated with 0.1 mol kg^{-1} hydrochloric acid (HCl) in two stages. First, a single aliquot of HCl is dosed to the cell to bring the pH of the sample between 3.5 and 4.0. Then, the solution is stirred for a period of time, which removes the evolved CO_2. The titration is then continued until the sample reaches a pH of about 3.0. The open cell application has the advantage that the total dissolved inorganic carbon (C_T) in the sample is approximately zero in pH regions around 3.0 and 3.5. The titration is monitored by a pH glass electrode/ reference electrode cell. The A_T of the seawater sample is calculated from the volume of the sample, the HCl volume and the electromagnetic field (emf) measurements from the electrode combination using a non-linear least-squares approach.

Figure 3.1 shows the Versatile Instrument for the Determination of Titration Alkalinity (VINDTA) built by Marianda, Germany, which is used in our laboratory at the GEOMAR. It applies the in Dickson et al. (2007) described SOP. A thermostat bath (Julabo F 25, JULABO GmbH, Germany) constantly controls the temperature of the seawater sample, the pipette and the titration cell to 25 °C. The Metrohm 719 S Titrino (Metrohm, Schweiz) serves as titrator for the HCl solution.

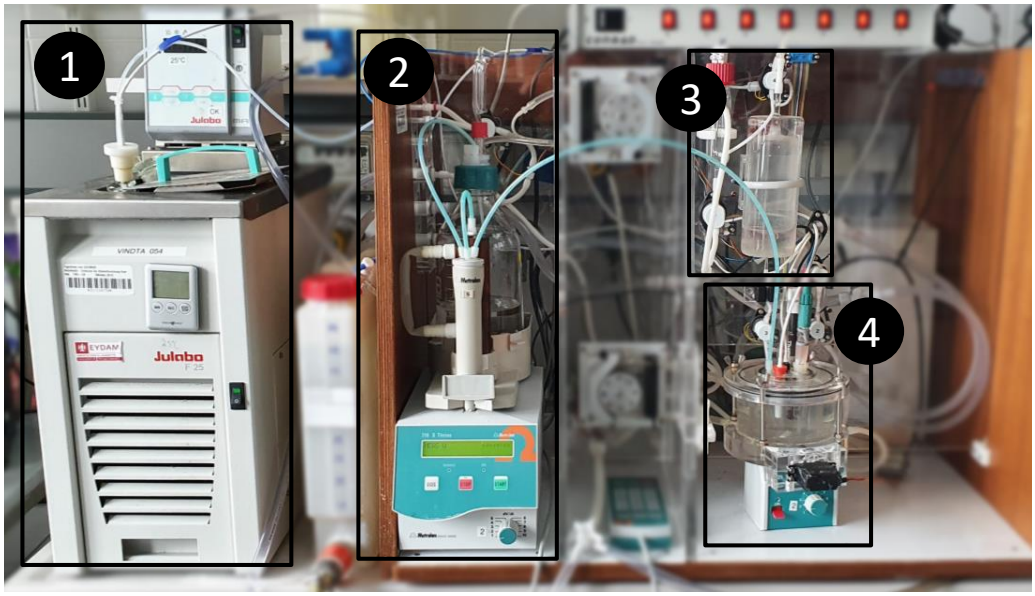

Figure 3.1: VINDTA measurement system at the GEOMAR. 1) Thermostat bath, 2) titrator for HCl solution, 3) jacketed pipette, and 4) titration cell assembly with stirrer and pH electrodes.

During the doctoral research period, this analyzer has served as referencing system by measuring the discrete samples taken throughout the participated cruises. Its measurement quality was monitored by regular Certified Reference Material (CRM) measurements.

This traditional method has several disadvantages. The pipette has to be precisely calibrated. The thermostat has to be capable of maintaining the temperature in the bath, the pipette and the cell to better than ± 0.05 °C. Furthermore, the calibration of the pH electrodes has to be carried out frequently to ensure high-quality pH measurements (Millero et al. 1993). Other disadvantages are the relatively long measurement time per sample (10 to 20 min), and the need of well-trained technicians in an air-conditioned laboratory. However, the main disadvantage of analyzers applying the traditional method is the fact that the measured seawater must be provided as a bottled and typically poisoned discrete sample. Direct measurements e.g. on ships are not possible or only possible with high effort and, additionally, not autonomously.

3.2.2 Spectrophotometric method

Since the late 1980's, spectrophotometric pH determination techniques using sulphonephthalein indicator dyes have been utilized for ocean carbon observations (Robert-Baldo et al. 1985; Byrne 1987; Byrne and Breland 1989; King and Kester 1989). Spectrophotometric A_T measurements require that both the indicator acid and the indicator base are detectable in the pH range of the acidified seawater

($\approx$ 3.0 - 4.5). Breland and Byrne (1993) discovered that the indicator dye bromocresol green (BCG) is suitable for the spectrophotometric pH determination around 3.4 and 4.6, and therefore, suitable for A_T measurements. After that, several authors described different measurement systems based on this finding (e.g. Yao and Byrne 1998; Aßmann 2012; Li et al. 2013). Besides BCG, the sulphonephthalein indicator dyes bromocresol purple (BCP) and bromophenol blue (BPB) were also used for spectrophotometric pH measurements for the determination of A_T (e.g. King and Kester 1989; Haraldsson et al. 1997; Okamura et al. 2010; Liu et al. 2015; Nand and Ellwood 2018).

Most of these developments follow the principle of an open cell, single-point titration with subsequent spectrophotometric pH determination: A known volume of seawater is titrated with a fixed volume of HCl to a pH between 3.0 and 4.5. A fixed volume of BCG solution is added either together with the HCL solution as one titrant or separately. A degassing procedure (stirring or inline CO_2 remover like a membrane) removes the evolved CO_2. Afterwards, a spectrophotometer measures the light absorbance at certain wavelengths (e.g. 444 nm and 616 nm for BCG). The pH of the acidified and dyed seawater is calculated by the following general equation:

$$\mathrm{pH} = \mathrm{p}K_\mathrm{I} + \log_{10} \frac{[\mathrm{I}^{2-}]}{[\mathrm{HI}^{-}]} \tag{3.1}$$

with the concentrations of the indicator base $[\mathrm{I}^{2-}]$ and the indicator acid $[\mathrm{HI}^{-}]$ and the dissociation constant of the indicator acid $\mathrm{p}K_\mathrm{I}$. The $\mathrm{p}K_\mathrm{I}$ has to be known as a function of the salinity and temperature, which requires an intensive and accurate characterization of the used indicator. Both indicator concentrations can be calculated from their light absorbances. Due to the known amount of added acid and the known seawater volume, the A_T can be calculated from the pH and other known coefficients. The detailed A_T calculation based on spectrophotometric pH detection can be found in Sect. 4.2.1.

All developments based on spectrophotometric A_T determinations showed comparable measurement quality to the traditional method. Additionally, most of the described systems were intended to directly measure A_T at sea without the need of discrete sampling. Some of them were also capable to run autonomously. Thus, the spectrophotometric method overcomes most of the disadvantages of the traditional method. Furthermore, as it only uses relative values like absorbance ratios for pH calculation, a calibration is not necessary.

One shortcoming of this method is the fact that impurities in the indicator dye may effect and deteriorate the resulting pH measurements and, consequently, the A_T measurements (Yao et al. 2007; Liu et al. 2011).

3.3 CONTROS HydroFIA® TA analyzer

3.3.1 Measurement principle and instrumental design

The measurement principle of the CONTROS HydroFIA® TA analyzer is based on a single-point, open cell titration of the seawater sample with subsequent spectrophotometric pH detection using BCG as indicator. It is a commercially available product offered by -4H-JENA engineering GmbH, Germany (since February 2020). Before February 2020, it was purchased by Kongsberg Maritime Contros GmbH, Germany. The CONTROS HydroFIA® TA is an autonomous, flow-through analyzer and, therefore suitable for A_T measurements at sea.

More details to the systems measurement principle and instrumental design can be found in Sect. 4.2.1 and 4.2.2.

3.3.2 Field deployments

In order to test the CONTROS HydroFIA® TA under field conditions, I participated in two major research cruises. The first one was a South Atlantic crossing on RV *Meteor* (M 133) from Cape Town, South Africa to Stanley, Falkland Islands (15. December 2016 - 13. January 2017). The second cruise was in the eastern North Atlantic on RV *Maria S. Merian* (MSM 68/2) from Emden, Germany to Mindelo, Cape Verde (03. November 2017 - 14. November 2017). A detailed description to both field deployments can be found in Chapter 4.

The final installation of the analyzer on the Ship of Opportunity (SOOP) was done in the last third of 2018. Since then, the merchant vessel MV *Atlantic Sail* (Atlantic Container Line, ACL) serves as SOOP line in the North Atlantic Ocean. The ship operates between Europe and North America. A detailed description of the installation on the SOOP line can be found in Chapter 6.

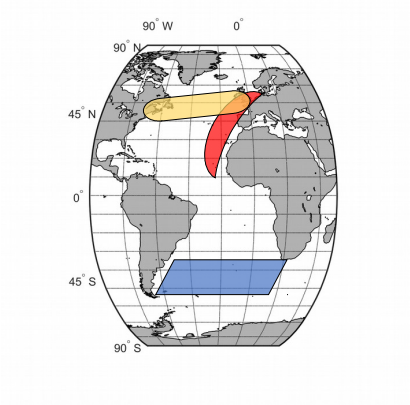

Figure 3.2: Approximate measuring regions of the field deployments, where the blue area represents the first research cruise (M 133), the red area represents the second research cruise (MSM 68/2), and the yellow area represents the SOOP line region.

In order to get a rough idea of the measured regions, Fig. 3.2 shows the measurement areas of each field deployment.

Figure 3.3 shows pictures of the respective field deployments. Although the housing color of the shown analyzer is different, the technical equipment of each system is similar. There were just two changes after the second research cruise: 1) The degasser unit was revised and improved by the manufacturer, and 2) a second inlet for reference measurements was installed.

Figure 3.3: Installations of the CONTROS HydroFIA® TA during field deployments

3.3.3 Laboratory experiments

All conducted laboratory experiments regarding measurements with the CONTROS HydroFIA® TA are explained in detail in the following chapters (see Sect. 4.3.1, Sect. 5.2.2 and Sect. 6.2.2).

3.4 Indicator dye purification

In order to investigate the impacts of impurities in BCG indicator dye on spectrophotometric A_T measurements using the CONTROS HydroFIA® TA analyzer, pure BCG was necessary as reference. At the time of this study, pure BCG was not purchasable and a purification method did not exist. Therefore, a high performance

liquid chromatography (HPLC) purification method was developed. A detailed description of the development and the BCG purification procedure can be found in Sect. 5.2.1.

An HPLC is an analytical technique in chemistry used to separate, identify, and quantify components in a mixture. In a nutshell, the technique works with the following principle: A liquid solvent (mobile phase), which contains the to separate sample mixture, is pumped with high pressure (50 – 350 bar) through a column. This column is filled with a solid adsorbent material (stationary phase) of varying polarity. Each component in the sample mixture interacts differently with the absorbent material, causing different flow rates for the different components. Finally, this leads to a separation of the components as they flow out of the column. A subsequent installed detector, which needs to be suitable for the detectable components, identifies and quantifies them. As this method separates colored compounds, an UV-VIS detector was used. The HPLC method described here is mainly based on the reversed-phase chromatography, which means that the stationary phase is non-polar and the mobile phase is moderately polar. Furthermore, due to the used column material, the separation of the indicator dye is supported by an ion-exchange mechanism.

Figure 3.4 shows the HPLC system, which was used both for analytical and preparative separation. A detailed list of the used components can be found in Sect. 5.2.1.

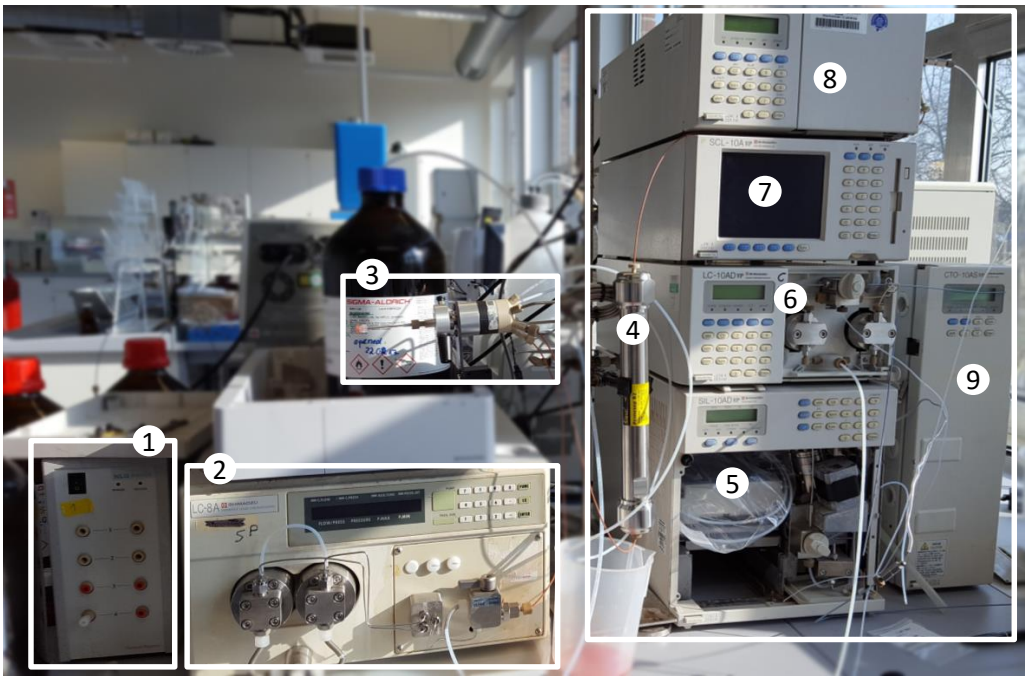

Figure 3.4: HPLC system for analytical (A) and preparative (P) separation: 1. Mobile phase degasser (P), 2. HPLC pump (P), 3. 10 mL injection loop (P), 4. preparative column (P), 5. auto sampler (A), 6. HPLC pump (A), 7. HPLC controller (A+P), 8. single channel UV-VIS detector (A+P), and 9. column oven with analytical column (A)

References

Aßmann, S. **2012**. Entwicklung und Qualifizierung autonomer Messsysteme für den pH-Wert und die Gesamtalkalinität von Meerwasser. Doctoral thesis. Available at: `https://macau.uni-kiel.de/receive/diss_mods_00010645`.

Breland, J. A. and R. H. Byrne. **1993**. Spectrophotometric procedures for determination of sea water alkalinity using bromocresol green. Deep Sea Research Part I: Oceanographic Research Papers. 40: 629–641, doi: 10.1016/0967-0637(93)90149-W

Byrne, R. H. **1987**. Standardization of standard buffers by visible spectrometry. Analytical Chemistry. 59: 1479–1481, doi: 10.1021/ac00137a025

Byrne, R. H. and J. A. Breland. **1989**. High precision multiwavelength pH determinations in seawater using cresol red. Deep Sea Research Part A. Oceanographic Research Papers. 36: 803–810, doi: 10.1016/0198-0149(89)90152-0

Dickson, A. G., C. L. Sabine, and J. R. Christian. **2007**. Guide to best practices for ocean CO_2 measurements. PICES Special Publications 3.

Haraldsson, C., L. G. Anderson, M. Hassellöv, S. Hulth, and K. Olsson. **1997**. Rapid, high-precision potentiometric titration of alkalinity in ocean and sediment pore waters. Deep Sea Research Part I: Oceanographic Research Papers. 44: 2031–2044, doi: 10.1016/S0967-0637(97)00088-5

King, D. and D. R. Kester. **1989**. Determination of seawater pH from 1.5 to 8.5 using colorimetric indicators. Marine Chemistry. 26: 5–20, doi: 10.1016/0304-4203(89)90061-3

Li, Q., F. Wang, Z. A. Wang, D. Yuan, M. Dai, J. Chen, J. Dai, and K. A. Hoering. **2013**. Automated Spectrophotometric Analyzer for Rapid Single-Point Titration of Seawater Total Alkalinity. Environ. Sci. Technol. 47: 11139–11146, doi: 10.1021/es402421a

Liu, X., M. C. Patsavas, and R. H. Byrne. **2011**. Purification and characterization of meta-cresol purple for spectrophotometric seawater pH measurements. Environ. Sci. Technol. 45: 4862–4868, doi: 10.1021/es200665d

Liu, X., R. H. Byrne, M. Lindemuth, R. Easley, and J. T. Mathis. **2015**. An automated procedure for laboratory and shipboard spectrophotometric measurements of seawater alkalinity: Continuously monitored single-step acid additions. Marine Chemistry. 174: 141–146, doi: 10.1016/J.MARCHEM.2015.06.008

Millero, F. J., J.-Z. Zhang, K. Lee, and D. M. Campbell. **1993**. Titration alkalinity of seawater. Marine Chemistry. 44: 153–165, doi: 10.1016/0304-4203(93)90200-8

Nand, V. and M. J. Ellwood. **2018**. A simple colorimetric method for determining seawater alkalinity using bromophenol blue. Limnology and Oceanography: Methods. 16: 401–410, doi: 10.1002/lom3.10253

Okamura, K., H. Kimoto, and T. Kimoto. **2010**. Open-cell Titration of Seawater for Alkalinity Measurements by Colorimetry Using Bromophenol Blue Combined with a Non-linear Least-squares Method. Analytical Sciences. 26: 709–713, doi: 10.2116/analsci.26.709

Robert-Baldo, G. L., M. J. Morris, and R. H. Byrne. **1985**. Spectrophotometric determination of seawater pH using phenol red. Analytical Chemistry. 57: 2564–2567, doi: 10.1021/ac00290a030

Yao, W. and R. H. Byrne. **1998**. Simplified seawater alkalinity analysis: Use of linear array spectrometers. Deep Sea Res., Part I. 45: 1383–1392, doi: 10.1016/S0967-0637(98)00018-1

Yao, W., X. Liu, and R. H. Byrne. **2007**. Impurities in indicators used for spectrophotometric seawater pH measurements: Assessment and remedies. Marine Chemistry. 107: 167–172, doi: 10.1016/j.marchem.2007.06.012

Chapter 4

Characterization of a novel autonomous analyzer for seawater total alkalinity: Results from laboratory and field tests

Published as: Seelmann, K., S. Aßmann, A. Körtzinger. **2019**. Characterization of a novel autonomous analyzer for seawater total alkalinity: Results from laboratory and field tests. Limnol Oceanogr Methods, 17: 515-532. doi:10.1002/lom3.10329

Abstract High quality seawater total alkalinity (A_T) measurements are essential for reliable ocean carbon and acidification observations. Well established manual multi-point potentiometric titration methods already fulfill these requirements. The next step in the improvement of these observations is the increase of the spatial and temporal measuring resolution with minimal personnel and instrumental effort. For this, a rapid, automated underway analyzer meeting the same high requirements as the traditional method is necessary. In this study, we carried out a comprehensive characterization of the flow-through analyzer CONTROS HydroFIA® TA (Kongsberg Maritime Contros GmbH, Kiel, Germany) for automated seawater A_T measurements in the laboratory and in field with overall more than 5000 measurements. Under laboratory conditions, the analyzer featured a precision of ± 1.5 µmol kg^{-1} and an accuracy of ± 1.0 µmol kg^{-1}, combined in an uncertainty of 1.6 — 2.0 µmol kg^{-1}. High precision (± 1.1 µmol kg^{-1}) and accuracy (0.3 ± 2.8 µmol kg^{-1}), and low uncertainty (2.0 — 2.5 µmol kg^{-1}) were also achieved during field trials of four and six weeks duration. Although a linear drift appears to be the typical behavior of the system, this can be corrected for by regular reference measurements giving consistent measurement results. Another advantage of regular reference measurements is the early detection of any kind of malfunction due to its direct impact on the measurement performance. Based on the present study, recommendations for automated long-term deployments are provided in order to gain optimal performance characteristics, aiming at the requirements for A_T measurements.

4.1 Introduction

The total alkalinity (A_T) of a seawater sample is defined by Dickson (1981) as "the number of moles of hydrogen ion equivalent to the excess of proton acceptors (bases formed from weak acids with a dissociation constant $K \leq 10^{-4.5}$ at 25 °C and zero ionic strength) over proton donors (acids with $K > 10^{-4.5}$) in 1 kg of sample". Therefore, A_T is a measure of the seawater buffering capacity. Together with the other parameters, pH, $p(CO_2)$, and total dissolved inorganic carbon (C_T), it is one of the four measurable parameters that allow to analytically describe the marine carbonate chemistry using the corresponding thermodynamic relationships (Millero 2007). Therefore, A_T measurements are essential components of ocean carbon observation. However, measuring this parameter both precisely and accurately is very challenging due to its high background signal (A_T of average seawater ≈ 2300 µmol kg^{-1}) compared to the small natural variability in the open ocean (Millero et al. 1998; Lee et al. 2006) and the required high accuracy for reliable cross calculations. The Guide to Best Practices for Ocean CO_2 Measurements (Dickson et al. 2007) describes the most-common standard method for measuring A_T based on a manual multi-point potentiometric titration of a seawater sample in an open or closed cell with a strong acid (here: hydrochloric acid). The method described there can achieve a precision (1σ) of better than 1 µmol kg^{-1} and an overall bias of about 2 µmol kg^{-1}. This, however, requires exact weighing of the seawater sample within 0.01 g or a precisely calibrated, thermostatted pipette as a volume-based substitute. Furthermore, the calibration of the pH electrode used for the potentiometric titration must be carried out frequently to ensure proper pH measurements (Millero et al. 1993). Other disadvantages of the traditional method are the relatively long measurement time per sample (approximately 10 to 20 min), the need of well-trained technicians in an air-conditioned laboratory, and the fact that the measured seawater must be provided as a bottled and typically poisoned discrete sample. This procedure often expands the time period between the seawater sampling during a field campaign and the actual measurement in the laboratory. Further, a potential sampling error can significantly affect the quality of the A_T measurement. Rapid seawater A_T measurements at sea with a simple and robust flow-through analyzer that can also be operated in autonomous mode would overcome most of these challenges. Several authors described different automated flow-through measurement systems for seawater A_T using potentiometric and spectrophotometric pH determination, respectively, with good accordance to the high quality requirements (for example: Roche and Millero 1998; Watanabe et al. 2004; Li et al. 2013). But none of these systems have become fully designed, commercially available products. At the time of this study, only the Submersible Autonomous Moored Instrument for alkalinity (SAMI-alk) that was developed and tested by Spaulding et al. (2014) was available as a product for unattended A_T measurements. Its measurement principle is based on a tracer monitored titration (TMT) approach, introduced by Martz et al. (2006) using a colorimetric tracer for simultaneous pH detection and acid concentration determination.

In this study, we test the CONTROS HydroFIA® TA, a novel commercially available flow-through analyzer for autonomous seawater A_T measurements built by Kongsberg Maritime Contros GmbH. Its general principle is based on open-cell single-point titration with spectrophotometric pH determination. Here we report the results of a suite of experiments carried out with this novel instrument both in the laboratory and in the field, i. e., two major research cruises to the North and South Atlantic Ocean. The goal of this study is to characterize the performance of the analyzer as well as its behavior under laboratory and real field conditions in view of potential long-term deployments. In order to evaluate, whether the measurement quality of the analyzer is suitable for underway A_T measurements in the open ocean, we compare the results with quality targets stated within the oceanographic community's established guides: 1) The "Guide to best practices for ocean CO_2 measurements" by Dickson et al. (2007) provides precision (standard deviation, σ) and accuracy (bias, ΔA_T) requirements for standard open-cell A_T titrators. 2) The "Global Ocean Acidification Observing Network: Requirements and Governance Plan" by Newton et al. (2015) provides uncertainty targets for A_T measurements in order to identify relative spatial patterns and short-term variations ("weather" goal), and to assess long-term trends with a defined level of confidence ("climate" goal), respectively. These targets are particularly important for the ocean acidification observing community. It must be taken into account, that the requirement for the "climate" goal is "only achievable by a very limited number of laboratories and is not typically achievable for all parameters by even the best autonomous sensors" (Newton et al. 2015). The certain targets of both guidelines are outlined in Tab. 4.1.

Table 4.1: Quality targets

Dickson et al. (2007)	Newton et al. (2015)[a]
Precision (1σ):	"Weather" goal:
$\pm$ 1 µmol kg^{-1}	u(c) = 10 µmol kg^{-1}
Accuracy (ΔA_T):	"Climate" goal:
$\pm$ 2 µmol kg^{-1}	u(c) = 2 µmol kg^{-1}

[a] Uncertainties with 68.3 % confidence interval

4.2 Materials and methods

4.2.1 Measurement principle

The measurement principle of the analyzer is oriented to the open-cell titration as described in the Guide to Best Practices for Ocean CO_2 Measurements (Dickson et al. 2007). Accordingly, a known amount of seawater is titrated with a solution of hydrochloric acid (HCl) to a final pH of about 3.0 to 3.5. A mixing and degassing

procedure allows the escape of all CO_2 deliberated from the sample's dissolved inorganic carbon content. The guide describes a potentiometric pH monitoring of the mixture over the entire titration. Following the definition of total alkalinity (Dickson et al. 2007), A_T at any titration point is given by

$$\begin{aligned}\frac{-m_{sw} \times A_T + m_A \times C_A}{m_{sw} + m_A} = {} & [H^+]_F + [HF] + [HSO_4^-] + [H_3PO_4] - \\ & [HCO_3^-] - 2 \times [CO_3^{2-}] - [B(OH)_4^-] - \\ & [OH^-] - [HPO_4^{2-}] - 2 \times [PO_4^{3-}] - \\ & [SiO(OH)_3^-] - [NH_3] - [HS^-]\end{aligned} \tag{4.1}$$

where $[H^+]_F$ is the free concentration of hydrogen ions, m_{sw} is the mass of the seawater sample, m_A is the mass of the added acid with the concentration C_A. Due to the working pH range of 3.0 to 3.5 and complete CO_2 removal, the majority of the terms in Equ. 4.1 can be ignored (Dickson et al. 2003). Hence, Equ. 4.1 can be reduced to

$$\frac{-m_{sw} \times A_T + m_A \times C_A}{m_{sw} + m_A} = [H^+]_F + [HF] + [HSO_4^-] \tag{4.2}$$

Deviating from the guide, the used analyzer determines the pH spectrophotometrically through a single-point titration of the seawater similar to the A_T measurement principle of Yao and Byrne (1998) and Li et al. (2013). Here, the titrant consists of two separate solutions: An acid (HCl) and an indicator solution of bromocresol green sodium salt (BCG). Based on the definition of Dickson (1981), the added BCG is regarded as a proton donor in the sample-titrant mixture due to its dissociation constant K_I at 25° C being slightly greater than $10^{-4.5}$ (exact definition of K_I later in this section, see Equ. 4.11). Thus, Equ. 4.2 must be extended by an indicator term

$$\frac{-m_{sw} \times A_T + m_t \times C_t}{m_{sw} + m_t} = [H^+]_F + [HF] + [HSO_4^-] + [HI^-] \tag{4.3}$$

where $[HI^-]$ is the concentration of the protonated (i. e. acidic) form of BCG, m_t is the sum of the masses of the two titrant solutions ($m_t = m_{acid} + m_{indicator}$) and C_t is the acid concentration in the combined titrant solution. Here, it is calculated by:

$$C_t = \frac{C_A \times m_A}{m_t} \tag{4.4}$$

For a spectrophotometric pH detection using BCG as indicator, the ideal pH range of the sample-titrant mixture is around an absorbance ratio (R) of $R \approx 1$ (further explanation later in this section). This corresponds to a pH range of about 3.5 to 4.0 and is achieved by adjusting the amount of added acid. Li et al. (2013) show that the reduction of Equ. 4.1 to Equ. 4.2 is also valid for this pH range, provided that CO_2 is quantitatively removed. Furthermore, within an autonomous measurement routine, volumes are easier to handle than masses. Hence, Equ. 4.3 is modified to

$$\frac{-V_{\mathrm{sw}} \times \rho_{\mathrm{sw}} \times A_{\mathrm{T}} + V_{\mathrm{t}} \times \rho_{\mathrm{t}} \times C_{\mathrm{t}}}{V_{\mathrm{sw}} \times \rho_{\mathrm{sw}} + V_{\mathrm{t}} \times \rho_{\mathrm{t}}} = [\mathrm{H^+}]_{\mathrm{F}} + [\mathrm{HF}] + [\mathrm{HSO_4^-}] + [\mathrm{HI^-}] \tag{4.5}$$

where V_{sw} and V_{t} are the volumes of the seawater sample and the added titrant, respectively, and ρ_{sw} and ρ_{t} are the densities of the seawater sample and the added titrant, respectively. Following Li et al. (2013), a volume mixing ratio γ_{v} ($\gamma_{\mathrm{v}} = V_{\mathrm{sw}}/V_{\mathrm{t}}$), a density ratio γ_{ρ} ($\gamma_{\rho} = \rho_{\mathrm{sw}}/\rho_{\mathrm{t}}$), and a mass mixing ratio γ ($\gamma = \gamma_{\mathrm{v}} \times \gamma_{\rho}$) are introduced to simplify the equation:

$$\frac{-\gamma \times A_{\mathrm{T}} + C_{\mathrm{t}}}{1+\gamma} = [\mathrm{H^+}]_{\mathrm{F}} + [\mathrm{HF}] + [\mathrm{HSO_4^-}] + [\mathrm{HI^-}] \tag{4.6}$$

The last three terms in Equ. 4.6 can be calculated using the dissociation equilibria described in Dickson et al. (2007). An additional rearrangement leads to

$$\begin{aligned} A_{\mathrm{T}} \times \gamma = C_{\mathrm{t}} - (1+\gamma) \\ \times \left([\mathrm{H^+}]_{\mathrm{F}} + \frac{S_{\mathrm{T}} \times \frac{\gamma}{1+\gamma} \times [\mathrm{H^+}]_{\mathrm{F}}}{[\mathrm{H^+}]_{\mathrm{F}} + K_{\mathrm{S}}} + \frac{F_{\mathrm{T}} \times \frac{\gamma}{1+\gamma} \times [\mathrm{H^+}]_{\mathrm{F}}}{[\mathrm{H^+}]_{\mathrm{F}} + K_{\mathrm{F}}} \right. \\ \left. + \frac{I_{\mathrm{T}} \times \frac{1}{1+\gamma} \times [\mathrm{H^+}]_{\mathrm{F}}}{[\mathrm{H^+}]_{\mathrm{F}} + K_{\mathrm{I}}} \right) \end{aligned} \tag{4.7}$$

where S_{T} and F_{T} are the total sulfate and the total fluoride concentration in the seawater sample, I_{T} is the total BCG concentration in the titrant, K_{S} and K_{F} are the dissociation constants of HF and HSO_4^- and K_{I} is the second dissociation constant of BCG. The factors $\gamma/(1+\gamma)$ and $1/(1+\gamma)$ represent the dilution factors of the seawater sample and the titrant, respectively. In Equ. 4.7, all dissociation constants are on the free scale, and concentrations are given in moles per kilogram solution ($\mathrm{mol\,kg^{-1}}$). The free concentration of hydrogen ions, $[\mathrm{H^+}]_{\mathrm{F}}$, or $\mathrm{pH_F}$, in the sample-titrant mixture is measured spectrophotometrically. Following Breland and Byrne (1993) and Yao and Byrne (1998), $\mathrm{pH_F}$ is described by

$$\mathrm{pH_F} = -\log K_\mathrm{I} + \log\left(\frac{R - e_1}{e_2 - R \times e_3}\right) \tag{4.8}$$

with

$$e_1 = \frac{\lambda_2 \epsilon_{\mathrm{HI^-}}}{\lambda_1 \epsilon_{\mathrm{HI^-}}} \quad e_2 = \frac{\lambda_2 \epsilon_{\mathrm{I^{2-}}}}{\lambda_1 \epsilon_{\mathrm{HI^-}}} \quad e_3 = \frac{\lambda_1 \epsilon_{\mathrm{I^{2-}}}}{\lambda_1 \epsilon_{\mathrm{HI^-}}} \tag{4.9}$$

and

$$R = \frac{A_{\lambda_2}}{A_{\lambda_1}} \tag{4.10}$$

where e_1, e_2 and e_3 represent ratios of absorption coefficients, $\lambda_\mathrm{i}\epsilon_\mathrm{x}$ for each indicator form, x, at wavelength 1 (λ_1) and 2 (λ_2), where the acid ($\mathrm{HI^-}$) and the base indicator form ($\mathrm{I^{2-}}$) have their absorbance maxima. R is the absorbance ratio at λ_1 and λ_2. For BCG, the following values are available from the literature: $\lambda_1 = 444$ nm, $\lambda_2 = 616$ nm, $e_1 = 0.0013$, $e_2 = 2.3148$, and $e_3 = 0.1299$; e_1, e_2 and e_3 are considered to be independent of salinity (Breland and Byrne 1993; Yao and Byrne 1998). Breland and Byrne (1993) reported the salinity dependence ($20 \leq S \leq 35$) of K_I for BCG at 25°C as

$$-\log K_\mathrm{I} = 4.4166 + 0.0005946 \times (35 - S) \tag{4.11}$$

where S is the salinity of the seawater sample. Yao and Byrne (1998) described an advanced salinity range up to 37 for this dependence. Due to the dilution of the seawater sample by the reagents made up in deionized (DI) water, the salinity S of the sample-titrant mixture must be adjusted as followed:

$$i_\mathrm{sw} = 0.72 \times \left(\frac{S}{35}\right) \tag{4.12}$$

$$i_\mathrm{mix} = \frac{i_\mathrm{sw} \times V_\mathrm{sw} \times \rho_\mathrm{sw} + C_\mathrm{A} \times V_\mathrm{A} \times \rho_\mathrm{A} + C_\mathrm{BCG} \times V_\mathrm{BCG} \times \rho_\mathrm{BCG}}{V_\mathrm{sw} \times \rho_\mathrm{sw} + V_\mathrm{t} \times \rho_\mathrm{t}} \tag{4.13}$$

$$S_\mathrm{mix} = 35 \times \left(\frac{i_\mathrm{mix}}{0.72}\right) \tag{4.14}$$

where i_sw and i_mix are the ionic strengths of the seawater and the seawater-titrant mixture, respectively, V_BCG and ρ_BCG are the volume and the density of the added indicator solution with the BCG concentration C_BCG, V_A and ρ_A are the volume and the density of the added HCl solution, and S_mix is the resulting salinity of

the seawater-titrant mixture. This calculation assumes the activity coefficient of BCG to be 1 and that a salinity of 35 corresponds to an ionic strength of 0.72 (Dickson 1990). Hence, the pH of the seawater-titrant mixture at 25°C within the valid salinity range of 20 to 37 can be calculated as followed

$$\mathrm{pH_F} = 4.4166 + 0.0005946 \times (35 - S_{\mathrm{mix}}) + \log\left(\frac{R - 0.0013}{2.3148 - R \times 0.1299}\right) \quad (4.15)$$

For this calculation, Breland and Byrne (1993) also described the temperature effect on the absorbance measurements between 18 and 32°C as followed

$$R_{25} = R_{\mathrm{t}} \times [1 + 0.00907 \times (25 - t)] \quad (4.16)$$

where R_{25} and R_{t} are the absorbance ratios at 25°C and at the exact temperature t (°C) of the sample-titrant mixture, respectively.

Finally, the A_{T} of a temperature controlled seawater sample with known salinity can be determined by a spectrophotometric pH measurement using Equ. 4.16, 4.15 and 4.7. Almost all variables in these equations are known or can be calculated. For the present analyzers, the volumes of the added reagents ($V_{\mathrm{t}} = V_{\mathrm{HCl}} + V_{\mathrm{BCG}}$) are fixed and thus known due to the usage of injections loops with a defined length of tubing (see Sect. 4.2.2). The densities (ρsw and ρ_{t}) at the measured temperatures of the seawater sample with known salinity, and the reagents with known chemical composition were determined using the equations reported in Dickson et al. (2007). The calculation of K_{S} and K_{F} is also based on the equations of Dickson et al. (2007) using the salinity of the seawater-titrant mixture; the calculation basis of S_{T} and F_{T} is their well characterized relationship to seawater salinity.

Due to the character of an absolute method, a calibration is principally not necessary. However, the exact volume of the seawater sample V_{sw} is the only unknown variable, which must be practically determined utilizing a one point CRM measurement. With the known A_{T} value of the CRM, it is possible to calculate V_{sw} using the same equations as for A_{T} determination. Consequently, all inevitable uncertainties (e. g. errors in the dissociation constants, the exact concentration of the titrant, impurities of the indicator dye or minor uncertainties in the titrant volume) are combined in V_{sw} and thereby taken into account for subsequent A_{T} measurements.

4.2.2 Instrumental design

4.2.2.1 Analyzer setup

For this study we used two units of the commercially available AT analyzer CONTROS HydroFIA® TA (Kongsberg Maritime Contros GmbH, Kiel, Germany).

For simplification, they are called ”red system” and ”gray system” in the following sections due to their different housing color. Otherwise, as long as there is no other information provided, the two analyzer can be regarded as being identical. Fig. 4.1 shows the schematic set-up of the analyzer showing the involved components in the measurement routine.

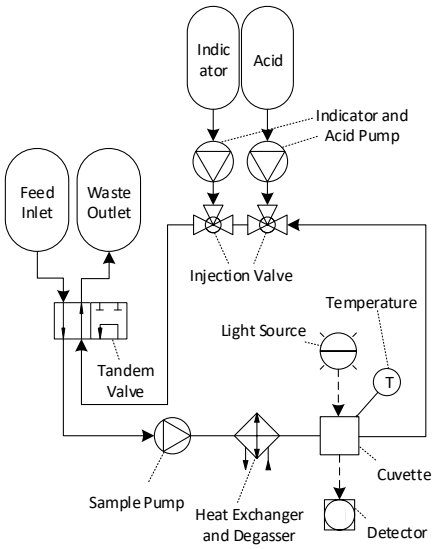

Figure 4.1: Schematic diagram of the CONTROS HydroFIA® TA system set-up. Solid lines represent fluid paths for sample water, acid or indicator solution. Dashed lines are light paths for the absorption measurement. Dotted lines are for naming and description. Oval forms represent reservoirs for the respective solutions. The indicator and acid reservoirs are closed while the feed and waste reservoirs are open.

The acid and indicator reservoirs are closed and kept in gas-tight and light-tight bags preventing any alteration of the solutions. Both solutions are separately pumped by piston pumps through injections loops with fixed length and thus fixed volume. These loops are used for injection into the sample circuit using injection valves. The injection valves are connected to the sample circuit in which the solution is pumped by a membrane pump. Depending on the position of the tandem valve, the sample solution is circulated within the sample circuit or is pumped through the open circuit to waste. While circulating, the sample is constantly temperature controlled to 25°C by the heat exchanger and at the same time the CO_2 is removed by the degassing unit which is combined with the heat exchanger (see Fig. 4.2). The temperature control is realized by a Peltier element and temperature measurement directly behind the cuvette. CO_2 removal is done by soda lime behind a membrane. The absorption measurement for the pH detection is realized by means of a flow-through cuvette with 1 cm path length, a broad-band white LED light source and a CCD spectrometer resolving the full absorption spectrum. With this setup, both can be measured simultaneously, the two absorption maximums of the indicator dye (444 nm and 616 nm) for pH calculation as well as the non-absorbing wavelength

730 nm for correction of a potential baseline shift during the measurement routine.

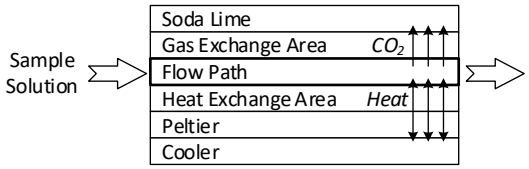

Figure 4.2: Schematic diagram of the degassing / heat exchange unit. The sample solution is flowing through the flow path being connected to tubing leading to the other parts of the measurement system (compare Fig. 4.1). For temperature control of the sample solution, the titanium heat exchange area is used separating the Peltier element from the fluid. For CO_2 stripping, the membrane gas exchange area is used separating the soda lime from the fluid.

4.2.2.2 Differences between used systems

For evaluating different working ranges of the analyzers during the second field study (see Sect. 4.3), each analyzer was equipped with different lengths of acid loop tubing. The red system was equipped with tubing 14.5 % longer than the gray system resulting in a lower final pH value after acid addition when measuring at a given A_T. Due to further developments of the analyzer during the course of this study, the red and the gray system were equipped with a modified degasser unit leading into a longer degassing time. The change was done after the first field deployment.

4.2.2.3 Measurement routine

The A_T measurement routine for each sample is structured as follows: (1) The sample pump flushes all tubing with fresh seawater to remove the residual solution from the previous analysis run. (2) This is followed by a conditioning phase with stopped seawater flow, where the system is conditioned to the pH of seawater to avoid memory effects from the large pH changes during the measurement. (3) Another flush routine collects the seawater sample for the actual measurement (either from a continuous seawater flow or a connected sample bottle), followed by the closing of the sample loop. (4) Now, the sample treatment starts. Dark and blank spectra are measured with the untitrated sample in the cuvette. (5) Both injection loops are filled with HCl solution and BCG solution, respectively, and the reagents are simultaneously injected into the sample loop. (6) This sample-titrant mixture is continuously pumped in the closed loop until completely homogenized. During this, the degasser unit, which is included in the sample loop, removes the CO_2 across a membrane, while constantly controlling the sample temperature to 25.0°C ± 0.1°C. (7) After equilibration and degassing, which takes about 5 minutes, the spectra of the CO_2 free and fully temperature controlled sample-titrant mixture are measured in the cuvette, and the A_T of the seawater sample

is calculated following the equations in Sect. 4.2.1. The whole measurement cycle (maximum measurement frequency) took approximately 7 min during the first field experiment and approximately 10 min with the modified degasser membrane during the second field test.

4.2.2.4 Seawater sample treatment

Bottled samples (i.e. CRM) were connected to the analyzer with PVC tubing using the same inlet as for underway measurements without any pretreatment. For autonomous underway measurements, the system was installed in bypass to a continuously pumped seawater flow using PVC tubing. Due to the very small tubing diameters of 0.8 mm ID inside the system, the seawater was filtered using a flow-through filter with 50 µm pore size on the first cruise and a cross-flow filter with 0.2 µm pore size on the second cruise. These filters only remove particular matter (e.g. sediment particles) which is important for not having particles dissolved during the sample treatment routine of the analyzer thus altering the A_T measurement result. An adsorption of dissolved organic matter (DOM) onto the filter material interfering with A_T measurement is not given to our knowledge. Furthermore, within the scope of this study, DOM contributions to A_T are not significant in the open ocean (e.g. McElligott et al. 1998; Lee et al. 2000; Millero et al. 2002; Ko et al. 2016).

4.2.3 Solutions and standards

The concentration of the used HCl and BCG solution was 0.1 mol kg^{-1} and 0.002 mol kg^{-1}, respectively. Both reagents were made up in DI water and provided custom-made and in ready-to-use cartridges by Kongsberg Maritime Contros GmbH. The BCG solution was made up by dissolving the sodium salt of BCG. The used BCG was not purified, but the development of an HPLC purification method for BCG and testing its impact on the A_T measurement is in progress and will be described elsewhere. Certified reference material, CRM, (batches 142, 143, 150, and 160) was obtained from A. G. Dickson at the Scripps Institution of Oceanography of the University of California, San Diego. For laboratory experiments, a seawater substandard was prepared out of leftover seawater samples poisoned with mercury chloride. For this, the samples were freshly mixed and the resulting A_T was measured using the reference method (see below).

4.2.4 Reference measurements

For accuracy monitoring, the analyzer measured CRM daily throughout all field campaigns. Every morning and evening, five repetitive CRM measurements were carried out. Furthermore, the measurements of the analyzer were compared to the results from discrete seawater samples measured on a standard open-cell alkalinity system using potentiometric titration (VINDTA 3S, Marianda, Germany). For these measurements, discrete samples were on average taken twice per day throughout

all field campaigns and measured in the home lab (GEOMAR Helmholtz Centre for Ocean Research Kiel, Germany) following the recommendations in Dickson et al. (2007).

4.2.5 Statistical calculations

For evaluating the precision of the system both in the laboratory and in field, the standard deviation σ of consecutive measurements of a reference sample (e.g. CRM) is calculated as followed

$$\sigma = \sqrt{\frac{\sum_{i=1}^{n}(x_i - \bar{x})^2}{n-2}} \tag{4.17}$$

with

$$\bar{x} = \frac{1}{n} \times \sum_{i=1}^{n} x_i \tag{4.18}$$

where n is the number of measurements, x_i is the i-th measurement of n measurements and $\bar{x}$ is the mean of the measurements.

For evaluating the accuracy in field, the bias ΔA_T between the A_T value of the system and the A_T value of the reference sample (CRM and discrete samples) is calculated as followed:

$$\Delta A_\mathrm{T} = A_\mathrm{T,Analyzer} - A_\mathrm{T,Reference} \tag{4.19}$$

The accuracy in the laboratory is determined in a different way and will be explained in Sect. 4.4.

In order to compare the measurement quality of the analyzer with the targets of the ocean acidification observing community (Newton et al. 2015), an approximation of the standard uncertainty both in the laboratory and in field is necessary. Due to the usage of CRM for "calibration" and validation of the analyzer, we utilize the within-laboratory validation approach of measurement uncertainty estimation known as "top down" for the first approximation of the measurement uncertainty. The best-known formalization of this approach is the so-called Nordtest™ described by Magnusson et al. (2017), which is based on the guide by Ellison (2012). There, the combined standard uncertainty $u(\mathrm{c})$ (approximates to a 68.3 % confidence interval) is calculated by:

$$u(\mathrm{c}) = \sqrt{u(\mathrm{RW})^2 + u(\mathrm{bias})^2} \tag{4.20}$$

where u(Rw) is the uncertainty estimate of the precision (random effects) and u(bias) is the uncertainty estimate of possible laboratory and procedural bias (systematic effects).

4.3 Experiments

4.3.1 Laboratory experiments

4.3.1.1 Scope

The first part of this study consists of experiments carried out under laboratory conditions. This means, the analyzer did not run for longer than 200 consecutive measurements (equaling approximately up to 24 h) and was set up in an air-conditioned room. Furthermore, the system was shut off overnight between the measurement days. At the start of each measurement day the analyzer carried out several conditioning measurements to ensure good system stability.

4.3.1.2 Performance characteristics

Tests on the performance characteristics in the laboratory were carried out as standard addition experiment. Therefore, a stable seawater sample (relatively high A_T) was titrated with a HCl solution (0.1 mol kg^{-1}) to lower its A_T in five steps (general range of resulting A_T: 2000 – 2450 µmol kg^{-1}). The titration was carried out by adding different precisely known volumes of HCl to a known volume of seawater resulting in five seawater aliquots with stepwise decreasing A_T. The theoretical A_T ($A_{T,theo}$) was calculated from the volumes of added acid and seawater, the concentration of the acid, and the original A_T of the seawater. To determine the practical A_T ($A_{T,prac}$), each of these aliquotes was repeatedly measured with the analyzer for five times. This experiment was carried out for each analyzer before and after the cruises.

4.3.1.3 Overlapping Allan experiment

Regular reference measurements are obligatory for quality assurance and performance monitoring of the analyzer during long term deployments. To achieve best results, the optimal number of repeated reference measurements with the smallest averaging error had to be determined. For this, we performed a stability estimation by determining the overlapping Allan deviation at different averaging times. To improve the confidence of the stability estimate, we used the overlapping Allan deviation instead of the normal Allan deviation. The overlapping Allan deviation $\sigma_y(\tau)$ makes maximum use of the data set by utilizing all possible combinations of samples at each averaging time τ (Riley 2008). It is estimated by the expression

$$\sigma_y(\tau) = \sqrt{\frac{1}{2 \times AF^2 \times (n - 2 \times AF + 1)} \times \sum_{\mathrm{j}=1}^{n-2\times AF+1} \left\{ \sum_{\mathrm{i}=\mathrm{j}}^{\mathrm{j}+AF-1} [y_{\mathrm{i}+AF} - y_{\mathrm{i}}] \right\}^2} \quad (4.21)$$

where n is the total number of measured samples, τ is the averaging time that is calculated as $\tau = \mathrm{AF} \times \tau_0$, where AF is the averaging factor and τ_0 is the basic measurement interval, and y_{i} is the i-th of n fractional frequency values averaged over τ. In this experiment, n was the total number of A_{T} measurements ($n = 30$), τ_0 was the measurement interval of the analyzer ($\tau_0 = 10\mathrm{min}$), AF was the number of averaged replicates of the reference measurement, and y represented the A_{T} values. In an optimal system with only statistical noise, a higher number of averaged replicates, that means longer averaging time, would lead to a higher precision of the measurement. However, due to long-term drift effects on the analyzer, the Allan deviation starts to increase again at some point. The minima in the overlapping Allan plot ($\sigma_{\mathrm{y}}(\tau)$ vs. AF) indicate the optimal number of averaged replicates. For this experiment, a stable seawater substandard was repeatedly measured 30 times in row with a measurement interval of 10 min on four different measurement days.

4.3.2 Field experiments

4.3.2.1 Scope

In order to test the performance of the analyzer under field conditions, we participated in two major research cruises: RV *Meteor* cruise 133 (M 133), from Cape Town, South Africa to Port Stanley, Falkland Islands; 15.12.2016 – 13.01.2017, and RV *Maria S. Merian* cruise 68/2 (MSM 68/2), from Emden, Germany to Mindelo, Cape Verde; 03.11.2017 - 14.11.2017. In both cases, the analyzer measured continuously pumped surface seawater (underway measurement mode) during the entire cruise with the fastest measurement interval of min during M 133 and 10 min during MSM 68/2, except when separate experiments were carried out. The different intervals were due to the degasser membrane change as mentioned in Sect. 4.2.2.

While we only used the red system on cruise M 133, we had the possibility to run both the red and gray system in parallel on cruise MSM 68/2.

At the beginning of both cruises each analyzer performed several conditioning measurements to ensure system stability. After stabilization, the internal seawater sample volume was determined with a freshly opened CRM.

4.3.2.2 Working range

Due to the measurement principle of the system, the working range of the analyzer is limited by the pK_{a} value of BCG, its absorption coefficients of the acid and base

form and the absorbance ratio R of the sample-titrant mixture, and therefore by the resulting pH of the sample-titrant mixture. The final pH value of a sample with given A_T after acidification can be freely adjusted by the amount of added acid or its concentration to meet the range of seawater A_T in the measured area. The A_T range is limited to seawater with salinities between 20 and 37 as specified by the characterization of BCG (Breland and Byrne 1993; Yao and Byrne 1998). Due to the constant temperature control of the sample water to 25°C, there is only the limitation of the analyzer's temperature controlling capability ranging from 5°C to 30°C for *in situ* temperatures. To take advantage of two analyzers running in parallel during the MSM 68/2 cruise, the influence of two different acid volumes was tested. For this, each analyzer was equipped with different lengths of acid loop tubing (see Sect. 4.2.2). The goal of this experiment was to investigate the influence of different pH ranges on the performance of the measurements. This experiment was only carried out on cruise MSM 68/2.

4.3.2.3 Performance characteristics

The precision under field conditions was evaluated by measuring CRM on both cruises. Additionally, during the cruise M 133, a long-term precision experiment was conducted. For this, a stable seawater substandard was prepared and measured 178 times consecutively with a measurement interval of 7 min.

The accuracy evaluation was carried out by comparing the measurements of the analyzer with both the certified values of the CRM (twice per day throughout both cruises), and the A_T values of taken discrete samples (on average twice per day throughout both cruises) measured with the reference system VINDTA 3S.

4.3.2.4 Initial drift after idle time

For longer idle times ($\geq$ 1 day), it is recommended to flush the analyzer with DI water to avoid any deposits inside the tubing, e.g. from the last colored and acidified sample. These idle times could be necessary for example during harbor time between field campaigns. Harbor seawater often is very dirty and should not be run through the system. Since the analyzer is flushed with DI water, the system is conditioned to low ionic strength, causing an extended stabilization phase (initial drift) when measuring again after these idle times. To examine the extent of such a drift, the system was flushed with DI water and did not measure any sample for 48 h, except for the very first measurements at the beginning of the cruise. Therefore, the initial idle time matched the storage and transportation time of the analyzer before the cruise ($\approx$ three months). Afterwards, a seawater substandard taken during the cruise was measured until the measurements were stable (standard deviation of the last three measurements $\leq$ 2 µmol kg^{-1}). This 48 h idling experiment was carried out three times during the whole cruise M 133: at the beginning, after 1304 measurements, and after 2183 measurements.

4.4 Results and discussion

4.4.1 Laboratory experiments

4.4.1.1 Performance characteristics

The comparison and discussion of the laboratory performance before and after a field deployment is most useful for an analyzer without any hardware problems during this deployment. Consequently, only the results for the red system before and after the MSM 68/2 cruise are shown and interpreted in the following part as the gray system suffered from a leakage in the degasser unit (see Sect. 4.4.2).

Figure 4.3 shows the results of the standard addition experiment observed with the red system before and after the MSM 68/2 cruise. For accuracy evaluation in the laboratory, the root mean square error (RMSE) of the measured A_{T} values was determined as followed

$$\mathrm{RMSE} = \pm\sqrt{\frac{1}{n} \times \sum_{i=1}^{n} (A_{\mathrm{T,fitted,i}} - A_{\mathrm{T,prac,i}})^2} \tag{4.22}$$

where n is the number of titration steps, $A_{\mathrm{T,fitted,i}}$ is the i-th A_{T} value calculated with the linear regression equation with $A_{\mathrm{T,theo,i}}$ as x variable.

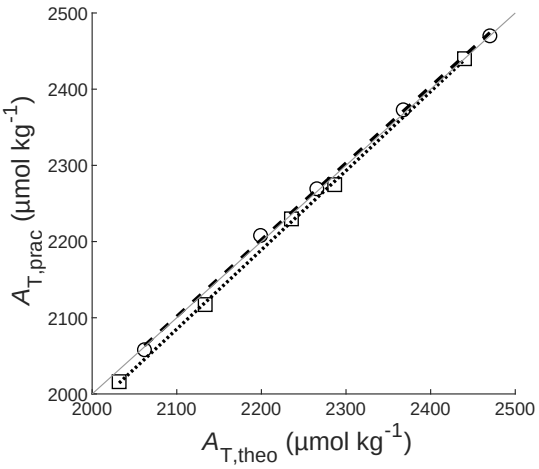

Figure 4.3: $A_{\mathrm{T,prac}}$ as a function of $A_{\mathrm{T,theo}}$ of each titration step measured with the red system before (open squares) and after (open circles) the MSM 68/2 cruise in the laboratory. $A_{\mathrm{T,prac}}$ is the average of five repeated measurements for each aliquot. The black dashed and dotted line indicates the linear fit of the data points with the following resulting linear equations: Before: $y = (1.03 \pm 0.01) \times x - (97.6 \pm 28.4), R^2 = 0.999$, and after: $y = (1.01 \pm 0.02) \times x - (11.4 \pm 40.6), R^2 = 0.999$. The gray solid line indicates the 1-to-1 line of this plot.

Before the campaign, the RMSE was determined with ± 5.5 µmol kg^{-1}; afterwards, it is improved to ± 1.0 µmol kg^{-1}. This big difference is due to a change of the experiment procedure. Before the cruise, the titrated seawater samples were manually changed and each measurement was started by hand. Afterwards, a more optimized experiment procedure was applied using an autosampler for these purposes. This custom made autosampler is part of the system calibration setup at the Kongsberg Maritime Contros GmbH laboratory and is used for routine calibrations automatically changing sample solutions of defined A_T levels. By using this autosampler, uncertainties, caused by the operator are partly removed resulting in better performance of the experiment itself. Furthermore, due to the worse slope and the large intercept of the linear regression of the data set before the cruise, it is possible that some unknown additional errors occurred during the experiment. However, the after-cruise evaluation shows a very satisfactory correlation between $A_{T,prac}$ and $A_{T,theo}$ with a slope of 1.01 ± 0.02 and an intercept of -11.4 ± 40.6 which are as expected (slope = 1, intercept = 0) within their found uncertainty. Furthermore, its laboratory accuracy of ± 1.0 µmol kg^{-1} is in full agreement with the requirements of Dickson et al. (2007) for the standard A_T titration methods for which an accuracy of ± 2 µmol kg^{-1} is required.

The precision in the laboratory is determined by using the standard deviation of the five single measurements at each titration step. General precision for each titration step was found to be approximately ± 2 µmol kg^{-1} for this analyzer (data not shown). This general precision also agrees with precision values determined by Kongsberg Maritime Contros GmbH for any HydroFIA analyzer. The explained laboratory performance characteristic is a standard procedure at Kongsberg Maritime Contros GmbH for each CONTROS HydroFIA® TA system and is carried out regularly. A performance characteristic test carried out with the gray system after the MSM 68/2 cruise and maintenance of the manufacturer (no leakage) shows an overall precision of ± 1.5 µmol kg^{-1}. Because both analyzers are treated similarly in the laboratory, and the modified method with autosampler is stable, robust and part of the quality management system of the company, it is possible to generalize this precision for all laboratory performance characteristics.

For estimating the combined standard uncertainty of this experiment in the laboratory (only shown for after-cruise experiment), the laboratory precision was utilized as random uncertainty component, and the root mean square error (RMSE) of the measured A_T values as systematic uncertainty component, respectively. Both components were estimated with a freshly "calibrated" analyzer using CRM. The relative combined laboratory standard uncertainty was estimated at 0.08 %, which results in a combined laboratory standard uncertainty of 1.6 – 2.0 µmol kg^{-1} at A_T values from 2000 – 2450 µmol kg^{-1} (see Appendix 4.9 for more details of the calculations). This laboratory uncertainty approximation is in full agreement with the "weather" goal requirements of Newton et al. (2015). Even the very high requirement of the "climate" goal is achieved. Thus, the laboratory standard uncertainty of the analyzer is sufficient for ocean acidification measurements.

4.4.1.2 Overlapping Allan experiment

Figure 4.4 shows the results of the overlapping Allan analysis with each curve representing one specific measurement day. As expected, each Allan plot shows a minimum representing the optimal number of averaging replicate measurements. The minima range from AF = 3–6 with resulting overlapping Allan deviations $\sigma_y(\tau)$ of (0.5 - 1.0) µmol kg^{-1}, each determined at $A_T \approx 2270$ µmol kg^{-1} ($pH_{sample-titrantmixture} \approx 3.6$).

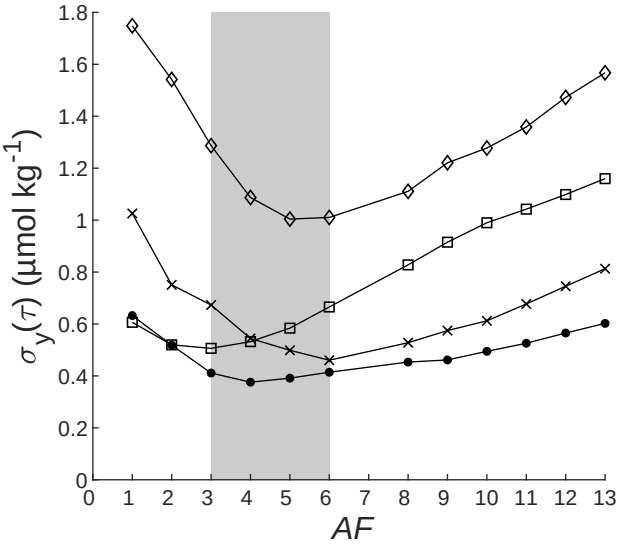

Figure 4.4: Overlapping Allan deviations $\sigma_y(\tau)$ as a function of the number of averaged replicates of the reference measurement, AF. Each curve represents one measurement day. The gray area indicates the range of the observed minima in the experiments.

This means, a reference sample used for performance monitoring should be repeatedly measured at least three times to minimize the impact of statistical noise. On the other hand, more than six repetitions lead into a regime affected by instrument drift or changes of environment / sample solution and causes the precision to deteriorate. The ideal number of repeated reference measurements depends on different factors: The available volume of stable reference seawater during the deployment, the length of the deployment, and the required number of quality assurance measurements per day. Also possible outliers within these reference measurements should be taken into account. For the performance monitoring during the two research cruises, we decided to repeatedly measure the reference samples (here: CRM) five times every morning and evening.

4.4.2 Field experiments

4.4.2.1 General information

During the MSM 68/2 cruise, the red analyzer ran without any hardware problems. Consequently, its performance characterization is discussed in detail in the following parts. However, because of the early development level of the system, both the M 133 analyzer as well as the gray analyzer during the MSM 68/2 cruise suffered from a leakage in the degasser unit. The effects of such a malfunction on the performance are briefly discussed afterwards.

4.4.2.2 Underway measurements

To give an overview of the measured underway variables (A_T, sea surface salinity [SSS] and sea surface temperature [SST]) in the monitored regions, Fig. 4.5a and 4.5b show their time-series over the course of each cruise (Note: shown A_T values are corrected). The red filled circles in the A_T time-series (Fig. 4.5a) represent the discrete samples taken during each cruise. Figure 4.5c illustrates the track of the M 133 and MSM 68/2 cruise, respectively. The scientific interpretation of these underway data is not part of this report as the focus here lies on the assessment of instrument performance under typical field deployment conditions. However, to get an rough idea of the consistency between the underway A_T values measured by the analyzer and the A_T range and variability in the measured region, we compared the corrected A_T data sets to calculated A_T values based on the parameterization described by Lee et al. (2006). This calculation utilize SSS and SST data. The consistency is estimated by calculating the RMSE of the $A_{T,Analyzer}$ and $A_{T,Calculated}$ following Equ. 4.22. A plot of the comparison is shown in the attached supporting information (Fig. S4.1). An RMSE of $\pm$ 12.7 µmol kg^{-1} and $\pm$ 4.9 µmol kg^{-1} was calculated for the M 133 cruise (South Atlantic Ocean) and the MSM 68/2 cruise (North Atlantic Ocean), respectively. The error of the parameterization is $\pm$ 8.4 µmol kg^{-1} and $\pm$ 6.4 µmol kg^{-1} for the North and South Atlantic Ocean, respectively. By taking these errors into account, both field data sets seem to be consistent with the A_T range and variability in the measured region, which is also proved by the comparison to discrete samples (see Sect. 4.4.2.4).

4.4.2.3 Working range

Figure 4.6 illustrates the possible A_T working range as a function of the pH of the sample-titrant mixture observed with analyzers using spectrophotometric pH measurements with BCG. In this figure, the A_T working ranges of the red and the gray system are based on the resulting pH working range observed with the MSM 68/2 underway measurements (pH_{min} to pH_{max}, see Fig. 4.7). On the one hand, the configuration of the red system yields in a wider measurement range, where small pH steps correspond to larger A_T steps, which makes it more attractive for regions with high A_T variability. On the other hand, the gray system is more

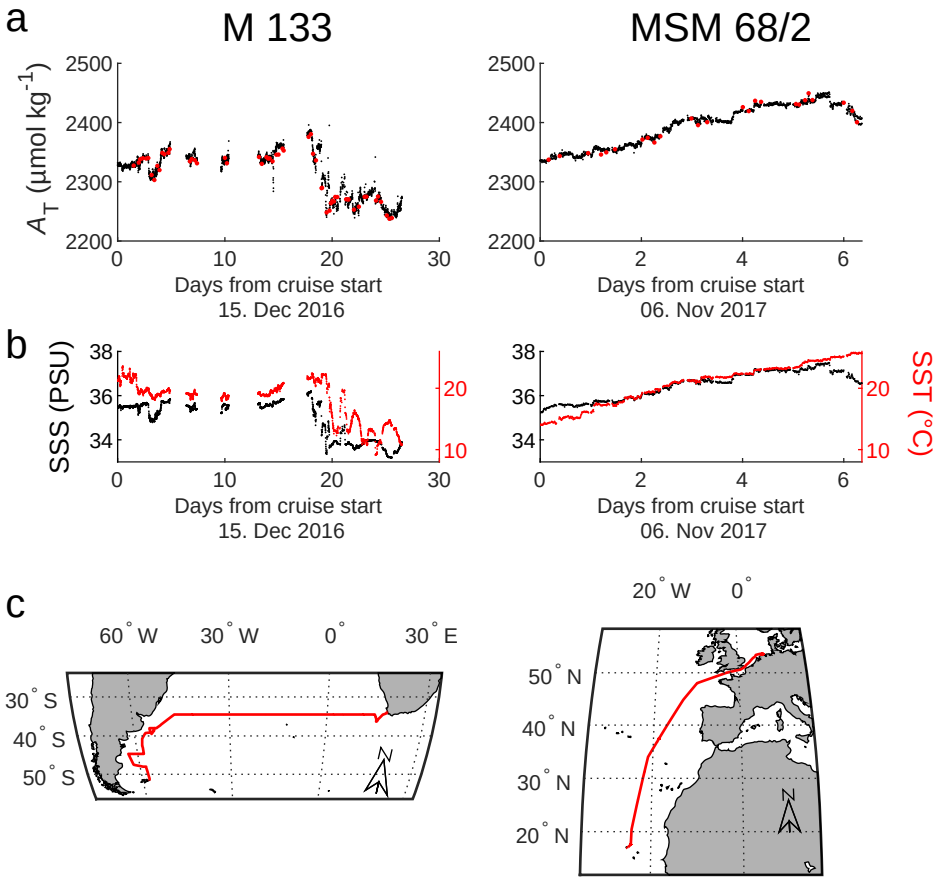

Figure 4.5: a) Time-series of the measured A_T values during the M 133 and MSM 68/2 cruise, respectively. Each filled red circle represents the A_T value of a discrete sample taken at a certain time during the cruise. **b)** Time-series of the measured sea surface salinity (SSS) with the left y-axis and sea surface temperature (SST) with the right y-axis during the M 133 and MSM 68/2 cruise, respectively, where the black filled circles represent SSS and the red filled circles represent SST. **c)** Track of M 133 cruise (Start: Cape Town, South Africa; End: Stanley, Falkland Islands) and MSM 68/2 cruise (Start: Emden, Germany; End: Mindelo, Cape Verde).

precise due to larger pH steps corresponding to smaller A_T steps. To take advantage of this better precision, the choice of a higher pH range (4.0 - 4.5) is more useful for regions, where small A_T changes are expected.

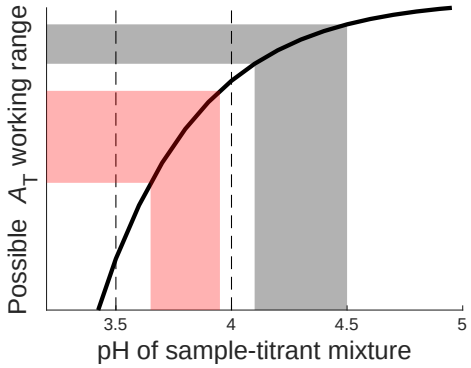

Figure 4.6: Possible A_T working range as a function of the sample-titrant mixture pH. The red and the gray area indicates the measured A_T range of the red and the gray system, respectively, during the cruise MSM 68/2. The vertical dashed lines indicate the optimal pH range of 3.5–4.0 given by Breland and Byrne (1993) and Li et al. (2013).

Another potential problem with pH ranges above 4.0 is the unknown validity of the A_T calculation following Equ. 4.7 (see Sect. 4.2.1). Li et al. (2013) only validate this calculation within pH values of 3.5–4.0. In this range, the concentrations of the terms $[H_3PO_4], [B(OH)_4^-], [OH^-], [HPO_4^{2-}], [PO_4^{3-}], [SiO(OH)_3^-], [NH_3]$ and $[HS^-]$ can be neglected. Following the calculation procedure of Li et al. (2013), recalculation of these concentrations at higher pH values results in an overall increase of the corresponding alkalinity contributions from approximately 0.4 µmol kg^{-1} at pH 4.0 up to approximately 0.9 µmol kg^{-1} at pH 4.5, and, consequently, in an increase in the systematic error of the method. However, it has to be noted that the total concentrations of these species, on which the calculation of Li et al. (2013) is based, are much higher than those of typical open ocean seawater (worst case scenario). Based on this fact, it can be assumed that the concentrations of the above listed terms can still be neglected within the given instrument uncertainties, thus Equ. 4.7 is also valid up to a pH of 4.5. Additionally, laboratory performance tests similar to that in Sect. 4.4.1 with another CONTROS HydroFIA® TA system (similar configurations to the gray system, but no leakage) support this finding. There, a linear slope of (1.01 ± 0.01), and (1.000 ± 0.003) measured with a maximum pH of 4.6, and 4.3, respectively, was observable (data not shown), which indicates unbiased performance of the system. Just an increase of the RMSE with increasing pH is detectable (ΔRMSE = 1.8 µmol kg^{-1}). The found decrease in accuracy at those high pH values can be explained by the limit of the spectrophotometer's ability determining the very low concentrations of the remaining indicator acid. Because of that, it is not recommended to measure A_T at pH values greater than 4.6.

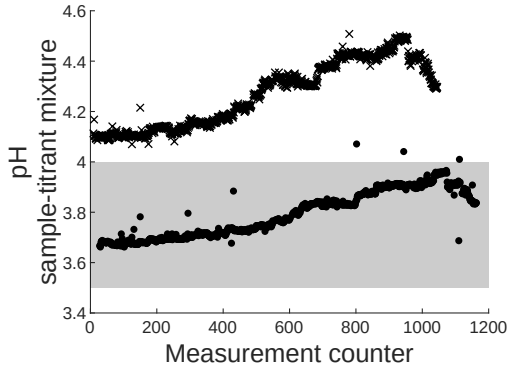

Figure 4.7: pH of the sample-titrant mixture (after degassing) of the MSM 68/2 underway measurements as a function of the measurement counter, where filled circles and crosses represent the red and the gray system, respectively. The gray area indicates the optimal pH range of 3.5–4.0 given by Breland and Byrne (1993) and Li et al. (2013).

4.4.2.4 Performance characteristics

In this part, only the performance characteristic of the red analyzer during the MSM 68/2 cruise is shown and discussed. Because it had no malfunctions during its deployment, these results are representative for the behavior of the system as such.

For evaluating precision, the standard deviation σ ($n = 5$) of each repeated measurement was determined. Figure 4.8 shows these standard deviations as a function of the measurement counter. The averaged field precision is determined at $\pm$ 1.2 µmol kg^{-1}. For an autonomous system, such a level of precision is in good agreement with the requirements of Dickson et al. (2007) as stated for standard A_T titration methods for which a standard deviation of better than $\pm$ 1 µmol kg^{-1}is required.

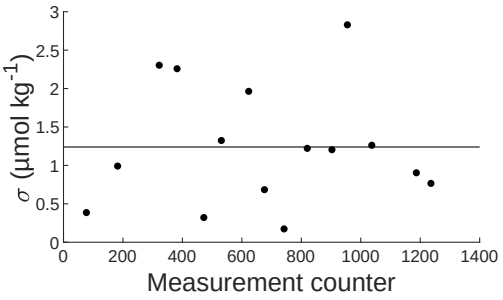

Figure 4.8: Standard deviation σ of repeated CRM measurements as a function of the measurement counter of the red analyzer during the cruise MSM 68/2. The horizontal black line indicates the averaged standard deviation.

For evaluating accuracy, the bias ($\Delta A_T = A_{T,Analyzer}$ - $A_{T,Reference}$) between the analyzer A_T measurements and the A_T values of the reference samples is calculated. Figure 4.9 shows the biases of the red system as function of the measurement counter both with raw data (Fig. 4.9a) and with linearly drift corrected data (Fig. 4.9b). This correction is necessary, because the analyzer shows a linearly increasing ΔA_T from -2 µmol kg^{-1}at the beginning up to +15 µmol kg^{-1} at the end of the cruise. The conducted CRM measurements are used for this drift correction resulting in a mean bias of (-0.3 ± 2.8) µmol kg^{-1} ($n = 28$) between the red system and the reference data from discrete samples measured by standard open-cell titrator (including the sampling error). Such a level of accuracy is comparable to standard A_T titration methods. Furthermore, by plotting the A_T values of the analyzer (already corrected against the drift using the CRM measurements) against the reference A_T values, the linear function $y = (0.98 \pm 0.01) \times x + (40 \pm 23)$ ($R^2 = 0.997$) results. Taking all uncertainties in account, this result proofs the good sensitivity of the analyzer over the whole working range.

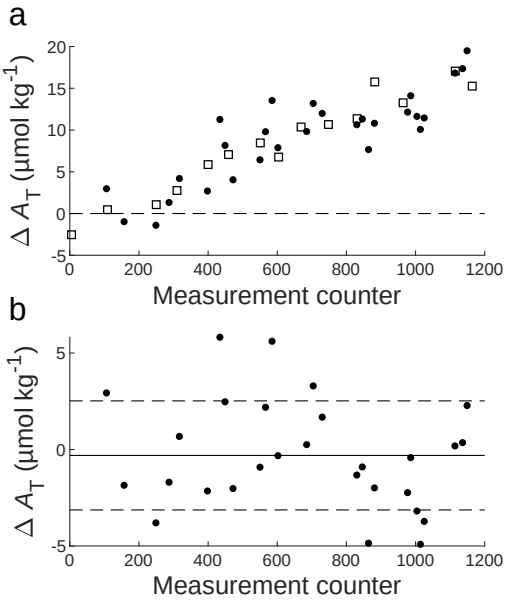

Figure 4.9: a) Bias plot for the intercomparison of A_T measurements between the red analyzer and the reference samples during the cruise MSM 68/2, where open squares represent the CRM, and filled circles represent the discrete samples measured with the standard open-cell titrator in the laboratory. The horizontal dashed line indicates $\Delta A_T = 0$ µmol kg^{-1}. **b)** Bias plot (discrete samples) after a linear drift correction using the CRM measurements. The horizontal black line indicates the mean bias, $\overline{\Delta A_T}$, while the dashed lines indicate $\overline{\Delta A_T} \pm \sigma$ (For this data set: (-0.3 ± 2.8) µmol kg^{-1}).

We discovered, that the observed linear drift with increasing measurement number occurs because of material deposits in the optical pathway. As a result, the light intensity decreases and therefore the absorbance A at 444 nm and

616 nm changes. Usually, such an intensity loss is corrected by the dark and blank spectrum within the measurement routine, but the optical measurements showed systematic deviations over time at the different wavelengths. Figure 4.10 shows the absorbance changes at 444 nm and 616 nm of the red system's CRM measurements in dependence of the measurement counter during the MSM 68/2 cruise, and also the resulting change in the absorbance ratio R. Theoretically, the absorbance ratio of a CRM measurement should not change, provided the same batch is measured. In reality, Fig. 4.10c proves, that this is not the case. R increases over time due to the different behavior of the absorbances at 444 nm and 616 nm, and an increasing R leads to increasing A_{T} values. We hypothesize, that the deposits are caused by colored substances, possibly by a decomposition of the BCG indicator or impurities, which cannot be completely prevented at the moment. Consequently, the observed linear drift towards higher A_{T} values has to be accepted as typical behavior. Fortunately, the drift can be easily corrected for by regular reference measurements. Even by applying one reference measurement in the beginning and one in the end of a deployment in our case would have been sufficient because of the linear character of the drift.

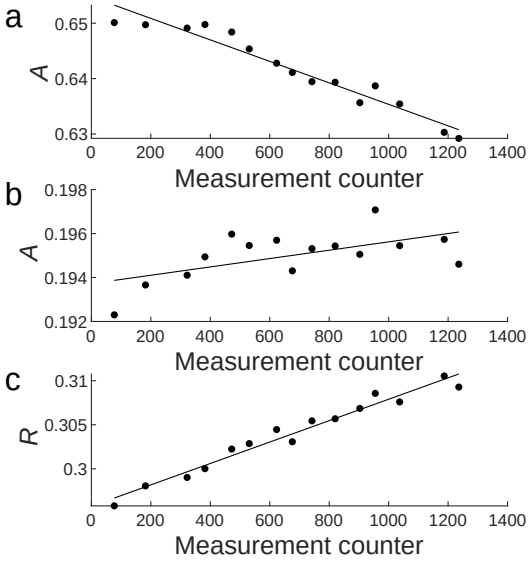

Figure 4.10: Absorbance A at the wavelengths of the indicator absorption maxima **a)** 444 nm, and **b)** 616 nm of the CRM measurements with the red system as a function of the measurement counter during the MSM 68/2 cruise. **c)** Absorbance ratio R ($R = A_{616\mathrm{nm}}/A_{444\mathrm{nm}}$) of these CRM measurements as a function of the measurement counter.

Recent results from other deployments show a similar drift magnitude but over a much longer time period with lower measurement interval of 90 min. Consequently, a small residual deposit is left on the optical window after each measurement

leading to accumulation over time as a function of number of measurements. This indicates that this pattern is related to the number of conducted measurements (number of indicator injections) rather than the pure deployment time.

For approximating the combined standard uncertainty in field, the daily CRM measurements were used. The precision of each repeated CRM measurement was utilized as random uncertainty component, and the root mean square (RMS) of the biases to the certified value of the measured CRM ($\Delta A_T = A_{T,CRM} - A_{T,Analyzer}$) as systematic uncertainty component, respectively. Additionally, the uncertainty contribution of the drift correction to the systematic uncertainty was estimated and implemented by using the RMSE of the linear regression. The relative combined field standard uncertainty of the analyzer was estimated with 0.10 % at 2212.44 µmol kg^{-1} (certified value of CRM Batch No. 160). Due to the proven linearity of the analyzer over the working range of 2000 – 2450 µmol kg^{-1}, the combined field standard uncertainty is estimated with 2.0 - 2.5 µmol kg^{-1} (see Supporting Information for more information). This field uncertainty approximation is in full agreement with the "weather" goal requirements of Newton et al. (2015). The very high requirement of the "climate" goal is almost be achieved in the field by being only 0.5 µmol kg^{-1} higher than the target of 2 µmol kg^{-1}. Thus, the field standard uncertainty of the analyzer is sufficient for ocean acidification measurements.

4.4.2.5 Long-term precision

The result of the long-term precision experiment during the M 133 cruise is shown in Fig. 4.11. The standard deviation of the long-term measurements is determined with ± 2.4 µmol kg^{-1} ($n = 178$), which is higher than the averaged short-term precision of ± 1.2 µmol kg^{-1} observed with the red analyzer during the MSM 68/2 campaign. This reduced precision is due to the instrument long-term drift, and changes of the environmental or sample conditions, that was already reported in the overlapping Allan experiment results. Unfortunately, it has to be mentioned, that this experiment was carried out after the leakage in the degasser unit appeared. A functional analyzer would probably show better results. However, while long-term standard deviation of ± 2.4 µmol kg^{-1} does not reach the requirements for standard open-cell titrators it still is in an acceptable range.

Another outcome of this experiment is the appearance of outliers. Overall 11 outliers are recognizable in the data set, which is 6.2 % of the measurements. This outlier rate seems to be relatively high, but, especially during long-term deployments, the measurement resolution of the CONTROS HydroFIA® TA system (measurement time per sample: < 10 min) is high enough to compensate these outliers. Additionally, removing these outliers using an algorithm (e.g. Grubbs outlier test by Grubbs (1969)) is very well possible during the post-processing, since appear as spike outliers in the regular dataset. The reasons for the occurrence of these outliers are still unclear. We hypothesize, that the sample pump supplies a minimally higher volume of seawater to the sample loop than usual. Also bubbles

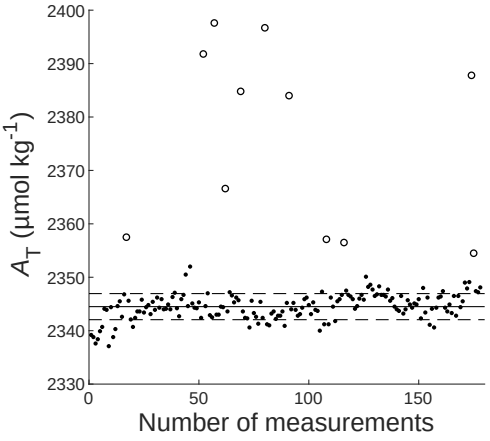

Figure 4.11: A_T long-term measurements of a stable seawater substandard as a function of the measurement counter of the red system during the cruise M 133, where filled circles indicate the regular measurements, and open circles the outliers in this data set (Grubbs outlier test, $\alpha = 0.05$, two-sided, $n = 178$). The horizontal black line represents the resulting mean A_T value, $\overline{A_T}$, without outliers. The dashed black lines indicate $\overline{A_T} \pm \sigma$.

in the sample loop could be possible.

4.4.2.6 Initial drift after idle time

Figure 4.12 shows the results of the initial drift experiment during the M 133 cruise. After the very first start of the system following an idle time of approximately three months, the required standard deviation of ≤ 2 µmol kg^{-1} is reached after 25 measurements. But the longer the analyzer has been operated continuously, the faster stable measurements are reached. After 2183 measurements followed by an idling time of 48 h, the analyzer only needs two measurements to reach stable A_T values. Therefore, relatively short idle times (around 48 h) with a DI water flush during a long-term deployment have a negligible effect on the measurements afterwards; provided, the analyzer runs constantly between these short idle times.

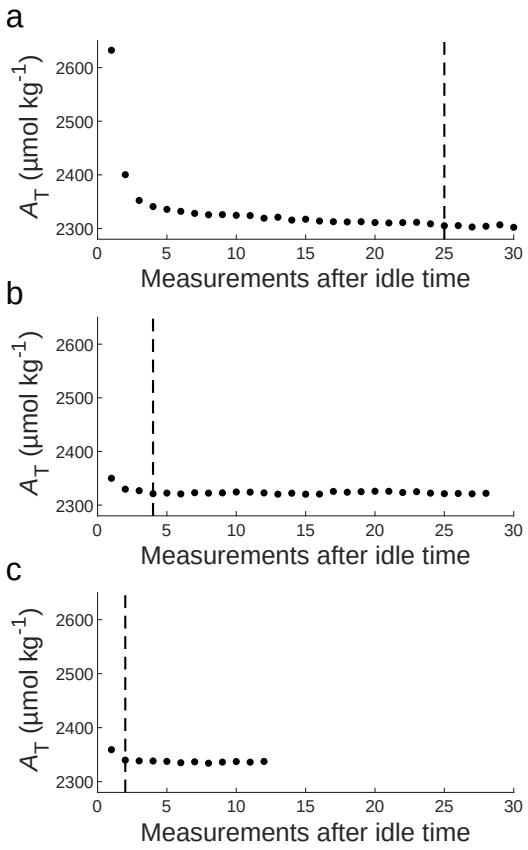

Figure 4.12: Measured A_T of a stable substandard as a function of the number of measurements after a DI water flush followed by an idle time of **a)** three months, and **b), c)** 48 h, respectively. The vertical black dashed lines indicate the number of measurements, after which the stability criterion of standard deviation of ≤ 2 µmol kg^{-1} is reached. The experiment was carried out **a)** at the beginning of the M 133 cruise, **b)** after 1304 consecutive measurements, and **c)** after 2183 consecutive measurements, respectively.

4.4.2.7 Observed failure modes

At the time of this study, a leakage in the degasser unit was the only malfunction of the CONTROS HydroFIA® TAsystem during its early development phase. The following discussion includes all precision and accuracy results both of the M 133 cruise, and of the gray system during the MSM 68/2 cruise. Figure 4.13 shows the precision evaluation of both the red analyzer during the cruise M 133, and the gray analyzer during the cruise MSM 68/2. Table 4.2 summarizes the results of the precision evaluation.

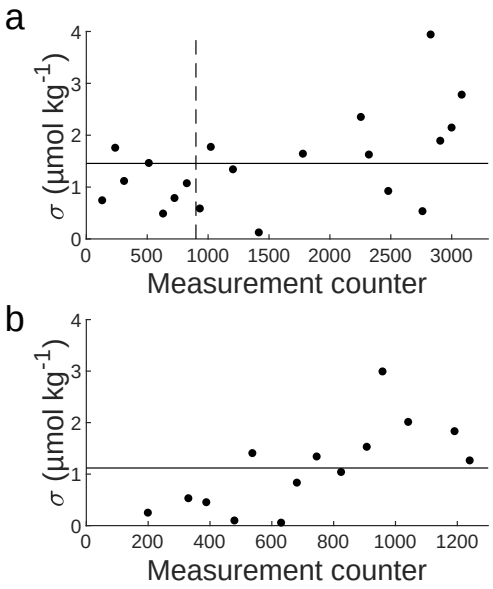

Figure 4.13: Standard deviation σ of repeated CRM measurements as a function of the measurement counter of **a)** the red analyzer during the cruise M 133, and **b)** the gray analyzer during the cruise MSM 68/2. In both plots, the horizontal black line indicates the averaged standard deviation: **a)** ± 1.5 µmol kg^{-1}, **b)** ± 1.1 µmol kg^{-1}. In plot **a)**, the vertical dashed line indicates the appearance of the leakage.

Table 4.2: Results of the precision evaluation

	Min σ - Max σ (µmol kg^{-1})	Mean σ (µmol kg^{-1})
M 133 cruise		
Red system	± (0.5 - 1.8)	± 1.0
Red system[a,b]	± (0.1 - 3.9)	± 1.8
MSM 68/2 cruise		
Red system	± (0.2 - 2.8)	± 1.2
Gray system[a]	± (0.1 - 3.0)	± 1.1

[a] Leakage occurred during the course of the cruise
[b] With leakage

It is obvious, that the averaged precision does not differ significantly much to the functional analyzer. However, a systematically increasing spread around the averaged σ over time is observable. This phenomenon is caused by an evolving dead volume within the degasser unit, which has an increasing effect on the random error of the measurement.

The effects of a leaking degasser on the accuracy of the system is shown in Fig. 4.14a and 4.14b. Different to the typical behavior, as shown in Fig. 4.9, there is a downward drift observable. Furthermore, as seen in Fig. 4.14b, a discrepancy between $\Delta A_{\mathrm{T,CRM}}$ and $\Delta A_{\mathrm{T,discreteSamples}}$ could occur. By plotting the A_{T} values of the analyzer (already corrected against the drift using the CRM measurements) against the reference A_{T} values, the linear function $y = (0.913 \pm 0.005) \times x + (193.4 \pm 13.4)$ ($R^2 = 0.999$) results. Because the slope is significantly smaller than 1.000, there must be a sensitivity loss induced by the leaking degasser. Both phenomena, the downward drift and the sensitivity problem, are caused by the loss of degasser functionality. Additionally, an analyzer, that runs with a leaking degasser for a longer time (approximately $>$ 2000 measurements), could show unpredictable effects like the increasing drift in Fig. 4.14a after 2500 measurements. The reasons for these effects are still unclear. However, the measured A_{T} values are still correctable in a way similar to the correction explained in Sect. 4.4.2.4. Deviating from this correction, both the CRM and the discrete sample measurements must be utilized. Figure 4.14c and 4.14d show the resulting biases of the analyzer A_{T} values after such a correction to the A_{T} values measured with a standard open-cell titrator. The mean bias of the corrected M 133 data is (0.2 ± 7.8) µmol kg^{-1}, and (0.2 ± 1.6) µmol kg^{-1} for the corrected MSM 68/2 data observed with the gray system. Obviously, the correction of the data observed with a system, which runs with a malfunction for a longer time (red analyzer during M 133 cruise), results in less accurate values. For the MSM 68/2 campaign, both analyzers show comparable results after correction. Although, it has be taken into account that the correction of the leaking gray analyzer had to rely on discrete samples measured with a reference technique in addition to the regular CRM measurements performed by the analyzer itself.

Summing up, we can say, that the effects of a leakage can occur in different unpredictable ways that do not necessarily appear at the same time. Thus, if the system shows a different performance behavior within the quality assurance routine other than the typical bias drift to higher A_{T} values, a leaking degasser unit might be the reason. However, after the experiments and campaigns carried out in this study, the degassing unit of the analyzer was revised and improved by the manufacturer solving the leakage problem (further information: see Sect. 4.6).

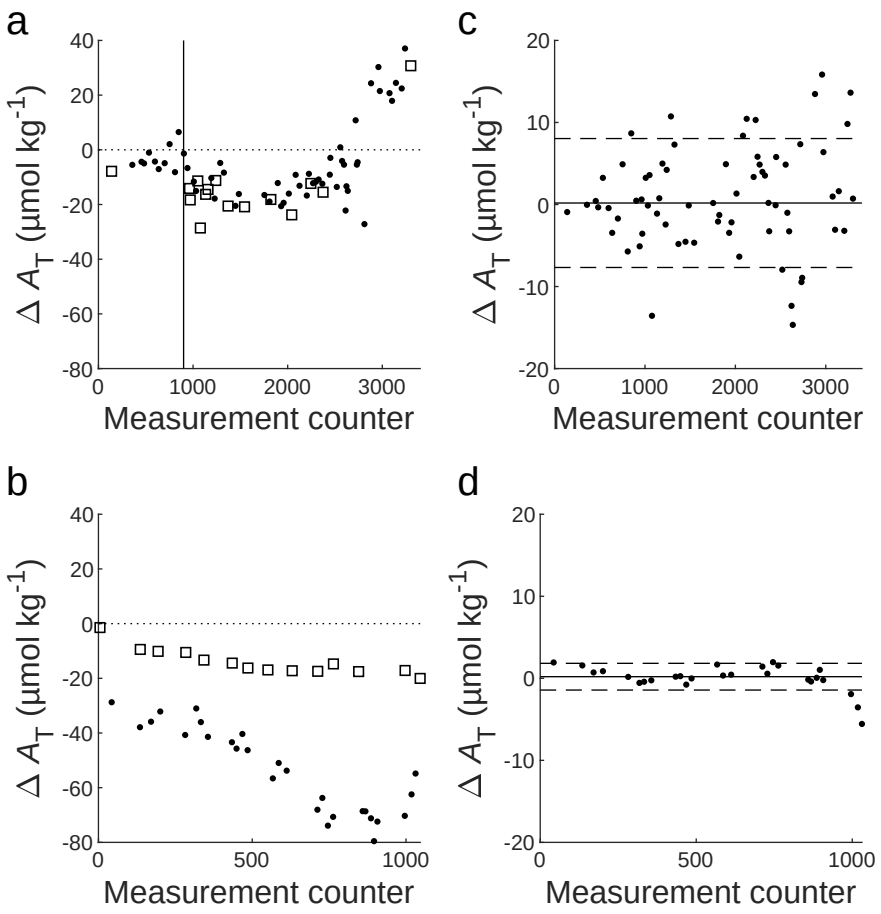

Figure 4.14: Results obtained with leaking analyzers: Bias plot for the intercomparison of A_T measurements between the analyzer and the reference samples **a)** during the cruise M 133, and **b)** during the cruise MSM 68/2 (gray system), where open squares represent the CRM, and filled circles represent the discrete samples measured with the standard open-cell titrator. The horizontal dotted line indicates $\Delta A_T = 0$ µmol kg^{-1}, and the vertical solid line in **a)** indicates the approximate appearance of the leakage. Bias plots (only discrete samples shown) after correction using both the CRM and discrete sample measurements for **c)** during the cruise M 133, and **d)** during the cruise MSM 68/2 (gray system). The horizontal black line indicates the mean bias, $\overline{\Delta A_T}$, while the dashed lines indicate $\overline{\Delta A_T} \pm \sigma$. Here: **c)** (0.2 ± 7.8) µmol kg^{-1}, and **d)** (0.2 ± 1.6) µmol kg^{-1}.

4.5 Conclusions

The performance tests of the first commercially available autonomous analyzer for total alkalinity, CONTROS HydroFIA® TA reveal several important features relevant for the future field application of this system. Table 4.3 summarizes the laboratory and field performance results obtained with the analyzer. While the system reaches the accuracy requirement for standard open-cell titrators provided by Dickson et al. (2007) both in the laboratory and in field, the precision requirement cannot be completely met. However, for an autonomous analyzer with spectrophotometric pH determination, such a level of precision is still in favorable comparison to the standard A_T titration methods. Furthermore, uncertainty approximations both in the laboratory and in field are in full agreement with the "weather" goal requirements by Newton et al. (2015) for ocean acidification observations. The very high requirement of the "climate" goal is achieved in the laboratory and almost be achieved in the field by being only 0.5 µmol kg^{-1} higher than the target of 2 µmol kg^{-1}.

Table 4.3: Results of the laboratory and field performance tests

	Precision σ (µmol kg^{-1})	Accuracy ΔA_T (µmol kg^{-1})	Uncertainty $u(c)$[f] (µmol kg^{-1})
Laboratory	± 1.5	± 1.0 [a]	1.6 - 2.0 [e]
Field	± 1.1	-0.3 ± 2.8 [b]	2.0 - 2.5 [b,e]
With leakage	± 1.3	0.2 ± 7.9 [b] 0.2 ± 1.6	
Required	± 1 [c]	± 2 [c]	10 / 2 [d]

[a] RMSE of the linear regression
[b] After drift correction against reference measurements
[c] For standard open cell titrator (Dickson et al. 2007)
[d] "Weather" / "Climate" goal (Newton et al. 2015)
[e] Working range of 2000 - 2450 µmol kg^{-1}
[f] With 68.3 % confidence interval

Another important outcome is, that the analyzer appears to show a linear drift (offset drift) caused by so far unavoidable colored deposits in the optical pathway. Currently, this drift has to be accepted as typical behavior and therefore must be corrected for by measurements of Seawater Certified Reference Material (CRM) with known A_T values or by regular reference samples to reach the required accuracy. Consequently, a regular quality assurance routine has to be implemented for long-term deployments. This routine should contain regular CRM measurements each consisting of 3 to 6 repetitive measurements, but if deemed sufficient, it could be lowered to one pre- and one post-deployment CRM measurement due the linear character of the drift. A stability estimation in the laboratory utilizing the overlapping Allan deviation plot showed that fewer than 3 or more than 6 replicates

are not recommendable due to the effects of statistical noise and long-term drift effects on the analyzer, respectively. Another major advantage of regular quality assurance measurements is the detection (with backward tracking and correction possibility) of malfunctions without the need to perform manual functionality checkups of single components. Fortunately, a leakage always shows a more or less abrupt change within the precision and/or accuracy evaluation of the analyzer. In addition, one of the following observations can point at a malfunction within the system: i) Higher spread of the standard deviation around the averaged value, ii) abrupt change in the accuracy or offset drift, iii) direction change of the offset drift, and/or iv) discrepancy between CRM and discrete samples biases (loss of sensitivity). Furthermore, it has to be taken into account that not all leakage effects appear necessarily at the same time. Figure 4.15 summarizes the behavior of the instrument being within the quality assurance routine during long-term deployments.

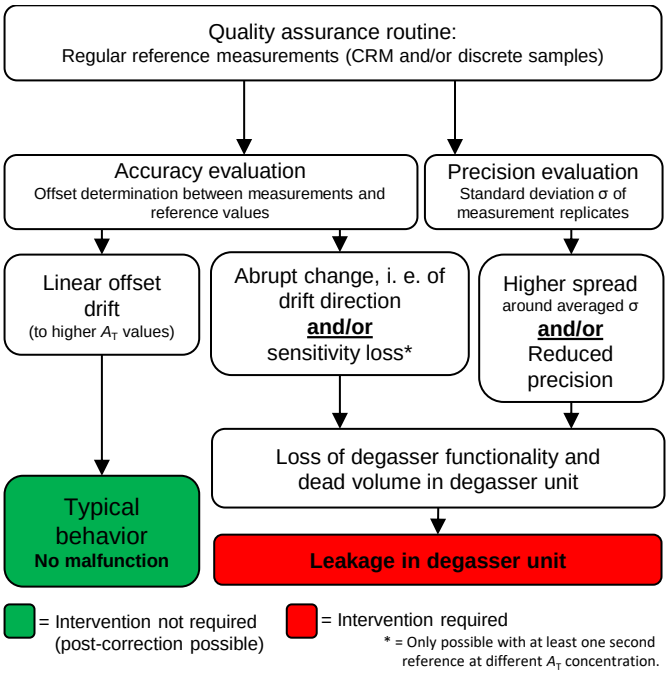

Figure 4.15: Overview of the behavior of the CONTROS HydroFIA® TA system within the quality assurance routine during a long-term deployment.

Experiments dealing with different pH ranges of the system show that its good performance is still maintained at pH values > 4.0, additionally with higher precision. However, the accuracy worsens at pH values between 4.3 and 4.5 ($\Delta = 1.8$ µmol kg^{-1}). The use of such high pH ranges might be useful for regions, where small A_T changes must be detected. Due to the detection limit of the spectrophotometer, it is not recommended to measure at pH values > 4.5.

4.6 Outlook

Recently, the degasser unit of the analyzer, a frequent cause for malfunctions in early versions of the instrument, was revised and improved by the manufacturer. Its newly developed membrane is more robust, and test measurements in the laboratory confirm the high resistance against leakages. A long-term deployment of the system with this new degasser unit in field is ongoing. Furthermore, this new membrane is more robust against organic solvents, allowing to flush the system with isopropanol to remove the colored deposits in the optical pathway. Future work dealing with possible improvements within the measurement routine will possibly overcome the drifting behavior of the analyzer. So, one option could be a regular cleaning procedure with isopropanol (only possible with the improved degasser membrane) to reduce the influence of the material deposits in the optical pathway and eliminating the observed bias. Another option may be the use of purified BCG indicator to possibly minimize its decomposition in solution. Using purified BCG could also improve the spectrophotometric measurement, similar to meta-cresol purple for spectrophotometric seawater pH measurements (Yao et al. 2007; Liu et al. 2011). For this, a preparative HPLC purification method is under development. Another crucial task during automated long-term deployments is the provision of enough reference seawater for regular quality assurance measurements. A standard CRM bottle of 500 mL, as provided by A. G. Dickson, is not sufficient for an automated long-term deployment. Due to the autonomous character of such deployments, changing the standard bottles by hand is also no option. Hence, an alternative stable larger volume storage (minimum 5 L) for standard seawater must be found. For this purpose, we are currently testing several types of containers, such as gas sampling bags, infusion bags, different canisters or bottles.

4.7 Recommendations for automated long-term deployments

Due to the fact, that the CONTROS HydroFIA® TA system is a commercially available analyzer, it is already being used by the oceanographic community. But not all of these users have the time or resources to fully characterize and test the system for their purposes. Based on our experiences and the present study, we provide recommendations for automated long-term deployments of this analyzer:

- After very long idle times (>> 48 h), e. g. after storage and/or transportation of the system), flush the system with 0.1 M HCl solution to shorten stabilization phase (initial drift) before starting measurements.
- At the beginning of a deployment, carry out stabilization measurements. Stabilization measurements should be carried out with stable seawater substandard. The absolute A_T value is not important as long as it is in the working range of the analyzer. The measurements are considered stable when

a standard deviation of $\leq$ 2 µmol kg^{-1} of the last three measurements is reached.

- After stabilization, "calibrate" (sample volume determination) the system always with a freshly opened CRM standard.
- Pumped underway seawater must be filtered, e. g. using a cross-flow filter before running it through the analyzer. Particles or particulate matter must be avoided in the measured sample water.
- Carry out regular quality assurance measurements (e. g. with CRM or any other suitable seawater standard). For this, 3–6 replicates are recommended. These quality assurance routine is important for the drift correction of the data during the post-processing. The frequency depends on the lengths of the deployment. For shorter deployments ($<$ 20 days), daily measurements are recommended (based on our experiences during field campaigns). The more reference data are collected, the better the drift correction of the system is. For longer campaigns, they can be reduced to every two or three days.
- Evaluate the quality assurance measurements on regular basis. These can be used to identify malfunctions (e. g. leakage in the degasser unit) without the need to manually inspecting the system. For identifying such malfunctions, use Fig. 4.15 as a guidance.
- In case quality assurance measurements indicate a problem of the analyzer functionality, increase the frequency of standard measurements to verify this.
- If there is a leakage in the degasser unit, stop the deployment as soon as possible for instrument maintenance by the manufacturer. The longer a leaking system runs, the more difficult the data post-correction becomes. The measured A_T values lose plausibility because of increasingly unpredictable effects caused by the leakage.
- Higher pH ranges (4.0–4.5) of the acidified sample may be used for regions with small A_T variability to detect small changes more precisely. The pH range can be adjusted by changing the length of the acid loop tubing (only by manufacturer) or by adjusting the acid concentration (consultation of manufacturer should be taken; post processing needed due to changed parameters).

4.8 Acknowledgments

The research leading to these results has received funding from the European Union's Horizon 2020 research and innovation programme under grant agreement No 633211(AtlantOS project). A thank you goes to the Captain and crew of RV *Meteor* and RV *Maria S. Merian*, respectively, for their support during the field campaigns. Another huge thank you goes to Nadja Kinski from Kongsberg Maritime Contros GmbH for the always fast and supportive help regarding all technical issues with the analyzer.

4.9 Appendix: Supporting Information

4.9.1 Comparison of measured underway A_T data with calculated A_T data

(Compare Sect. 4.4.2)

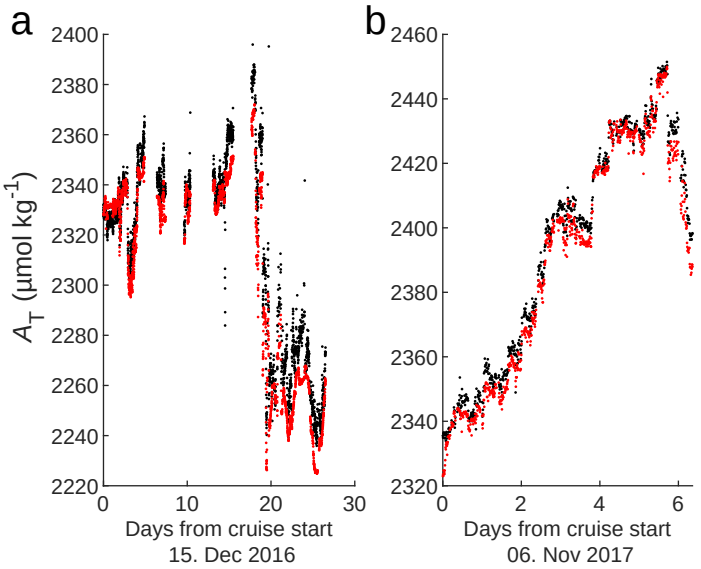

Figure S4.1: Time-series of the A_T values of **a)** the M 133 cruise and **b)** the MSM 68/2 cruise, where the black filled circles represent the A_T values of the analyzer and the red filled circles represent the calculated A_T values based on the parameterization described by Lee et al. (2006).

4.9.2 Standard uncertainty *u*(c) approximation in the laboratory

(Compare Sect. 4.4.1)

Systematic component of the uncertainty *u*(bias)

$u(\text{bias}) = \text{RMSE}_{\text{linearRegression}}$

Absolute: $u(\text{bias}) = 1.0\ \mu\text{mol}\,\text{kg}^{-1}$

Relative: $u(\text{bias}) = 0.04399898\ \%$

Random component of the uncertainty *u*(RW)

$u(\text{RW}) = \sigma_{\text{Laboratory}}$

Absolute: $u(\text{RW}) = 1.5\ \mu\text{mol}\,\text{kg}^{-1}$

Relative: $u(\text{RW}) = 0.06599847\ \%$

Relative combined laboratory uncertainty *u*(c)

$u(\text{c}) = \sqrt{u(\text{RW})^2 + u(\text{bias})^2}$

$$\underline{\underline{u(\text{c}) = 0.07932\ \%}}$$

4.9.3 Standard uncertainty *u*(c) approximation in the field (using CRM)

(Compare Sect. 4.4.2)

Information to CRM Batch No. 160 and calculation of uncertainty of the reference sample *u*(Cref)

$A_{\mathrm{T,CRM}} = 2212.44 \pm 0.67\ \mu\mathrm{mol\,kg^{-1}}$
(certified value of CRM Batch No. 160, provided by A. G. Dickson)

$u(\mathrm{Cref}) = (0.67\ /\ 2212.44) \times 100\ \%$

$$\boldsymbol{u(\mathrm{Cref}) = 0.03028331\ \%}$$

Uncertainty *u*(Corr) of drift correction

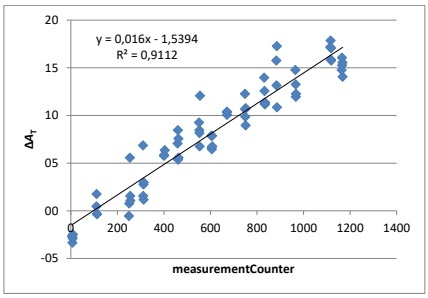

Figure S4.2: Bias (ΔA_{T}) between measured A_{T} and $A_{\mathrm{T,CRM}}$ as a function of the measurement counter for drift correction purposes. The black solid line represents the linear regression of the data points.

$$\mathrm{RMSE} = \sqrt{\frac{\sum (A_{\mathrm{T,fitted}} - A_{\mathrm{T,measured}})^2}{n-2}}$$

$$u(\mathrm{Corr}) = \frac{\mathrm{RMSE}}{A_{\mathrm{T,CRM}}} \times 100\%$$

$$\boldsymbol{u(\mathrm{Corr}) = 0.078085733\ \%}$$

Uncertainty of bias *u*(bias)

$$bias = \frac{A_{\mathrm{T,corr,mean}} - A_{\mathrm{T,CRM}}}{A_{\mathrm{T,CRM}}} \times 100\%$$

Table S4.1: Corrected data

measurement counter	$A_{\mathrm{T,corr}}$ ($\mu\mathrm{mol\,kg^{-1}}$)	
5	2211.5	
109	2212.8	
250	2211.1	
310	2211.8	
400	2213.4	
459	2213.6	
551	2213.5	
604	2211.0	
669	2213.5	
748	2212.5	
831	2211.8	
882	2215.4	
964	2211.5	
1115	2212.8	
1164	2210.2	
mean $A_{\mathrm{T,corr}}$	2212.4	$\mu\mathrm{mol\,kg^{-1}}$
standard deviation	1.33603259	$\mu\mathrm{mol\,kg^{-1}}$
s_{bias}	0.06038729	%
n	5	
bias	-8.22×10^{-14}	%

$$u(\text{bias}) = \sqrt{bias^2 + \frac{s^2_{\text{bias}}}{\sqrt{n}} + u(\text{Cref})^2 + u(\text{Corr})^2}$$

$$\boldsymbol{u(\text{bias}) = 0.0891965\ \%}$$

Uncertainty of the precision *u*(RW)

$$u(\text{RW}) = \sigma_{\text{Field}}$$

Absolute: $u(\text{RW}) = 1.2\ \mu\text{mol}\,\text{kg}^{-1}$

$$\textbf{Relative: } \boldsymbol{u(\text{RW}) = 0.05423876\ \%}$$

Relative combined standard uncertainty *u*(c)

$$u(\text{c}) = \sqrt{u(\text{RW})^2 + u(\text{bias})^2}$$

$$\underline{\underline{\boldsymbol{u(\text{c}) = 0.1044\ \%}}}$$

References

Breland, J. A. and R. H. Byrne. **1993**. Spectrophotometric procedures for determination of sea water alkalinity using bromocresol green. Deep Sea Research Part I: Oceanographic Research Papers. 40: 629–641, doi: 10.1016/0967-0637(93)90149-W

Dickson, A. G. **1981**. An exact definition of total alkalinity and a procedure for the estimation of alkalinity and total inorganic carbon from titration data. Deep Sea Research Part A. Oceanographic Research Papers. 28: 609–623, doi: 10.1016/0198-0149(81)90121-7

Dickson, A. G. **1990**. Standard potential of the reaction: AgCl(s) + $^1/_2H_2$(g) = Ag(s) + HCl(aq), and the standard acidity constant of the ion HSO_4^- in synthetic sea water from 273.15 to 318.15 K. J. Chem. Thermodyn. 22: 113–127, doi: 10.1016/0021-9614(90)90074-z

Dickson, A. G., J. D. Afghan, and G. C. Anderson. **2003**. Reference materials for oceanic CO_2 analysis: A method for the certification of total alkalinity. Marine Chemistry. 80: 185–197, doi: 10.1016/S0304-4203(02)00133-0

Dickson, A. G., C. L. Sabine, and J. R. Christian. **2007**. Guide to best practices for ocean CO_2 measurements. PICES Special Publications 3.

Ellison, S. eds.: Williams, A. **2012**. Eurachem/CITAC guide: Quantifying uncertainty in analytical measurement, 3rd Ed. Eurachem.

Grubbs, F. E. **1969**. Procedures for Detecting Outlying Observations in Samples. Technometrics. 11: 1–21, doi: 10.1080/00401706.1969.10490657

Ko, Y. H., K. Lee, K. H. Eom, and I.-S. Han. **2016**. Organic alkalinity produced by phytoplankton and its effect on the computation of ocean carbon parameters. Limnology and Oceanography. 61: 1462–1471, doi: 10.1002/lno.10309

Lee, K., F. J. Millero, R. H. Byrne, R. A. Feely, and R. Wanninkhof. **2000**. The recommended dissociation constants for carbonic acid in seawater. Geophysical Research Letters. 27: 229–232, doi: 10.1029/1999GL002345

Lee, K., L. T. Tong, F. J. Millero, C. L. Sabine, A. G. Dickson, and others. **2006**. Global relationships of total alkalinity with salinity and temperature in surface waters of the world's oceans. Geophysical Research Letters. 33: L19605, doi: 10.1029/2006GL027207

Li, Q., F. Wang, Z. A. Wang, D. Yuan, M. Dai, J. Chen, J. Dai, and K. A. Hoering. **2013**. Automated Spectrophotometric Analyzer for Rapid Single-

Point Titration of Seawater Total Alkalinity. Environ. Sci. Technol. 47: 11139–11146, doi: 10.1021/es402421a

Liu, X., M. C. Patsavas, and R. H. Byrne. **2011**. Purification and characterization of meta-cresol purple for spectrophotometric seawater pH measurements. Environ. Sci. Technol. 45: 4862–4868, doi: 10.1021/es200665d

Magnusson, B., H. Näykki, M. Hovind, M. Krysell, and E. Sahlin. **2017**. Handbook for calculation of measurement uncertainty in environmental laboratories., 4th Ed. Nordtest Report TR 537.

Martz, T. R., A. G. Dickson, and M. D. DeGrandpre. **2006**. Tracer Monitored Titrations: Measurement of Total Alkalinity. Analytical Chemistry. 78: 1817–1826, doi: 10.1021/ac0516133

McElligott, S., R. H. Byrne, K. Lee, R. Wanninkhof, F. J. Millero, and R. A. Feely. **1998**. Discrete water column measurements of CO_2 fugacity and pH_T in seawater: A comparison of direct measurements and thermodynamic calculations. Marine Chemistry. 60: 63–73, doi: 10.1016/S0304-4203(97)00080-7

Millero, F. J., J.-Z. Zhang, K. Lee, and D. M. Campbell. **1993**. Titration alkalinity of seawater. Marine Chemistry. 44: 153–165, doi: 10.1016/0304-4203(93)90200-8

Millero, F. J., K. Lee, and M. Roche. **1998**. Distribution of alkalinity in the surface waters of the major oceans. Marine Chemistry. 60: 111–130, doi: 10.1016/S0304-4203(97)00084-4

Millero, F. J., D. Pierrot, K. Lee, R. Wanninkhof, R. Feely, C. L. Sabine, R. M. Key, and T. Takahashi. **2002**. Dissociation constants for carbonic acid determined from field measurements. Deep Sea Res., Part I. 49: 1705–1723, doi: 10.1016/S0967-0637(02)00093-6

Millero, F. J. **2007**. The Marine Inorganic Carbon Cycle. Chemical Reviews. 107: 308–341, doi: 10.1021/cr0503557

Newton, J., R. Freely, P. Williamson, and J. Mathis. **2015**. Global Ocean Acidification Observing Network: Requirements and Governance Plan, 2nd Ed. GOA-ON.

Riley, W. J. **2008**. Handbook of Frequency Stability Analysis. NIST Special Publication 1065.

Roche, M. P. and F. J. Millero. **1998**. Measurement of total alkalinity of surface waters using a continuous flowing spectrophotometric technique. Mar. Chem. 60: 85–94, doi: 10.1016/S0304-4203(97)00087-X

Spaulding, R. S., M. D. DeGrandpre, J. C. Beck, R. D. Hart, B. Peterson, E. H. De Carlo, P. S. Drupp, and T. R. Hammar. **2014**. Autonomous in Situ Measurements of Seawater Alkalinity. Environ. Sci. Technol. 48: 9573–9581, doi: 10.1021/es501615x

Watanabe, A., H. Kayanne, K. Nozaki, K. Kato, A. Negishi, and others. **2004**. A rapid, precise potentiometric determination of total alkalinity in seawater by a newly developed flow-through analyzer designed for coastal regions. Mar. Chem. 85: 75–87, doi: 10.1016/j.marchem.2003.09.004

Yao, W. and R. H. Byrne. **1998**. Simplified seawater alkalinity analysis: Use of linear array spectrometers. Deep Sea Res., Part I. 45: 1383–1392, doi: 10.1016/S0967-0637(98)00018-1

Yao, W., X. Liu, and R. H. Byrne. **2007**. Impurities in indicators used for spectrophotometric seawater pH measurements: Assessment and remedies. Marine Chemistry. 107: 167–172, doi: 10.1016/j.marchem.2007.06.012

Chapter 5

Impact of impurities in bromocresol green indicator dye on spectrophotometric total alkalinity measurements

Published as: Seelmann, K., M. Gledhill, S. Aßmann, A. Körtzinger. **2020**. Impact of impurities in bromocresol green indicator dye on spectrophotometric total alkalinity measurements. Ocean Sci. doi: 10.5194/os-16-535-2020.

Abstract Due to its accurate and precise character, the spectrophotometric pH detection is a common technique applied in measurement methods for carbonate system parameters. However, impurities in the used pH indicator dyes can influence the measurements quality. During our work described here, we focused on impacts of impurities in the pH indicator dye bromocresol green (BCG) on spectrophotometric seawater total alkalinity (A_T) measurements. In order to evaluate the extent of such influences, purified BCG served as a reference. First, a high-performance liquid chromatography (HPLC) purification method for BCG was developed as such a method did not exist at the time of this study. An analysis of BCG dye from four different vendors with this method revealed different types and quantities of impurities. After successful purification, A_T measurements with purified and unpurified BCG were carried out using the novel autonomous analyzer CONTROS HydroFIA® TA. Long-term measurements in the laboratory revealed a direct influence of impurity types and quantities on the drift behavior of the analyzer. The purer the BCG, the smaller was the A_T increase per measurement. The observed drift is generally caused by deposits in the optical pathway mainly generated by the impurities. However, the analyzers drift behavior could not be fully overcome. Furthermore, we could show that a certain impurity type in some indicator dyes changed the drift pattern from linear to non-linear, which can impair long-term deployments of the system. Consequently, such indicators are impractical for these applications. Laboratory performance characterization experiments revealed no improvement of the measurement quality (precision and bias) by using purified BCG as long as the impurities of the unpurified dye do not exceed a quantity

of 2 % (relationship of peak areas in the chromatogram). However, BCG with impurity quantities higher than 6 % provided A_T values, which failed fundamental quality requirements. Concluding, to gain optimal A_T measurements especially during long-term deployments, an indicator purification is not necessarily required as long as the purchased dye has a purity level of at least 98 % and is free of the previously named impurity type. Consequently, high-quality A_T measurements do not require pure but the purest BCG that is purchasable.

5.1 Introduction

Global observations of the marine carbonate system are of high importance to understand biogeochemical processes in the ocean effected by anthropogenic CO_2. The measurable key variables characterizing the ocean carbon cycle are pH, total alkalinity (A_T), $p(CO_2)$, and total dissolved inorganic carbon (C_T). Due to their thermodynamic relationships, it is only necessary to measure two of these four parameters for a full characterization of the marine carbonate system (Millero 2007). Traditionally, A_T and C_T were the preferred parameters for this purpose when measuring discrete samples. However, more recently, pH measurements have become more prominent within the oceanographic communities. During decades of ocean carbon observations, several analytical methods have been established, ranging from manual bench top systems for laboratory work via at-sea flow-through analyzers to *in situ* sensors. Among all these available methods, spectrophotometric pH determination techniques using sulphonephthalein indicator dyes are described as simple, fast, and precise (e.g. Clayton and Byrne 1993; Tapp et al. 2000; Bellerby et al. 2002; Aßmann et al. 2011). They have been utilized in marine research especially for ocean carbon observations since the late 1980's (Robert-Baldo et al. 1985; Byrne 1987; Byrne and Breland 1989; King and Kester 1989). Since Breland and Byrne (1993) showed that the sulphonephthalein indicator dye bromocresol green (BCG) is suitable for seawater pH determination in the pH range 3.4 to 4.6, it has been used in several spectrophotometric A_T measurement systems with comparable precision and accuracy as traditional methods (Yao and Byrne 1998; Li et al. 2013; Seelmann et al. 2019).

Investigations of Yao et al. (2007) on seawater pH measurements with the most common indicator dye, meta-cresol purple (mCP) from different vendors have revealed different types and quantities of light-absorbing impurities. These impurities can contribute to pH offsets of up to 0.01 pH units. To overcome the uncertainties caused by indicator impurities, Liu et al. (2011) developed a preparative high-performance liquid chromatography (HPLC) method to purify mCP and characterized this purified dye. Furthermore, to produce large batches of purified mCP, Patsavas et al. (2013a) developed a flash chromatography (FC) method resulting in a 3.5 times increased yield per run. However, not all users of spectrophotometric seawater pH measurement systems are able to purify or to purchase purified mCP. Therefore, Douglas and Byrne (2017) published a mathematical correction for accurate pH measurements using unpurified mCP.

In order to apply these findings to spectrophotometric A_T measurements, Nand and Ellwood (2018) described a simple colorimetric method for determining seawater A_T using purified bromophenol blue (BPB) as pH indicator dye. However, at the time of this study, there are no comparable detailed investigations on how indicator impurities in BCG may influence spectrophotometric seawater A_T measurements.

Since our previous work dealt with an open-cell single-point titration analyzer with spectrophotometric pH determination using BCG as indicator dye (Seelmann et al. 2019), we investigated the influences of any impurities in BCG from different

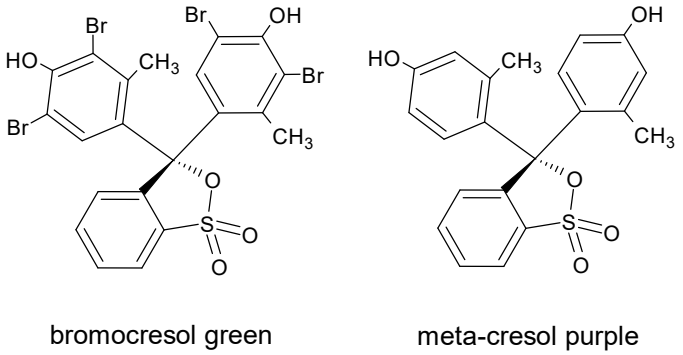

Figure 5.1: Chemical structure of bromocresol green and meta-cresol purple

vendors in comparison to purified BCG as reference. Hence, the first step of this study was to develop a purification method for BCG. Due to similarity in the chemical structure of BCG and mCP (see Fig. 5.1) and the available facilities in our laboratory, we decided to develop an HPLC analysis and purification method for BCG based on the mCP purification method published by Liu et al. (2011). Once the developed method was sufficient for BCG purification, a small batch of purified BCG was produced. Following this, comparative experiments were carried out with a novel autonomous analyzer for seawater A_T using purified and unpurified BCG in order to evaluate the influence of impurities in the indicator dye.

5.2 Materials and methods

5.2.1 HPLC method

5.2.1.1 Reagents and instrumentation

The BCG indicator (as sodium salt) was obtained from the following vendors: Acros Organics, Alfa Aesar, Carl Roth, and TCI. The solvents used in the HPLC purification were water (H_2O), acetonitrile (ACN), and trifluoroacetic acid (TFA). The ACN (HPLC grade) and the TFA (Purity: $\geq$ 99.9 %) were obtained from Fisher Scientific and Carl Roth, respectively.

A Shimadzu liquid chromatography (LC) system performed both the analytical and preparative chromatography. This system included an auto-sampler (SIL-10ADvp) (only for analytical mode), a isocratic preparative LC pump (LC-8A), an isocratic analytical HPLC pump (LC-10ADvp), a column oven (CTO-10ASvp), a single channel UV-VIS detector (SPD-10Avp), and an LC controller (SCL-10Avp).

The Primesep B2 HPLC columns were obtained from SIELC Technologies. This is a reverse-phase column with embedded basic ion-pairing groups that retains analytes by reverse-phase and ion-exchange mechanisms. For developing the purification method, an analytical Primesep B2 column (4.6 x 250 mm, particle size:

5 µm) was chosen. The purification was performed by a preparative Primesep B2 column (21.2 x 250 mm, particle size: 5 µm). Analytical separations were performed at 25 °C, but preparative chromatography was undertaken at room temperature.

5.2.1.2 Method development

The method development included the optimization of the mobile phase composition for BCG separation on the chosen column and was performed in analytical mode. For this purpose, a 10 $\mathrm{mg\,mL^{-1}}$ BCG solution of each vendor was prepared in the mobile phase and 20 µL were injected. One HPLC run with a flow-rate of 1.5 $\mathrm{mL\,min^{-1}}$ took 60 min and was monitored using the UV-VIS detector at 280 nm. The optimal mobile phase composition was determined by systematically changing the concentrations of the solvents starting from the conditions described by Liu et al. (2011). There, the mobile phase composition was 70:30 ACN:H_2O (volume:volume) with 0.05 % of TFA. Afterwards, the ACN and TFA concentration were increased by 5 % and 0.05 % increments, respectively, until the mobile phase consisted of 85 % ACN and 0.2 % TFA. One BCG injection was done per mobile phase composition each followed by a blank run. Blank runs were carried out by injecting the mobile phase as sample.

5.2.1.3 Comparison of BCG from different vendors

Once the optimal mobile phase composition was found, we tested BCG from different vendors for impurity types and quantities. For that, a BCG solution of each vendor was prepared and analyzed as described in Sect. 5.2.1.2 with the optimal mobile phase composition. To quantitatively compare the purity of each dye, we defined the relative purity of BCG at 280 nm wavelength (P_{BCG}), which was calculated as follows:

$$P_{\mathrm{BCG}} = \frac{A_{\mathrm{BCG}}}{\sum_{\mathrm{i}=1}^{n} A_{\mathrm{i}}} \times 100\% \tag{5.1}$$

where A_{BCG} is the area of the BCG peak, n is the number of peaks, and A_{i} is the area of the i^{th} peak.

5.2.1.4 Purification of BCG

The purification was performed by the LC system in preparative mode. A 7.5 $\mathrm{mg\,mL^{-1}}$ BCG solution was prepared in the mobile phase and 10 mL were injected onto the preparative column. Impurities were separated by isocratic flow (flow rate 31.2 $\mathrm{mL\,min^{-1}}$) with 75:25:0.1 ACN:H_2O:TFA as mobile phase. The pure BCG was collected manually in a round bottom flask at its retention time of about 52 min. Approximately 90 % of the mobile phase was removed from the BCG eluate using a rotary evaporator, with the final 10 % left to evaporate in a dark open box at room temperature. The pure crystalline dye was transferred to a brown flask for further experiments.

In order to verify the success of the purification, the purified BCG was analyzed by the analytical HPLC procedure as described in Sect. 5.2.1.2.

5.2.2 Total alkalinity measurements

5.2.2.1 Reagents and instrumentation

Total alkalinity measurements were performed using the novel autonomous analyzer CONTROS HydroFIA® TA (until 2019: Kongsberg Maritime Contros GmbH, Kiel, Germany; since 2020: -4H-JENA Engineering GmbH, Kiel, Germany). Its measurement principle is based on a single-point open-cell titration of the seawater sample with subsequent spectrophotometric pH detection using BCG as indicator (Breland and Byrne 1993; Yao and Byrne 1998; Li et al. 2013; Seelmann et al. 2019). The seawater sample was titrated with 0.1 mol kg^{-1} hydrochloric acid (HCl) obtained from Carl Roth and constantly temperature controlled to 25.0 ± 0.1 °C by the systems internal heat exchanger.

The A_T value of the sample was calculated by the following general equation:

$$\frac{-V_{sw} \times \rho_{sw} \times A_T + V_t \times \rho_t \times C_t}{V_{sw} \times \rho_{sw} + V_t \times \rho_t} = [H^+]_F + [HF] + [HSO_4^-] + [HI^-] \qquad (5.2)$$

where V_{sw} and V_t are the volumes of the seawater sample and the added titrant (HCl and BCG solutions), respectively, and ρ_{sw} and ρ_t are the densities of the seawater sample and the added titrant, respectively. C_t is the acid concentration in the combined titrant solution. $[H^+]_F$ is the free concentration of hydrogen ions, and $[HI^-]$ is the concentration of the protonated (i. e. acidic) form of BCG. [HF] and $[HSO_4^-]$ are the concentrations of hydrogen fluoride and the bisulfate ion in the seawater sample. $[H^+]_F$, or pH_F, in the sample-titrant mixture is measured spectrophotometrically. Following Breland and Byrne (1993) and Yao and Byrne (1998), pH_F is described by

$$pH_F = 4.4166 + 0.0005946 \times (35 - S_{mix}) + \log\left(\frac{R - 0.0013}{2.3148 - R \times 0.1299}\right) \qquad (5.3)$$

where S_{mix} is the salinity of the sample-titrant mixture, and R is the ratio between the absorbances at 444 and 616 nm.

Certified reference material, CRM, (batch 160, $A_{T,reference}$ = 2212.44 ± 0.67 µmol kg^{-1}) was obtained from A. G. Dickson at the Scripps Institution of Oceanography of the University of California, San Diego. The seawater for our experiments was prepared by diluting a commercially available 8.33-fold concentrate of seawater ("Absolute Ocean", ATI Aquaristik, Germany) with deionized water. Its absolute A_T value was not important as it was only used

for mimicking semi-continuous measurement conditions between the references. All total alkalinity measurements were carried out in an air-conditioned laboratory and after the system was "calibrated" with a freshly opened CRM. However, the "calibration" routine conducted by the CONTROS HydroFIA® TA is not a calibration in a true sense. It rather serves the determination of the exact sample volume by utilizing a one point CRM measurement. The seawater sample volume is the only unknown variable of the absolute A_T determination method (Seelmann et al. 2019).

5.2.2.2 Long-term measurements

For the long-term measurements, 0.002 mol kg^{-1} BCG solutions were prepared from unpurified BCG (from different vendors) and purified BCG and used as indicator dye in the analyzer. The unpurified dyes (sodium salts) were dissolved in deionized water (DI-water). The purified dye was dissolved in DI-water with sodium hydroxide (NaOH) as additive. The exact amount of NaOH was calculated by the molar ratios and molar masses of BCG and NaOH. This transferred the pure BCG to its sodium salt and improved its solubility. For both unpurified and purified BCG solutions the ionic strength was kept very low (only created by the dissolved BCG sodium salt itself) in order to realize high concentrations of BCG stock solution. However, the dilution of the sample seawater by the added BCG and HCl solution was accounted for in the A_T calculation procedure.

The prepared seawater sample ($\approx$ 25 L) was measured more than 300 times with a measuring interval of 15 min, which took about four days. For monitoring the drift, a freshly opened CRM was measured at the beginning and at the end of this experiment, as well as daily in between. Each of these CRM measurements consisted of five consecutive single measurements.

5.2.2.3 Standard addition experiment

In order to evaluate the impact of impurities on the measuring performance of the system, we carried out a standard addition experiment with each unpurified and the purified BCG. This experiment is the standard validation procedure for evaluating the performance of the analyzer under laboratory conditions. Therefore, a seawater sample (with relatively high A_T) was titrated with an HCl solution (0.1 mol kg^{-1}) to lower its A_T in five steps. The titration was carried out by adding different precisely known volumes of HCl to a known volume of seawater resulting in five seawater samples with stepwise decreased A_T. The theoretical A_T ($A_{T,titrated}$) was calculated from the volumes of added acid and seawater, the concentration of the acid, and the original A_T of the seawater. To determine the practical A_T ($A_{T,measured}$), each of these samples was repeatedly measured with the analyzer ($n = 5$).

The precision was determined by averaging the standard deviation (σ) of each sample measurement. The root mean square error (RMSE) of the linear regression

after plotting $A_{\mathrm{T,measured}}$ vs. $A_{\mathrm{T,titrated}}$ gave us information about the bias of the method. It was calculated by

$$\mathrm{RMSE} = \pm\sqrt{\frac{1}{n} \times \sum_{\mathrm{i}=1}^{n} (A_{\mathrm{T,fitted,i}} - A_{\mathrm{T,measured,i}})^2} \tag{5.4}$$

where n is the number of samples, $A_{\mathrm{T,fitted,i}}$ is the i^{th} A_{T} value calculated with the linear regression equation with $A_{\mathrm{T,titrated,i}}$ as x variable, where $A_{\mathrm{T,measured}}$ is the average of the five repeatedly measured A_{T} values of each titrated seawater sample. Slope and intercept of this regression were important for the evaluation of linearity and sensitivity. Within the standard validation procedure of the analyzer, these terms must fulfill within their uncertainties the following requirements: Slope = 1; intercept = 0.

5.3 Results and discussion

5.3.1 HPLC separation and purification of BCG

5.3.1.1 Method development

Table 5.1 summarizes the influence of the different mobile phase compositions on the BCG separation. For saving solvents and time, it is important to keep the time of each HPLC run under 60 min, but, at the same time, with an optimal separation of BCG from its impurities. Hence, the optimal separation of BCG was achieved with 75:25:0.1 ACN:H_2O:TFA as mobile phase. The pure BCG was eluted from the column as fast as possible (retention time: 52 min) with the best dye-impurity separation.

Table 5.1: Mobile phase compositions and their impact on the BCG separation

Mobile phase composition:			BCG separation:	
ACN (%)	H_2O (%)	TFA (%)	BCG peak (min)	Sufficient separation of impurities
70	30	0.05	no elution[a]	-
70	30	0.10	60	no[b]
70	30	0.15	no elution[a]	-
70	30	0.20	no elution[a]	-
75	25	0.10	52	yes
80	20	0.10	56	yes
85	15	0.10	60	no[b]

[a] Within 60 min run time
[b] Impurities found in subsequent blank run

5.3.1.2 Comparison of BCG from different vendors

Figure 5.2 shows the resulting analytical HPLC chromatograms. There, BCG from different vendors shows different types and quantities of impurities. The retention time of the pure BCG was 52 min in all chromatograms. Another similarity between all chromatograms was the cluster of several peaks around 3-5 min. Only the peak areas of these peaks strongly differed. As there are no peaks at these retention times in the blank chromatogram, this peak cluster had to be caused by the indicator and not by the solvent. BCG from Acros Organics, Alfa Aesar and Carl Roth showed an intensive peak around 58 min, which is not present in the BCG from TCI. However, BCG from TCI showed three other small peaks around 26 min, 29 min, and 42 min. Alfa Aesar BCG also showed the 42 min peak in addition to small peaks around 7 min, 10 min, and 35 min. These various quantities of total absorbance at 280 nm resulted in different P_{BCG}. The calculated P_{BCG} for each

vendor (following Equ. 5.1) are summarized in Table 5.2. It has to be taken into account that these quantities are only valid when using an UV detector. Other detectors may result in different purity levels.

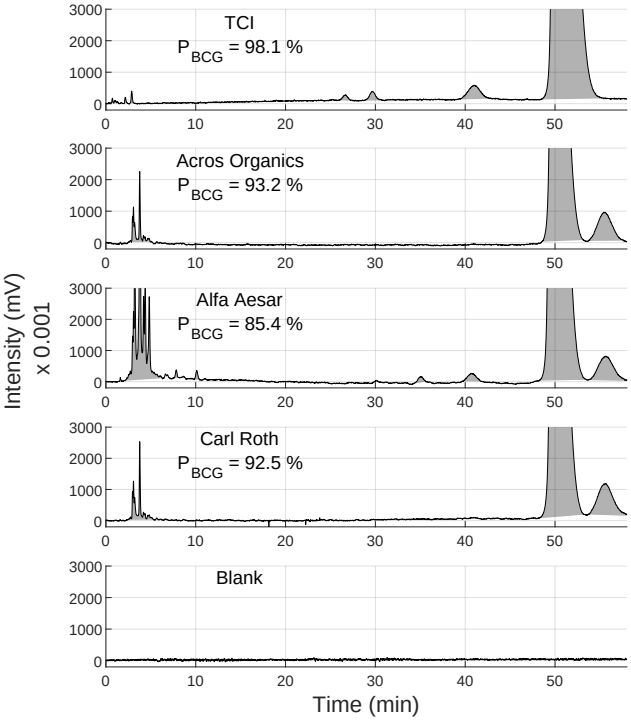

Figure 5.2: Analytical HPLC chromatograms of unpurified BCG from different vendors with their P_{BCG} and a chromatogram from a solvent injection without BCG (Blank). All peaks are highlighted with gray background color.

Table 5.2: Summary of analytical HPLC of unpurified BCG from different vendors

	Acros Organics	Alfa Aesar	Carl Roth	TCI
Number of peaks	3	7	3	5
P_{BCG} (%)	93.2	85.4	92.5	98.1

5.3.1.3 Purification of BCG

In order to test the effectiveness of the purification method, we decided to purify the least pure BCG from Alfa Aesar. Furthermore, to produce the most pure dye, also BCG from TCI was chosen for purification. The obtained yields were between 60 % and 70 % for both BCGs with around 50 mg purified BCG recovered per injection.

Figure 5.3 shows the analytical HPLC chromatograms of purified TCI BCG, and Alfa Aesar BCG. Both chromatograms still show the peak cluster around 3-5 min, but with much smaller areas, especially with purified Alfa Aesar BCG. Furthermore, the 42 min and 58 min peaks of Alfa Aesar BCG could not be totally removed. However, the purity of TCI BCG, and Alfa Aesar BCG improved to 99.6 %, and 99.3 %, respectively. The results are summarized in Table 5.3.

Table 5.3: Summary of analytical HPLC of purified BCG

	Purified from	
	TCI	Alfa Aesar
Number of peaks	2	4
P_{BCG} (%)	99.6	99.3

Since the relative purity of Alfa Aesar BCG was improved from 85.4 % to 99.3 %, the success of the purification was proven. Hence, the HPLC purification method developed here is considered sufficient for the nearly full removal of impurities from BCG.

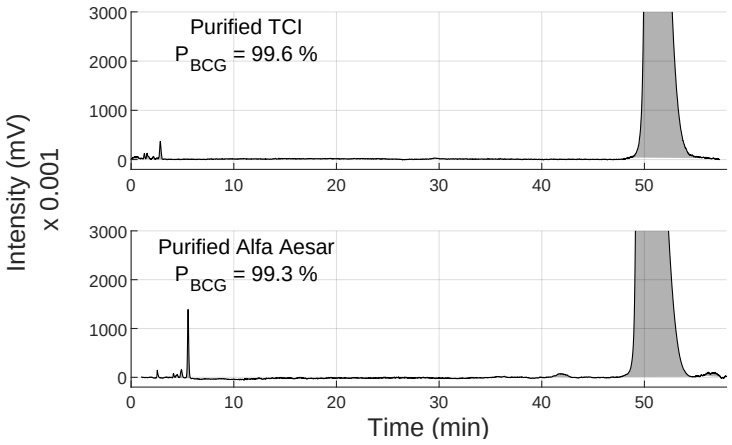

Figure 5.3: Analytical HPLC chromatograms of purified BCG from TCI, and Alfa Aesar with their P_{BCG}. All peaks are highlighted with gray background color.

5.3.2 Total alkalinity measurements

5.3.2.1 Long-term measurements

During previous studies with the CONTROS HydroFIA® TA analyzer, we found that a linear drift to higher A_T values appears to be the typical behavior of the system (Seelmann et al. 2019). We also found out that the drift is caused by deposits in the optical pathway. As a result, the light intensity decreases and therefore the absorbances at 444 and 616 nm (wavelengths where the acid and base form of BCG have their absorbance maxima) changes in a certain ratio so that the A_T values increases per measurement. In the present study we wanted to examine the impact of BCG impurities and the usage of purified BCG, respectively, on the drift behavior of the system.

In order to evaluate the drift of the system supposedly caused by impurities of the BCG indicator dye, the bias between the measured A_T value and the reference A_T value of the CRM ($\Delta A_T = A_{T,measured} - A_{T,reference}$) was plotted vs. the measurement counter. Figure 5.4 shows the results for A_T measurements with purified and unpurified TCI BCG, as well as unpurified BCG from Alfa Aesar and Acros Organics. Measurements with purified and unpurified TCI BCG resulted in a linear drift to higher values with the regression equation $y = (0.0193 \pm 0.0009) \times x + (-0.18 \pm 0.16)$, and $y = (0.0317 \pm 0.0004) \times x + (-0.16 \pm 0.10)$, respectively. However, unpurified Acros Organics and Alfa Aesar BCG showed a non-linear drift to higher values. All A_T measurements took into account the relative uncertainty of the analyzer, determined as 0.08 % (Seelmann et al. 2019). Figure 5.4 does not show these uncertainties as they are to small for the scaling of the y-axis.

One important outcome of this experiment is, that the magnitude and shape of the drift directly depends on the purity of the used BCG. The drift caused by purified TCI BCG is reduced by 0.0124 µmol kg^{-1} per measurement with respect to unpurified TCI BCG. This indicates that the drift of the system must be primarily caused by impurities of the BCG indicator and not by the indicator itself as hypothesized in our previous study (Seelmann et al. 2019). However, there is still a remaining small drift component even with the most pure TCI BCG. Hence, BCG purification appears to significantly reduce but not completely eliminate the observed system drift. For resetting the drift, a flush with ethanol or isopropyl alcohol removes any impurity deposits in the optical pathway caused by the indicator dye. The frequency of these cleanings during long-term deployments can be reduced by using purer dye. But finally, the user of the CONTROS HydroFIA® TA analyzer decides the cleaning interval as its frequency depends on the certain application of the system and how often measurements are conducted. Furthermore, there is a dependency on the measured water matrix as well, e.g. high turbidity coastal water requires more often cleanings than open ocean water. We can only make recommendations based on our experiences with the analyzer. During our field deployments of the analyzer (not part of this study), we ran a cleaning procedure using ethanol right before a new "calibration" of the system with CRM. As our

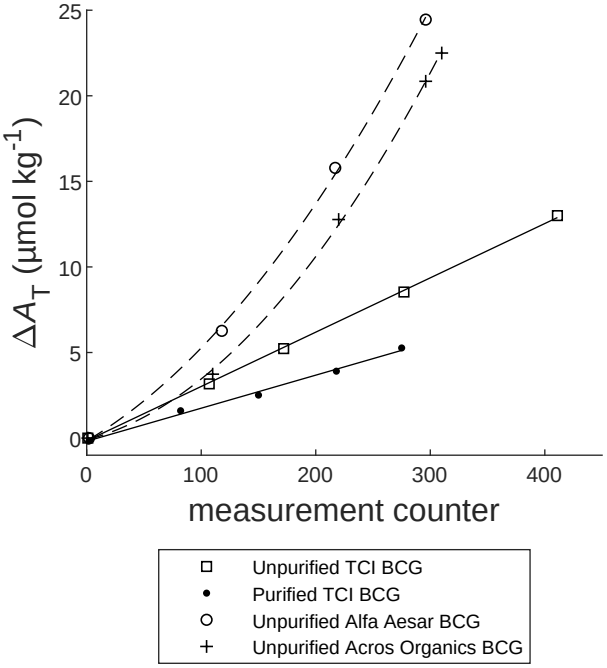

Figure 5.4: Bias (ΔA_T) between measured A_T and reference value of the CRM as a function of the measurement counter of the CONTROS HydroFIA® TA analyzer, where filled circles, open squares, crosses, and open circles represent the average of five repeated measurements made with purified BCG (TCI), unpurified TCI BCG, unpurified Acros Organics BCG, and unpurified Alfa Aesar BCG, respectively. The solid lines are the linear regressions of the associated measurement points. The dashed lines represent a non-linear regression.

analyzer measured around 1000 A_T values per month, we carried out an ethanol flush with a subsequent calibration on monthly basis. We also experienced that the subsequent drift correction is entirely manageable up to a maximum ΔA_T of approximately 30 µmol kg^{-1} (as observed during our field deployments, not part of this study). This $\Delta A_{T,max}$ can be used as a guidance for determining the cleaning frequency.

Another important outcome is that the shape of the drift differed with the amount of impurities. Below a certain purity grade (between 93.2 % and 98.1 %), the drift behavior appears to change from linear to non-linear. However, for unattended long-term installations of the CONTROS HydroFIA® TA analyzer it is highly preferable to have a linear drift. Under this condition, the correction during the post-processing of the data is easier and the necessary reference measurements can be reduced to a pre- and post-deployment measurement. Furthermore, the upper limit of the analyzer's working range will be reached faster with a non-linear increase

of the A_T values per measurement. Hence, there is the risk, that the measured A_T values are rendered useless towards the end of a long-term deployment.

Due to the nearly similar drift behavior of Acros Organics and Alfa Aesar BCG, we also hypothesize that the observed non-linear behavior was mainly caused by the impurity with the retention time around 58 min, which is only present in BCG from Acros Organics, Carl Roth, and Alfa Aesar. Additional tests with the Carl Roth indicator supported the hypothesis (results not shown). This certain impurity might be a molecule with a higher adsorption tendency to the glass wall of the cuvette compared to other impurities. If the used indicator dye contains this impurity type, the magnitude and shape of the drift is mainly driven by the presence of this molecule than by the BCG purity itself. As a consequence, the usage of BCG indicators containing this impurity should be avoided especially during long-term deployments.

Additional to the impacts on the drift, we also experienced, that the frequency of system cleanings has to be increased when using BCG with low purity. For unattended long-term deployments, this must be taken into account.

Table 5.4: Precision and bias of unpurified and purified BCG

	"High-purity" BCG: unpurified TCI	purified TCI	"Low-purity" BCG: unpurified Acros Organics	unpurified Alfa Aesar	Requirements for standard open-cell titrators[a]	Typical performance of the analyzer[b]
Precision σ ($\mu mol\,kg^{-1}$)	± 1.6	± 1.5	± 1.4	± 2.7	± 1	± 1.5
Bias (RMSE) ($\mu mol\,kg^{-1}$)	± 1.2	± 1.1	± 1.7	± 5.3	± 2	± 1.0

[a] Dickson et al. (2007)
[b] Seelmann et al. (2019)

5.3.2.2 Standard addition experiment

After this experiment was conducted, we experienced that "high-purity" ($P_{\mathrm{BCG}} > 98$ %) and "low-purity" BCG ($P_{\mathrm{BCG}} < 94$ %) showed different results. Hence, we decided to divide the results and discussion section of this experiment into two groups. Which type of BCG belongs to which group can be found in Table 5.4. We cannot say anything about the behavior of BCG with 98 % $> P_{\mathrm{BCG}} >$ 94 %, because none of the tested dyes fall in this range.

The results of the standard addition experiment carried out with purified and unpurified TCI BCG ("high-purity" BCG) are shown in Fig. 5.5. By plotting $A_{\mathrm{T,measured}}$ vs. $A_{\mathrm{T,titrated}}$, purified and unpurified TCI BCG show a linear equation of $y = (0.996 \pm 0.013) \times x + (11 \pm 29)$, and $y = (0.997 \pm 0.012) \times x + (7 \pm 26)$, respectively. Both correlations satisfy the quality requirements (slope = 1, intercept = 0) within their uncertainty, and they were statistically indistinguishable. Hence, the sensitivity and linearity of these measurements are considered satisfactory. The evaluation of precision and bias, which is summarized in Table 5.4, revealed no significant differences between measurements. Furthermore, both biases were in full agreement with previous laboratory performance characterizations of the system (Seelmann et al. (2019): ± 1.0 µmol kg^{-1}) and with the requirements of Dickson et al. (2007) for standard open-cell A_{T} titrators for which an overall bias of ± 2 µmol kg^{-1} is required. However, the requirement for precision (standard open-cell titrator: ± 1 µmol kg^{-1}) were not fully achieved, but both results are entirely comparable to our previous laboratory performance characteristic (Seelmann et al. (2019): ± 1.5 µmol kg^{-1}). Consequently, above a relative purity grade of 98 % no negative influence of indicator impurities on the measurement performance of the analyzer could be identified.

"Low-purity" indicators behaved completely different. The results of the standard addition experiment carried out with unpurified BCG from Acros Organics and Alfa Aesar are shown in Fig. 5.5 with their linear equations of $y = (1.097 \pm 0.013) \times x + (-228 \pm 29)$, and $y = (1.147 \pm 0.036) \times x + (-352 \pm 82)$, respectively. Clearly, these correlations were not satisfactory, and statistically different to the correlation of purified BCG. Hence, these "low-purity" dyes do not show the sensitivity and linearity behavior that is required for most accurate measurements with the analyzer. Table 5.4 shows that measurements with Acros Organics BCG ($P_{\mathrm{BCG}} = 93.2$ %) still fell within acceptable ranges regarding precision and bias requirements. However, measurements using Alfa Aesar BCG ($P_{\mathrm{BCG}} = 85.4$ %) did not meet the quality requirements.

Summing up, we can state that the uncertainty of A_{T} measurements only deteriorates significantly for a BCG purity grade below 94 %. Indicator dyes with $P_{\mathrm{BCG}} > 98$ % provide A_{T} measurements with a quality comparable to these measured with purified BCG. These findings partially support other studies dealing with different purified pH indicators for spectrophotometric pH (Yao et al. 2007; Liu et al. 2011; DeGrandpre et al. 2014; Lai et al. 2016) and A_{T} measurements (Nand and Ellwood 2018). There, indicator purification always led to an improvement in

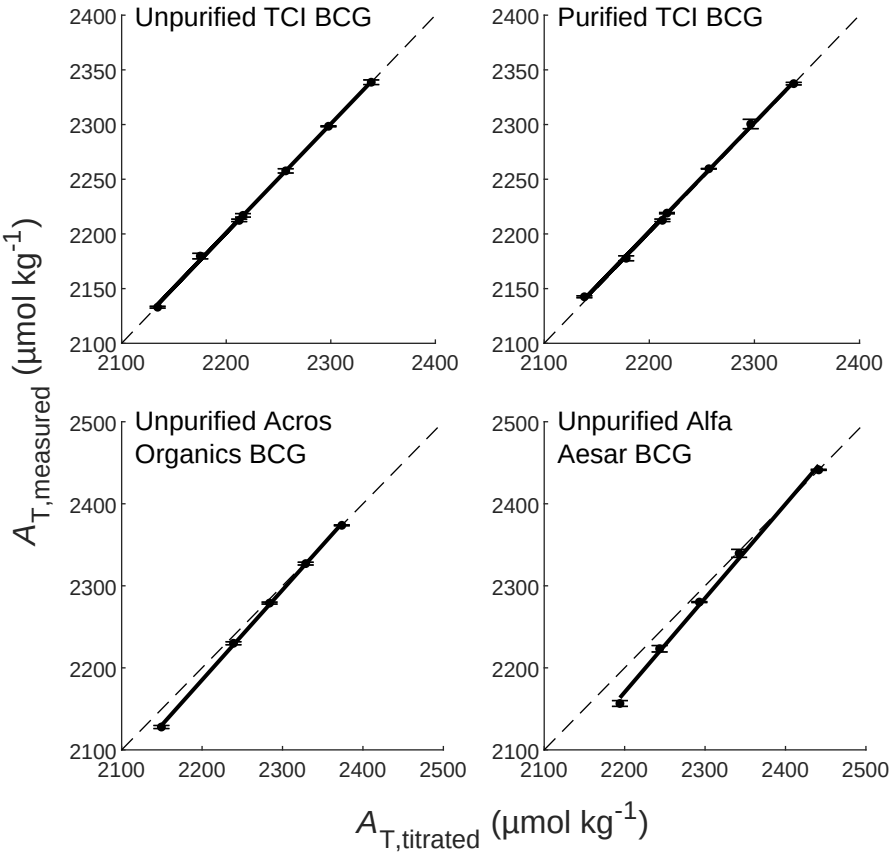

Figure 5.5: $A_{\mathrm{T,measured}}$ as a function of $A_{\mathrm{T,titrated}}$ of each titration step measured with purified and unpurified TCI BCG as well as unpurified BCG from Acros Organics and Alfa Aesar. The black filled circles represent the average of five repeated measurements for each sample with their standard deviations (σ) as errorbar. The black solid lines indicate the linear fit of the data points. The black dashed lines indicate the 1-to-1 line of these plots.

measurement precision. Under the scope of this study, we proved that purification of BCG is not necessary to improve the quality of the A_T measurements with the CONTROS HydroFIA® TA analyzer as long as the used BCG is purer than 98 %. The reason for the deviation to other studies lies in the measuring principle of the system. Before starting measurements with newly prepared solutions, it is obligatory to "calibrate" the system by measuring a CRM. However, this procedure is not a calibration in the real sense, as the method has an absolute character. During this routine, the exact volume of the analyzers internal seawater sample loop, V_{SW} is determined being the only unknown variable within this method. Hence, all inevitable uncertainties (including impurities of the indicator) are combined in V_{SW} and thereby taken into account for subsequent A_T measurements. The present results prove that this procedure is able to compensate any influences of indicator impurities on the measurement quality up to an impurity level of 2 %. Consequently, the usage of "low-purity" BCG is not recommended.

5.4 Cost-benefit analysis

5.4.1 Measurements with purified vs. unpurified BCG

This study proves that an HPLC purification of BCG is entirely feasible. But is the purification of BCG worths the efforts and costs involved? To answer this question we compare the costs incurred and the benefits gained for A_T measurements with the CONTROS HydroFIA® TA analyzer. Due to the relatively long HPLC run time of 60 min and a flow rate of 31.2 mL min^{-1}, the purification method needs about 1.5 L of ACN per run (including pre- and post-flushes). To carry out the long-term and standard addition experiment for this study (around 500 measurements), approximately 144 mg of purified BCG were needed. Hence, with a yield of around 50 mg pure BCG per purification run,a minimum of three injections was necessary. However, for long-term measurement campaigns with the analyzer, the typical volume of BCG solution is 500 mL, which is sufficient for at least 2300 measurements. This would need 700 mg of purified BCG, which corresponds to a minimum of 14 purification runs and 21 L of ACN. ACN with HPLC grade is a relatively expensive chemical, and it must be appropriately disposed. This causes additional costs. Furthermore, the whole purification process takes about a full working day per run.

Rough calculations on the actual costs per measurement with the CONTROS HydroFIA® TA analyzer revealed that indicator purification would approximately double measurement costs. The calculation for measurements with unpurified indicator are based on ready-to-use 500 mL cartridges for both chemicals (HCl and BCG) ordered from Kongsberg Maritime Contros GmbH without any preparation effort for the user.

To overcome this high increase in measurement costs, there could be the possibility to develop a flash chromatography (FC) purification method for BCG as described for mCP by Patsavas et al. (2013a) to increase the yield of purified dye

per run. According to the method description in this publication (Patsavas et al. 2013a), the solvent consumption of both methods (FC and HPLC) per purification run is approximately the same. Provided the FC method would increase the yield 3.5 times as it was described for mCP, only 4 injections will be necessary to produce enough purified BCG for a long-term deployment with at least 2300 measurements. The estimated measurement costs for such a FC method would be approximately a third of these for measurements using BCG purified by HPLC. Hence, if BCG purification would be necessary, the FC method would be the more cost-effective choice. However, it has to be taken into account that the calculations for these measurement costs (especially for the FC method) are just theoretically estimated and may differ from reality depending on availability of resources and equipment. Furthermore, a FC purification method for BCG is so far not developed and validated, which means additional costs and working time.

Finally, if we compare the purified BCG with "high-purity" BCG like from TCI, the only benefit gained from the purification is a reduced drift per A_T measurement. However, as long as the drift pattern is linear, its actual slope is irrelevant as it can be easily corrected by regular reference measurements. Furthermore, there is no improvement in the measurement quality (precision and bias) as long as the impurity level is 2 % or below. Since the drift behavior cannot fully overcome, it seems not worth the effort to purify BCG for A_T measurements with the CONTROS HydroFIA® TA analyzer.

The types and quantities of impurities can nevertheless have a strong influence on measurement quality in unattended long-term applications of the system as it was shown before (e.g. change of the drift behavior, non fulfillment of the quality requirements). Hence, the purity of the used BCG is not unimportant at all. To achieve the best long-term measurement experience with the analyzer it is not necessary to use purified BCG, as the purest available indicator (e.g. BCG from TCI) generate fully satisfying quality results. Users of the CONTROS HydroFIA® TA should take the consequences of indicator impurities into account when choosing their BCG supplier. From this perspective, it would be beneficial to invest into higher purity indicator avoiding the issues described above. If applicable, an HPLC analysis of the used indicator following the here described analytical method can show any types and quantities of impurities. However, if there is no HPLC available, long-term laboratory measurements as described here can help to evaluate whether the purchased indicator is suitable or not by evaluating the drift behavior. As there could be batch to batch variability in purity, the drift pattern should be also assessed for each batch of BCG provided by the same supplier.

5.4.2 BCG characterization

Most of the studies dealing with purification of indicator dyes for spectrophotometric seawater pH measurements conducted a subsequent characterization of the purified indicator (e.g. Liu et al. 2015; Patsavas et al. 2013b; Nand and Ellwood 2018). Due to impurity impacts, coefficients and constants of purified indicators may

be different to these of unpurified dyes. During our work with purified BCG, we decided to forgo of an indicator characterization. There were two reasons for this decision:

1. Li et al. (2013) investigated the impact of different BCG characteristics found in the literature on spectrophotometric A_T measurements and concluded that the influences are insignificant also with regard to possible impurities. They justified this conclusion with the calibration of the system using CRM. The CONTROS HydroFIA® TA analyzer follows a similar measurement principle as the analyzer described by Li et al. (2013) and also conducted a calibration routine. Therefore, any uncertainties regarding the coefficients are taken into account for subsequent measurements.

2. The measurement quality using both purified and unpurified "high-purity" BCG were fully satisfying and met the quality requirements for A_T measurements. Furthermore, both uncertainties did not significantly differ from each other.

Finally, we concluded that a characterization of purified BCG would not improve the measurement quality at all and therefore decided to not conduct it.

5.5 Conclusions

We successfully developed an HPLC purification method for BCG and subsequently tested the impact of using the purified and unpurified dye on measurements with a novel autonomous analyzer for seawater A_T, the CONTROS HydroFIA® TA.

Taking all the achieved results into account, we conclude that a purification of BCG is not strictly recommended to carry out high-quality measurements with the CONTROS HydroFIA® TA analyzer. But the usage of "high-purity" BCG ($P_{BCG} > 98$ %, e.g. from TCI) is highly recommended to avoid a non-linear drift behavior and resulting loss of measurement quality as it was observed with "low-purity" BCG ($P_{BCG} < 94$ %). Users of the CONTROS HydroFIA® TA analyzer should take these recommendations into account, if they want to prepare the BCG solution on their own. A preceding HPLC analysis of the indicator dye would be the preferred approach to test the BCG purity and avoid a loss of analytical performance. BCG indicator dyes showing a relatively big peak after the BCG peak should be avoided, because their usage results in a non-linear drift pattern. It must be noted that modified HPLC methods (e.g. with a different mobile phase composition, detector or column) may result in altered peak patterns or relative BCG purities. However, not every user of the .CONTROS HydroFIA® TA has the facilities for such HPLC analyses. In case of any doubts, the compatibility of the purchased BCG can be easily tested by applying the laboratory long-term measurement experiment explained in this study. Dyes resulting in a linear drift pattern can be used without any concern providing the cleaning intervals are performed regularly to limit the absolute drift to < 30 µmol kg^{-1}. Furthermore, the measurement quality should be

monitored on regular basis, especially if the BCG solution decomposes over time. These tests should be also conducted with a new batch of BCG from the same vendor, because there could be batch-to-batch variabilities in purity.

5.6 Acknowledgments

This work was supported by the European Union's Horizon 2020 Research and Innovation Programme (AtlantOS) (grant number: 633211).

References

Aßmann, S., C. Frank, and A. Körtzinger. **2011**. Spectrophotometric high-precision seawater pH determination for use in underway measuring systems. Ocean Science. 7: 597–607, doi: 10.5194/os-7-597-2011

Bellerby, R. G., A. Olsen, T. Johannessen, and P. Croot. **2002**. A high precision spectrophotometric method for on-line shipboard seawater pH measurements: the automated marine pH sensor (AMpS). Talanta. 56: 61–69, doi: 10.1016/S0039-9140(01)00541-0

Breland, J. A. and R. H. Byrne. **1993**. Spectrophotometric procedures for determination of sea water alkalinity using bromocresol green. Deep Sea Research Part I: Oceanographic Research Papers. 40: 629–641, doi: 10.1016/0967-0637(93)90149-W

Byrne, R. H. **1987**. Standardization of standard buffers by visible spectrometry. Analytical Chemistry. 59: 1479–1481, doi: 10.1021/ac00137a025

Byrne, R. H. and J. A. Breland. **1989**. High precision multiwavelength pH determinations in seawater using cresol red. Deep Sea Research Part A. Oceanographic Research Papers. 36: 803–810, doi: 10.1016/0198-0149(89)90152-0

Clayton, T. D. and R. H. Byrne. **1993**. Spectrophotometric seawater pH measurements: total hydrogen ion concentration scale calibration of m-cresol purple and at-sea results. Deep Sea Research Part I: Oceanographic Research Papers. 40: 2115–2129, doi: 10.1016/0967-0637(93)90048-8

DeGrandpre, M. D., R. S. Spaulding, J. O. Newton, E. J. Jaqueth, S. E. Hamblock, A. A. Umansky, and K. E. Harris. **2014**. Considerations for the measurement of spectrophotometric pH for ocean acidification and other studies. Limnology and Oceanography: Methods. 12: 830–839, doi: 10.4319/lom.2014.12.830

Dickson, A. G., C. L. Sabine, and J. R. Christian. **2007**. Guide to best practices for ocean CO_2 measurements. PICES Special Publications 3.

Douglas, N. K. and R. H. Byrne. **2017**. Achieving accurate spectrophotometric pH measurements using unpurified meta-cresol purple. Marine Chemistry. 190: 66–72, doi: 10.1016/j.marchem.2017.02.004

King, D. and D. R. Kester. **1989**. Determination of seawater pH from 1.5 to 8.5 using colorimetric indicators. Marine Chemistry. 26: 5–20, doi: 10.1016/0304-4203(89)90061-3

Lai, C.-Z., M. D. DeGrandpre, B. D. Wasser, T. A. Brandon, D. S. Clucas, and others. **2016**. Spectrophotometric measurement of freshwater pH with purified

meta-cresol purple and phenol red. Limnology and Oceanography: Methods. 14: 864–873, doi: 10.1002/lom3.10137

Li, Q., F. Wang, Z. A. Wang, D. Yuan, M. Dai, J. Chen, J. Dai, and K. A. Hoering. **2013**. Automated Spectrophotometric Analyzer for Rapid Single-Point Titration of Seawater Total Alkalinity. Environ. Sci. Technol. 47: 11139–11146, doi: 10.1021/es402421a

Liu, X., M. C. Patsavas, and R. H. Byrne. **2011**. Purification and characterization of meta-cresol purple for spectrophotometric seawater pH measurements. Environ. Sci. Technol. 45: 4862–4868, doi: 10.1021/es200665d

Liu, X., R. H. Byrne, M. Lindemuth, R. Easley, and J. T. Mathis. **2015**. An automated procedure for laboratory and shipboard spectrophotometric measurements of seawater alkalinity: Continuously monitored single-step acid additions. Marine Chemistry. 174: 141–146, doi: 10.1016/J.MARCHEM.2015.06.008

Millero, F. J. **2007**. The Marine Inorganic Carbon Cycle. Chemical Reviews. 107: 308–341, doi: 10.1021/cr0503557

Nand, V. and M. J. Ellwood. **2018**. A simple colorimetric method for determining seawater alkalinity using bromophenol blue. Limnology and Oceanography: Methods. 16: 401–410, doi: 10.1002/lom3.10253

Patsavas, M. C., R. H. Byrne, and X. Liu. **2013a**. Purification of meta-cresol purple and cresol red by flash chromatography: Procedures for ensuring accurate spectrophotometric seawater pH measurements. Marine Chemistry. 150: 19–24, doi: 10.1016/j.marchem.2013.01.004

Patsavas, M. C., R. H. Byrne, and X. Liu. **2013b**. Physical–chemical characterization of purified cresol red for spectrophotometric pH measurements in seawater. Marine Chemistry. 155: 158–164, doi: 10.1016/j.marchem.2013.06.007

Robert-Baldo, G. L., M. J. Morris, and R. H. Byrne. **1985**. Spectrophotometric determination of seawater pH using phenol red. Analytical Chemistry. 57: 2564–2567, doi: 10.1021/ac00290a030

Seelmann, K., S. Aßmann, and A. Körtzinger. **2019**. Characterization of a novel autonomous analyzer for seawater total alkalinity: Results from laboratory and field tests. Limnology and Oceanography: Methods. 17: 515–532, doi: 10.1002/lom3.10329

Tapp, M., K. Hunter, K. Currie, and B. Mackaskill. **2000**. Apparatus for continuous-flow underway spectrophotometric measurement of surface water pH. Marine Chemistry. 72: 193–202, doi: 10.1016/S0304-4203(00)00081-5

Yao, W. and R. H. Byrne. **1998**. Simplified seawater alkalinity analysis: Use of linear array spectrometers. Deep Sea Res., Part I. 45: 1383–1392, doi: 10.1016/S0967-0637(98)00018-1

Yao, W., X. Liu, and R. H. Byrne. **2007**. Impurities in indicators used for spectrophotometric seawater pH measurements: Assessment and remedies. Marine Chemistry. 107: 167–172, doi: 10.1016/j.marchem.2007.06.012

Chapter 6

Enhance ocean carbon observations: Successful implementation of a novel autonomous total alkalinity analyzer on a Ship of Opportunity

Submitted as: Seelmann, K., T. Steinhoff, S. Aßmann, A. Körtzinger. **2020**. Enhance ocean carbon observations: Successful implementation of a novel autonomous analyzer on a Ship of Opportunity. Manuscript submitted to: Frontiers in Marine Science.

Abstract Over recent decades, observations based on merchant vessels (Ships of Opportunity – SOOP) equipped with sensors measuring the CO_2 partial pressure ($p(CO_2)$) in the surface seawater formed the backbone of the global ocean carbon observation system. However, one severe shortcoming of the current SOOP observatory is the fact that it mostly only measures $p(CO_2)$. Full insight into the marine CO_2 system requires the measurement of at least two of the four measurable variables of the marine CO_2 system which are $p(CO_2)$, total alkalinity (A_T), dissolved inorganic carbon (C_T) and pH. One workaround is to estimate A_T values based on established temperature-salinity parameterizations, but this leads to higher uncertainties and the possibility of regional and/or seasonal biases. Therefore, autonomous SOOP-based A_T measurements are of great interest. Our study describes the implementation of a novel autonomous analyzer for seawater A_T, the CONTROS HydroFIA® TA system (-4H-JENA engineering GmbH, Germany) on a SOOP line operating in the North Atlantic. We present the installation in detail and address major issues encountered with autonomous measurements using this analyzer, e.g. automated cleaning and stabilization routines, and waste handling. Another issue during long-term deployments is the provision of reference seawater in large-volume containers for quality assurance measurements and drift

correction. Hence, a stable large-volume seawater storage had to be found. We tested several container types with respect to their suitability to store seawater over a time period of 30 days without significant changes in A_T. Only a gas sampling bag made of polyvinylidene fluoride (PVDF) satisfied the high stability requirement. In order to prove the performance of the entire setup, we compared the autonomous A_T measurements with A_T from discrete samples taken during the first two measuring campaigns. Although the measurement accuracy in unattended mode slightly deteriorated compared to our previous system characterization, its overall uncertainty fulfilled requirements for autonomous A_T measurements on SOOP lines. A comparison with predicted A_T values based on an established and often used parameterization pointed at regional and seasonal limitations of such A_T predictions. Consequently, better spatiotemporally covered A_T observations are needed, which are now possible with the method described here.

6.1 Introduction

The world ocean so far has taken up about 40 % of the cumulative anthropogenic CO_2 emissions since 1750 (Friedlingstein et al. 2019), which is a direct consequence of the enormous buffer capacity of the marine CO_2 system. The annual sink for anthropogenic CO_2 has been estimated with different, completely independent methods in reasonably good agreement, e.g. 2.0 ± 1.0 $Gt\,C\,a^{-1}$ (Takahashi et al. 2009), 2.2 ± 0.6 $Gt\,C\,a^{-1}$ (Manning and Keeling 2006), 2.6 ± 0.3 $Gt\,C\,a^{-1}$ (Gruber et al. 2019). The prestigious, annually published "Global Carbon Budget" (Friedlingstein et al. 2019) represents the best synthesis product which makes use of all available observation data that have undergone and passed thorough quality control. The relatively good understanding of the current global mean oceanic uptake of anthropogenic CO_2 is contrasted by a lack of knowledge how the natural carbon cycle will respond regionally to global change. It is beyond doubt that natural carbon reservoirs and fluxes will change in an ocean that is turning warmer, sourer and less oxygenated (Riebesell et al. 2009; Keeling et al. 2010). In view of the central role of the ocean's CO_2 sink and its vulnerability to global change we need to better observe and document the changing marine carbon cycle. This requires a globally concerted observational effort that makes use of the existing observation networks. The Ships of Opportunity network (SOOP), organized in the Surface Ocean CO_2 Network (SOCONET), forms the backbone of the global observation system for the oceanic CO_2 sink (Wanninkhof et al. 2019). It is of prime importance to quantify the net air-sea flux of CO_2 and its interannual variability, particularly in areas of high variability. The resulting high-relevance product – the "Surface Ocean CO_2 Atlas" (SOCAT) – is most dominantly based on data from SOOP lines (Bakker et al. 2016). The recent release of SOCAT version 2019 features 25.7 million quality-controlled CO_2 measurements from the period 1957-2019. A strong provider of high-quality ocean CO_2 data from waters around Europe - with participation of our working group - is the ocean component of the European research infrastructure "Integrated Carbon Observation System" (ICOS). Since 2016, ICOS has established a network of ship-based and fixed carbon observation stations with standardized CO_2 measurements (Steinhoff et al. 2019). Each station has to pass a labeling process, which includes the mandatory fulfillment of certain parameters, measurement frequency and quality requirements (for the ICOS-Oceans labeling document with all requirements see: `https://otc.icos-cp.eu`)(ICOS Ocean Thematic Centre 2020). The ICOS-Ocean labeling document is based on fundamental standard operating procedures (SOP) and guidelines, which are accepted in the oceanographic communities (e.g. Dickson et al. 2007; Pfeil et al. 2013; Newton et al. 2015). It is noteworthy that for a SOOP line to achieve the highest "class 1" label of ICOS additional routine measurements of C_T or A_T are required (ICOS Ocean Thematic Centre 2020). Since 2002, our working group at the GEOMAR Helmholtz Centre for Ocean Research Kiel has operated a subpolar North Atlantic SOOP line until today (with funding-related gaps) using several merchant vessels (M/V *Falstaff* [Wallenius Lines], M/V *Atlantic Companion*, M/V

Atlantic Cartier, since 2018: M/V *Atlantic Sail* [all Atlantic Container Line]). The line is an official observation component of ICOS. All $p(CO_2)$ data acquired from this operational observation platform are quality-controlled according to international standards and protocols and delivered at regular intervals to SOCAT.

One severe shortcoming of the current SOOP-based ocean CO_2 observation platforms is the fact that they mostly only measure $p(CO_2)$ which is required to calculate the net air-sea CO_2 flux. However, full insight into the marine CO_2 system for important aspects such as net biological production, ocean acidification, and marine calcification requires the measurement of at least two of the four measurable variables of the marine CO_2 system which are $p(CO_2)$, total alkalinity (A_T), dissolved inorganic carbon (C_T) and pH. The so far common workaround for this problem is the calculation of A_T from sea surface temperature (SST) and sea surface salinity (SSS) using established parameterizations (Millero et al. 1998; Lee et al. 2006). Unfortunately, this procedure leads to additional uncertainty and is particularly prone to regional and seasonal bias. To solve this problem, autonomous measurements of A_T are required. Kongsberg Maritime Contros GmbH (Germany) commercialized a novel autonomous flow-through analyzer for A_T in seawater under the brand name CONTROS HydroFIA® TA, which is sold by -4H-JENA engineering GmbH (Germany) since February 2020. Its measurement principle is based on single-point open-cell titration of a seawater sample with a strong acid and subsequent spectrophotometric pH detection. In a previous study dealing with a performance characterization of this analyzer in the laboratory and in the field we were able to show that its measurement quality fulfills the high-quality requirements for ocean A_T measurements (Seelmann et al. 2019). Therefore, it was deemed suitable for autonomous long-term deployments on SOOP lines. Voynova et al. (2019) successfully implemented the CONTROS HydroFIA® TA in their FerryBox systems operating in the Wadden Sea and North Sea. However, the methodology behind this installation is not described in detail. During our work we experienced that an implementation of this analyzer on our SOOP line was not as straightforward as expected. Several additional circumstances have to be taken into account: 1) A linear drift of the system to higher values over time, which requires regular reference measurements for correction, 2) cleaning of the inner sample tubing with deionized water (DI-water) after stopping the measurements to avoid deposits in the tubing, 3) stabilization measurements when starting the system after idle times longer than 48 h, and 4) proper waste handling.

This study describes in detail how we installed the CONTROS HydroFIA® TA analyzer on our SOOP line and addressed the named issues. One major problem during automated long-term campaigns was the provision of enough reference seawater for regular quality assurance measurements with subsequent drift correction. A standard CRM bottle (500 mL), as provided by the group of Andrew G. Dickson, is not sufficient for long-term deployments. Due to the unattended character of such deployments, changing the bottles manually is not an option. Hence, an alternative stable larger volume storage ($\approx$ 5 L) for standard seawater had to be found. For this purpose, we tested several types of containers, such as

gas sampling bags, infusion bags, different canisters, or bottles. Finally, we show sea surface A_T data from the first four campaigns and compare them to A_T values of discrete samples (only the first two cruises) as well as predicted A_T values based on the parameterization described by Lee et al. (2006) giving a first insight into the consistency between the measured values and the A_T range and variability in the monitored region.

6.2 Methods and materials

6.2.1 Instrumentation

6.2.1.1 Total alkalinity measurements

Autonomous A_T measurements were performed by the CONTROS HydroFIA® TA analyzer (since February 2020: -4H-JENA engineering GmbH, Germany; before: Kongsberg Maritime Contros GmbH, Germany). Its measurement principle is based on a single-point open-cell titration of a seawater sample with subsequent spectrophotometric pH detection using bromocresol green (BCG) as indicator. Its detailed design and functionality can be found in Seelmann et al. (2019).

The seawater sample is titrated with 0.1 $\mathrm{mol\,kg^{-1}}$ hydrochloric acid (HCl) obtained from Carl Roth and is temperature controlled to 25°C by the system's internal heat exchanger. Therefore, all A_T measurements are independent of the room temperature. The 0.002 $\mathrm{mol\,kg^{-1}}$ BCG solution was prepared by dissolving the sodium salt of BCG obtained from Tokyo Chemical Industry (TCI) in deionized (DI) water. Both titrants were prepared in the laboratory and filled in opaque and air-tight 500 mL bags. During the measurement campaigns they were stored inside the system.

The interval of the autonomous A_T measurements onboard the SOOP line, i.e. the time period between two consecutive measurements, was set to 15 min. For quality assurance and drift correction, reference measurements were carried out automatically once per day by the system during the campaigns. Each daily referencing consists of five consecutive single measurements with a measurement interval of 10 min, which are averaged for the subsequent evaluation and drift correction. For this referencing procedure, certified reference material (CRM, batch #160: 2212.44 ± 0.67 $\mathrm{\mu mol\,kg^{-1}}$) obtained from the group of Andrew G. Dickson (Scripps Institution of Oceanography of the University of California, San Diego) was transferred into a 5 L bag to provide a sufficient amount of reference seawater. For this purpose, several large-volume containers had previously been tested in the laboratory. The details of this experiment can be found in Sect. 6.2.2.

6.2.1.2 Crossflow filter

Autonmous A_T measurements by the CONTROS HydroFIA® TA analyzer require filtration of the surface seawater due to its very small inner tubing. A severe issue during long-term deployments is the clogging of the filter. Crossflow filters are not

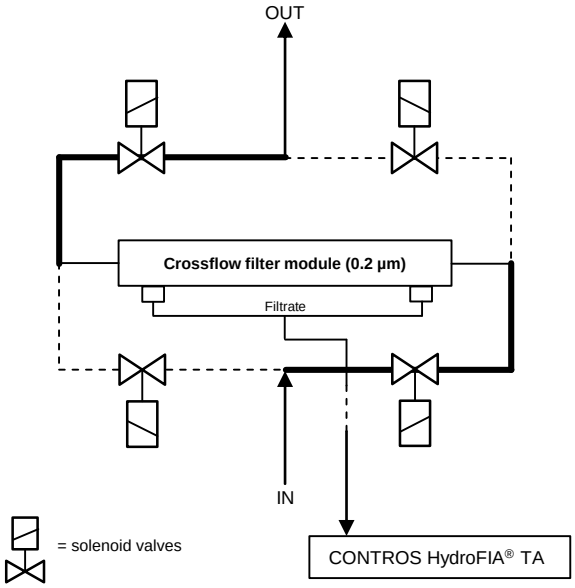

Figure 6.1: Schematic illustration (not to scale) of the crossflow filter device. The black bold solid lines and the black dashed lines represent the two respective flow paths achieved by opening and closing the solenoid valves.

prone to clogging and therefore suitable for long-term filtration. However, larger particles may clog the intake of the filter module. Regular changes of the flow direction through the filter module can solve this issue. Therefore, we installed the -4H-X-Flow-Flipper (-4H-JENA engineering GmbH, Germany) equipped with a 0.2 µm MiniKros® crossflow filter module (Spectrum Laboratories, USA). Figure 6.1 shows a scheme of this filter device. By opening and closing solenoid valves, the flow direction automatically changes every 15 min.

6.2.1.3 Temperature and salinity measurements

For measuring the intake seawater temperature, a SBE 38 Digital Oceanographic Thermometer (Sea-Bird Electronics, USA) is used as an inline temperature sensor. The salinity of the seawater is determined by a SBE 21 SeaCAT Thermosalinograph (Sea-Bird Electronics, USA). Both sensors are calibrated annually.

6.2.1.4 $p(CO_2)$ measurements

Autonomous $p(CO_2)$ measurements are carried out by a General Oceanics (GO) underway $p(CO_2)$ system 8050 (USA). As unattended $p(CO_2)$ measurements with this system onboard ships are well established within the oceanographic community (Pierrot et al. 2009), its installation and operation is not part of this report. The focus here lies on the implementation of the A_T analyzer. The quality-controlled

$p(CO_2)$ data measured on the North Atlantic SOOP line are delivered to SOCAT on regular basis.

6.2.2 Large-volume reference seawater storage test

6.2.2.1 Containers

For the purpose of stable storage of a larger volume of reference seawater, we tested several container types. The following criteria were important for our selection: 1) Handling on moving platforms like ships, 2) inertness of the inner material, 3) headspace above the seawater, 4) gas permeability, and 5) cost. Table 6.1 gives an overview of all tested containers. The numbering in Table 6.1 is for classifying the containers, where 1.x are gas sampling bags, 2.x are infusion bags, and 3.x are inflexible containers.

6.2.2.2 Stability tests

To test each container for seawater A_T stability over time, it was filled with about 5 L of a poisoned seawater sample (similar to CRM conditions). The seawater was prepared by diluting concentrated seawater solutions ("Absolute Ocean", ATI Aquaristik, Germany). Its absolute A_T value only had to be within the working range of the analyzer as only the temporal change between the starting value and the value after x days was of interest. The resulting A_T value was similar to that of the CRM ($\approx 2215\ \mu mol\,kg^{-1}$) measured by the CONTROS HydroFIA® TA in the laboratory. Each measurement day started with stabilization measurements and a "calibration" of the system with a freshly opened CRM. This procedure assured accurate and comparable measurements.

For determining the initial A_T value ($A_{T,start}$) of the seawater at the start of the storage experiment, the freshly filled container was connected to the analyzer and five repetitive measurements were carried out. $A_{T,start}$ therefore is the mean of these five measurements. After x days, the measuring procedure was repeated with a maximum storage time of 30 days ($x_{max} = 30$). The A_T value after x days ($A_{T,x}$) was calculated by averaging the five measurements on that day. For evaluating the A_T stability over time, the difference ($\Delta A_{T,x}$) between $A_{T,start}$ and $A_{T,x}$ was calculated for each day and container.

Table 6.1: Tested containers for large-volume reference seawater storage

No.	Container type	Inner material	Volume (L)	Supplier
1.1	Multi-foil gas sampling bag with polypropylene (PP) valve (opaque)	polyethylene (PE)	5	Sense Trading, Netherlands
1.2	Multi-foil gas sampling bag with PP valve (opaque)	PE	5	SKC Ltd., UK
1.3	Gas sampling bag with PP valve (transparent)	Polyvinylidene fluoride (PVDF)	5	Restek Corporation, USA
1.4	Nalophan™ bag (opaque)	Nalophan™	5	Olfasense GmbH, Germany
2.1	Infusion bag (transparent)	Ethylene-vinyl acetate (EVA)	5	IMPROMEDIFORM GmbH, Germany
2.2	Infusion bag (transparent)	EVA	5	Sartorius AG, Germany
2.3	Infusion bag (transparent)	PVDF	5	Meissner Filtration Products, USA
3.1	Waste canister (opaque)	PE	10	—
3.2	Glass bottle (transparent)	borosilicate glass	1	DWK Life Sciences GmbH, Germany
3.3	Canister	PP	5	Bürkle GmbH, Germany

6.2.3 North Atlantic SOOP line

6.2.3.1 The ship

Since 2018, the merchant vessel M/V *Atlantic Sail* operated by Atlantic Container Line (ACL) serves as SOOP line in the subpolar North Atlantic Ocean under the responsibility of our working group at the GEOMAR Helmholtz Centre for Ocean Research Kiel. It is a hybrid roll-on/roll-off container vessel (ConRo). This line is an official ocean observation station (DE-SOOP-Atlantic Sail) of the European research infrastructure "Integrated Carbon Observation System" (ICOS). The ship operates between Europe (Hamburg, Germany; Antwerp, Belgium; Liverpool, UK) and North America (Halifax, Canada; New York, USA; Baltimore, USA; Norfolk, USA). A full roundtrip of the ship takes about 5 weeks. Any maintenance of our installations is typically carried out during port calls in Hamburg, Germany. The seawater measurements are only carried out during the trans-Atlantic crossings between Liverpool, UK and Halifax, Canada.

6.2.3.2 Onboard installation

All facilities and instruments related to surface seawater measurements are installed on the lowest level of the engine room at the port side of the ship. Figure 6.2 shows a schematic illustration of the installations, where valve #1 is a pneumatic valve, and valves #2 - 4 are manual ball valves. Details about individual components can be found in Sect. 6.2.1. Photos of the onboard installation can be found in the Supplementary Information (Fig. S6.1).

The ship's lower sea chest was chosen as seawater intake. Its intake is located about 8-11 m below sea surface depending on the draught of the ship, which varies with cargo load. A centrifugal pump delivers seawater to the system. The seawater intake temperature is continuously measured with an inline temperature sensor (SBE 38). In order to split the seawater flow, a manifold with an integrated thermosalinograph (SBE 21) is installed. It provides the pCO_2 system and the crossflow filter device for A_T measurements with fresh seawater at a flow rate of 3 $L\,min^{-1}$ and 1 $L\,min^{-1}$, respectively. The A_T system only measures the filtrate of the crossflow filter. All waste seawater (with exception of measured A_T reference seawater) flows into a 100 L reservoir with a level sensor that controls a second centrifugal pump, which empties the content into the ship's higher sea chest when full. From there, the waste water leaves the ship into the ocean. The measured reference seawater from the A_T system is collected in a separate 100 L waste container as it is poisoned with mercury chloride. When this waste reservoir is full, its level sensor turnes off the CONTROS HydroFIA® TA, which serves as an emergency stop and prevents an overflow of the poisoned waste reservoir.

The main electric management of the entire system is organized in an electric box (see Fig. S6.1). This box also contains a computer, which controls all serially controllable devices such as the CONTROS HydroFIA® TA. Furthermore, the main switch is located there, which allows for easy the starting and stopping of

the complete system by member of the crew.

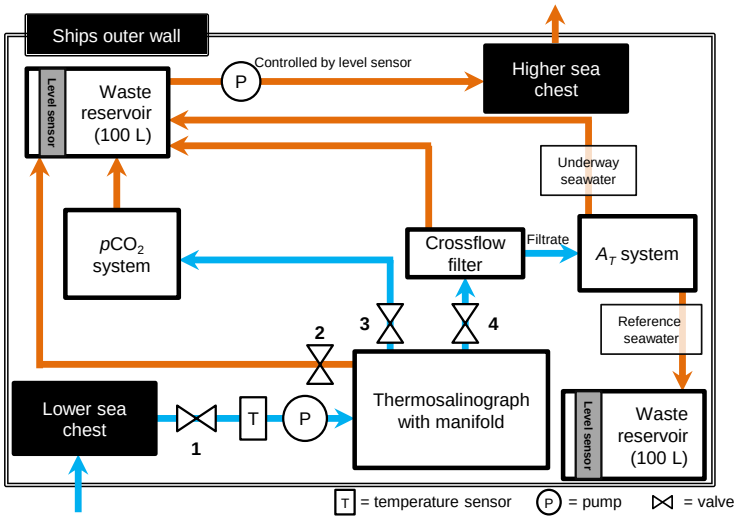

Figure 6.2: Schematic illustration (not to scale) of the onboard installation for seawater measurements. Black filled boxes represent ship facilities. White filled boxes represent our installations. Blue arrows, and orange arrows represent the water flow of fresh seawater, and waste seawater, respectively.

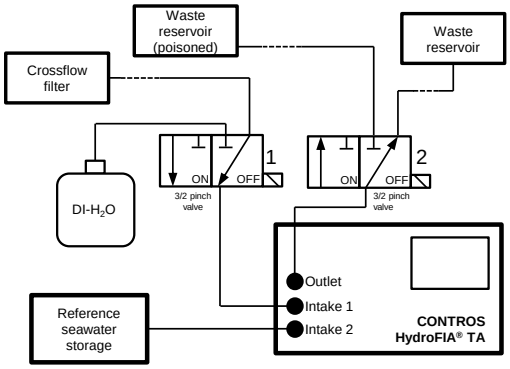

Figure 6.3: Schematic illustration (not to scale) of the onboard installation for seawater A_T measurements.

6.2.3.3 Autonomous A_T measurement procedure

Figure 6.3 shows the schematic set-up of the A_T analyzer installation. The current version of the analyzer is equipped with two inlets: One for continuous (inlet 1) and one for discrete measurements (inlet 2). In our SOOP application, inlet 2 is permanently connected to the reference seawater storage. Inlet 1 is connected to a 3/2-way pinch valve (#1) obtained from Bio-Chem Fluidics, USA, which can be electrically actuated. When not actuated, the analyzer receives seawater from the crossflow filter. When actuated, inlet 1 is connected to a 5 L DI-water reservoir. A second 3/2-way pinch valve (#2) downstream the system's outlet controls the waste water separation. When not actuated, the waste is routed to the regular seawater waste reservoir. When actuated, the waste water is routed to the poisoned waste reservoir. Both pinch valves are wired with the programmable outlet strip "MultiBox-pro seri" obtained from ANTRAX Datentechnik GmbH, Germany. Each socket of this outlet strip can be switched on or off via serial commands. The A_T analyzer is also controllable via serial commands. Therefore, both the CONTROS HydroFIA® TA as well the MultiBox are connected to the computer.

The workflow of the autonomous A_T measurements in autonomous SOOP line mode is illustrated in Fig. 6.4. During all named phases, the status of the main switch is permanently controlled by a software program written in Python. This script additionally sends and reads all serial commands to and from the analyzer and the MultiBox. By triggering the main power switch of the system and thereby starting the seawater flow, the stabilization phase of the analyzer is initiated. Both pinch valves are not actuated. The analyzer carries out 30 consecutive measurements using inlet 1 every 10 min. After these measurements, the analyzer starts with the actual measurement cycle. It consists of two parts: 1) Five consecutive reference measurements at 10 min interval using inlet 2 with actuated pinch valve #2 and not actuated pinch valve #1, and 2) 96 consecutive surface seawater measurements (underway) at 15 min interval using inlet 1 with both pinch valves being not actuated. This measurement cycle always starts with reference measurements and is only interrupted by switching off the main switch, which initiates the final flushing phase. During this phase, pinch valve #1 is actuated for 300 sec and #2 is not actuated. Meanwhile, the system flushes its inner tubing with DI-water and stops all measurements until the main switch is actuated again. In case the main switch is turned off during the stabilization phase, the analyzer skips the measurement cycle and directly starts with the flushing phase.

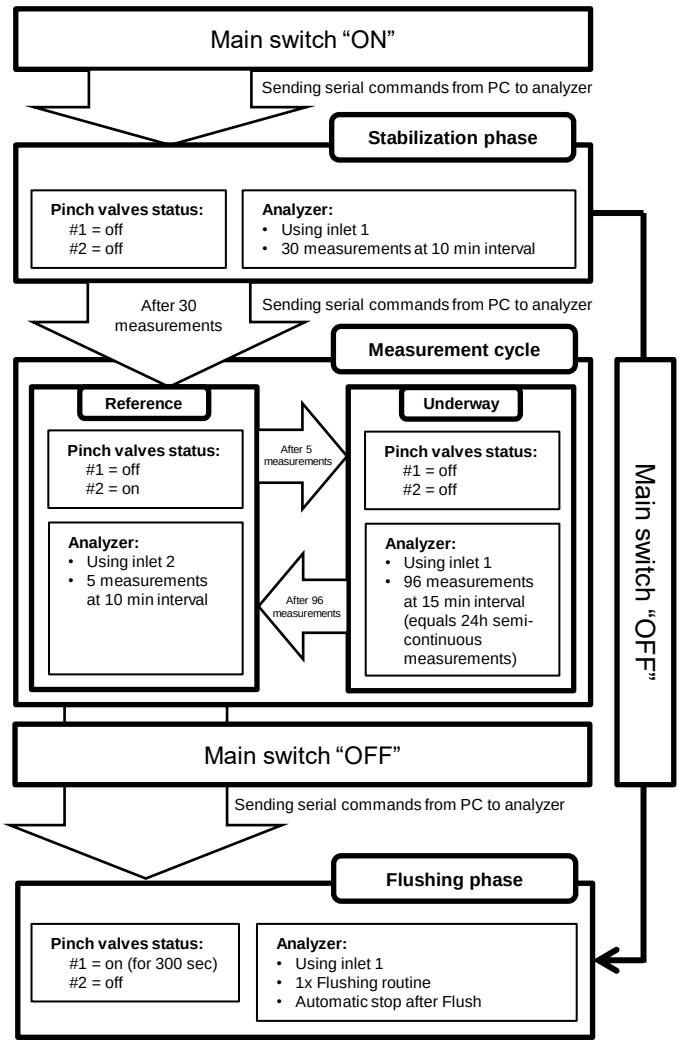

Figure 6.4: Workflow of the autonomous A_{T} measurements.

6.2.3.4 Discrete samples

In order to supervise and evaluate the new installation, we participated in the first two cross-Atlantic transits onboard the vessel: 1) From Liverpool, UK to Halifax, Canada (30 October 2018 - 06 November 2018), and 2) from Halifax, Canada to Liverpool, UK (05 February 2019 - 11 February 2019). During these transits, discrete samples for A_T and DIC were collected three times per day. They were bottled, poisoned and air-tight sealed following the recommendations of Dickson et al. (2007). Their measurement took place in the home laboratory (GEOMAR Helmholtz Centre for Ocean Research Kiel, Germany) using a standard open-cell alkalinity system with potentiometric titration (VINDTA 3S, Marianda, Germany) with an accuracy of about ± 2 µmol kg^{-1} (daily quality assurance using CRM). These measurements also followed the recommendations of Dickson et al. (2007). The A_T values of the discrete samples ($A_{T,ref}$) were used for accuracy evaluation and proof of the successful implementation of the CONTROS HydroFIA® TA analyzer. Besides the discrete sampling, no further interference with the unattended character of the installation onboard the ship occurred.

6.3 Results and discussion

6.3.1 Large-volume reference seawater storage tests

The main issue during autonomous long-term installations of the analyzer is the provision of enough reference seawater for regular quality assurance and drift correction. As 500 mL standard CRM bottles are insufficient for longer measurement campaigns, we tested several different container types in the laboratory.

Before we started with the actual testing, we set certain stability requirements, which needed to be fulfilled by the container: After 30 days of storage, each ΔA_{Tx} (including analyzer uncertainty) need to fall within the ± 10 µmol kg^{-1} uncertainty range required by ICOS for ship-based A_T measurements. This requirement is based on the "weather goal" introduced by Newton et al. (2015). Ideally, they would fall within the ± 2.2 µmol kg^{-1} uncertainty range of the analyzer. This value is based on the systems typical relative uncertainty of 0.1 % at a reference seawater A_T of ≈ 2215 µmol kg^{-1} under field conditions (Seelmann et al. 2019).

Figure 6.5 shows the results of the container stability tests without the standard error of the five repeated measurements at each point as the small numbers would not be properly visible with the y-axis scaling. Clearly, most of the tested containers do not meet the requirements. Gas sampling bags and infusion bags made out of materials such as PE or EVA (numbers: 1.1, 1.2, 2.1) show a clear trend towards decreasing A_T in the stored seawater. The same behavior is observed with the canisters made of PE and PP (numbers: 3.1, 3.3). We hypothesize that these materials contaminate the seawater with chemical substances, which bind or consume A_T relevant compounds. The infusion bag #2.2, which is also made of EVA, only shows a slight decrease in A_T at the beginning followed by a

subsequent increase after 24 days. This behavior suggests that the material causes less contamination with the increase in A_T being most likely caused by evaporation of water by the permeation through the foil. The majority of the $\Delta A_{T,x}$ of #2.2 lies within the ICOS uncertainty range, but only very close. The gas sampling bag #1.4 made of Nalophan™ shows a mostly increasing $\Delta A_{T,x}$ behavior. We hypothesizes that its barrier layer is not able to prevent water evaporation and/or initially releases alkalinity into the water. The infusion bag #2.3 made of PVDF shows a more unspecific, but highly unstable behavior and is therefore not suitable.

The most promising solution for a large-volume seawater storage is container #1.3. It fulfills both stability requirements with an average difference of (0.2 ± 1.3) µmol kg^{-1} over 30 storage days. But also the glass bottle (#3.2) stores the seawater in a comparably stable way. However, inflexible containers like bottles always have the problem of a constantly increasing headspace above the seawater and therefore, enhanced evaporation of water. This results in increasing A_T values over time. Although such a behavior does not show up in Figure 6.5(c), it has to be taken into account that the tested bottle only had a volume of 1 L. For unattended long-term measurements of the analyzer on SOOP lines, larger volumes of 5 L or more are preferable. Most likely the influence of the headspace is much stronger in a 5 L bottle. Furthermore, the handling of such a big glass bottle on a moving ship is not as straightforward as that of a flexible bags. Consequently, we decided to choose the PVDF gas sampling bag (#1.3) as large-volume storage for the reference seawater.

6.3.2 Cleaning procedure

Previously gained experiences with the analyzer show that a flush with DI-water at the end of a measuring campaign and before longer idle times (more than 48 h) prevents the formation of deposits in the inner tubing and therefore, enhances the long-term stability of the analyzer. It is also recommended by the manufacturer. The automated final flushing phase (see Fig. 6.4) is the easiest way to assure the best conditions for the idle state between two measuring campaigns, i.e. the DI-water remains in the tubing and the system stops until the seawater flow is restarted.

6.3.3 Stabilization measurements

Due to the DI-water in the tubing during idle times, the analyzer shows only a brief initial drift, when the measurements are restarted. Consequently, only a moderate number of stabilization measurements are necessary before the first reference seawater analyses. The number of such measurements mostly depends on how long the previous idle time was. Our first study with the analyzer revealed that the shorter the idle times are, the fewer stabilization measurements have to be carried out (Seelmann et al. 2019). However, this behavior requires that the analyzer continuously measures during the measuring phase. Furthermore, idle

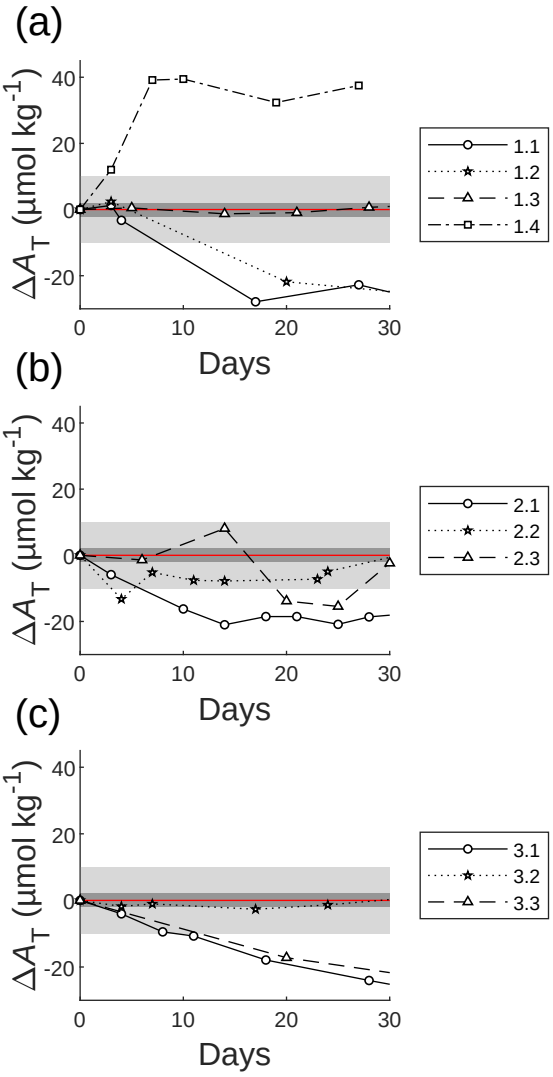

Figure 6.5: Difference between measured A_T after x days and $A_{T,start}$ ($\Delta A_{T,x}$) for each container type as a function of the measurement day x, where (a) shows the gas sampling bags, (b) the infusion bags, and (c) other container types. The numbers in the legend represent each tested container following the numbering in Table 6.1. The horizontal red line in each plot represents $\Delta A_{T,x} = 0$ µmol kg^{-1}. The light gray, and the dark gray areas indicate the ICOS required uncertainty of ± 10 µmol kg^{-1}, and the analyzers typical relative field uncertainty of 0.10 % (equals ± 2.2 µmol kg^{-1} at $A_T = 2215$ µmol kg^{-1}) (Seelmann et al. 2019), respectively.

times of less than 48 h shows no initial drift and a stabilization phase is not needed. As the idle times on our SOOP line are at least seven days, we decided to carry out 30 consecutive underway measurements with a measuring interval of 10 min during the stabilization phase. This high number of measurements includes a safe buffer for even longer idle times guaranteeing stable conditions for subsequent analyses. After the stabilization the measurement routine starts with the reference seawater followed by the measurement cycle (see Fig. 6.4).

6.3.4 Waste handling

Due to the poisoning of the reference seawater with mercury chloride, the waste water has to be collected separately after measurement and properly disposed. The waste from regular underway measurements is unproblematic for the environment and therefore it is disposed with the waste water of the $p(CO_2)$ installation (see Fig. 6.2). As the analyzer has only one outlet, we initially collected the entire waste water in the poisoned waste reservoir, whether it was from reference or underway measurements, and emptied the 100 L canister during port calls in Hamburg, Germany to dispose it properly. But this procedure was too laborious and time consuming. During one month of operation, about 50 L waste water is collected, which results in high emptying frequencies and disposal costs. Consequently, we installed an electrically actuated 3/2-way pinch valve downstream the analyzer's outlet. As long as the system measured underway seawater, the valve is not actuated and the waste water is routed into the regular waste reservoir, which is emptied into the ocean. During reference measurements, the valve is actuated and the waste water is routed to the poisoned waste reservoir. This procedure reduces the volume of the collected hazardous waste water to 2.5 L per month (with daily reference measurements of five consecutive single measurements). Through this waste separation routine, we are able to strongly reduce our maintenance effort during port calls and the disposal costs.

6.3.5 First unattended measurement campaigns

6.3.5.1 Cruise tracks and A_T time-series

Figure 6.6(a) shows the cruise tracks of the first four campaigns on the North Atlantic SOOP line, where the CONTROS HydroFIA® TA analyzer was installed and measured.

To give an overview of the measured A_T values in the monitored region during the first four measuring campaigns, Fig. 6.6(b) shows the A_T vs. the measured longitudes. The red filled circles in both plots on the top represent the A_T value of the discrete samples. Due to problems with the thermosalinograph, the measurement start of the analyzer was delayed during the November 2018 transit. The delayed start in February 2019 was due to a problem with the ship's sea chest. Throughout all campaigns, a total of 1700 A_T measurements were performed by the analyzer at a measurement interval of 15 min.

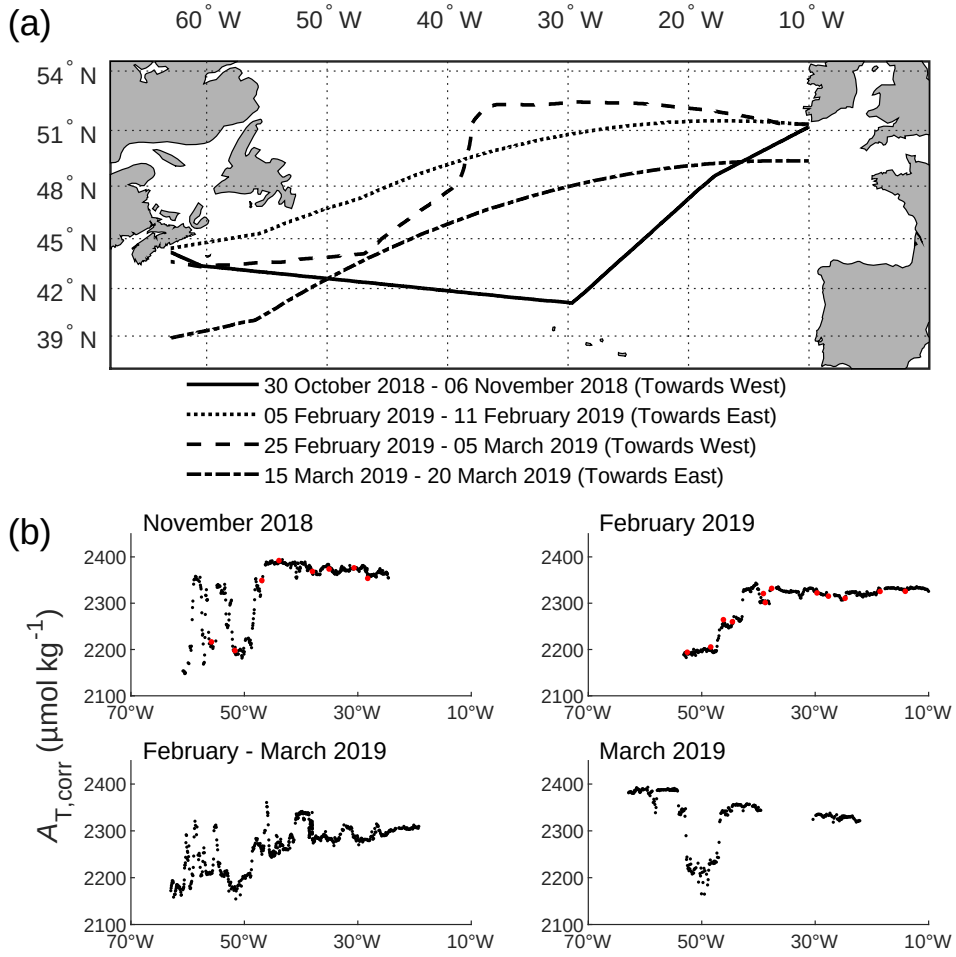

Figure 6.6: (a) Cruise tracks of the first four campaigns on the North Atlantic SOOP line. (b) Corrected A_T values during the first four measuring campaigns as a function of the measured longitudes. Each filled red circle represents the A_T value of a discrete sample taken at a certain time. Both plots on the left are from westward crossings, and both plots on the right are from eastward crossings.

The shown underway A_T values are fully post-processed, which means that the typical drift of the analyzer was corrected for by using the daily reference measurements from the storage bag. The complete correction procedure is not provided here, but can be found in Seelmann et al. (2019). Furthermore, a detailed scientific interpretation of the shown underway data is not part of the report. Here, the main focus lies on the performance assessment of the analyzer in unattended SOOP mode.

6.3.5.2 Data quality

In order to evaluate the accuracy of the A_T values acquired in continuous operation mode with the PVDF gas sampling bag as large-volume reference seawater storage, discrete samples were taken throughout the first two trans-Atlantic crossings (November 2018 and February 2019). Figure 6.7 shows the comparison between the drift-corrected A_T values measured with the CONTROS HydroFIA® TA analyzer and the A_T of discrete samples measured with the reference open-cell titrator VINDTA 3S. The averaged residuals between the two measurement systems were (-0.2 ± 4.7) µmol kg^{-1} for the November 2018 campaign, and (-0.5 ± 4.3) µmol kg^{-1} for the February 2019 campaign. Furthermore, a slightly increasing drift is still visible in both plots, which might be caused by the PVDF gas sampling bag. Although the bag showed stable A_T values under laboratory conditions (see Fig. 6.5), the changing conditions in the ship's engine room appear to deteriorate its ability to stably store the seawater. However, on average the analyzer shows no systematic offset, but the variation around the mean value is less accurate than the typical field accuracy observed during our previous characterization study (-0.3 ± 2.8 µmol kg^{-1}). It must be considered that the latter accuracy determination was based on daily CRM measurements (overall 15 measurements of five consecutive single measurements) using freshly opened CRM bottles each day (Seelmann et al. 2019), and it therefore represents a best case scenario. Furthermore we would like to note that the matching of autonomous underway measurements with data from discrete sampling is a complicated matter especially under conditions of high variable such as in the western part of the region. Imperfect matching inevitably introduces an additional element of noise which cannot be avoided even with greatest care in the matching. The accuracy and its variation is strongly effected by the stability of the CRM, and logically, we expected a slight accuracy deterioration when the CRM is stored in the large-volume PVDF gas sampling bag as compared to the original bottle. The high accuracy requirement ($\leq \pm 2$ µmol kg^{-1}) for standard A_T open-cell titrators described by (Dickson et al. 2007) can only be fulfilled by the mean offsets of -0.2 and -0.5 µmol kg^{-1}. However, the overall uncertainty of the systematic error is deteriorated due to the larger variation of the observed residuals. As long as there is no other stable option for the reference storage during long-term deployments, it must be accepted that the uncertainty of the possible bias is extended compared to freshly opened CRM bottles.

Throughout all measurement campaigns, the short-term precision of the analyzer

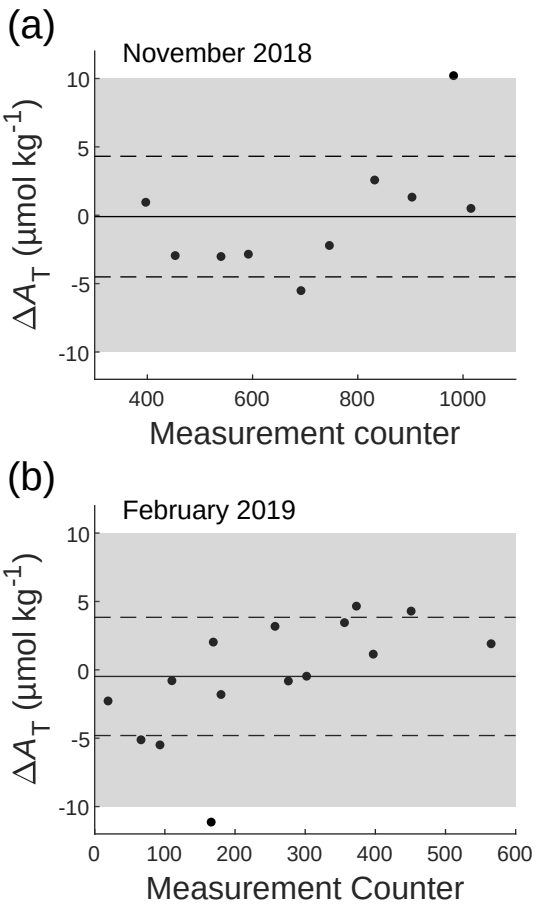

Figure 6.7: Residuals of the intercomparison of A_{T} measurements between the CONTROS HydroFIA® TA (drift corrected values) and the reference open-cell titrator (VINDTA 3S) for (a) the November 2018, and (b) the February 2019 transit. The horizontal black solid line indicates the averaged bias, $\overline{\Delta A_{\mathrm{T}}}$, and the horizontal black dashed lines indicate $\overline{\Delta A_{\mathrm{T}}} \pm \sigma$. The gray area represents the uncertainty of $\pm$ 10 µmol kg^{-1} required by ICOS.

(standard deviation of the consecutive reference measurements) exhibits the typical field precision of ± 1.1 µmol kg^{-1} found during our previous characterization study. Therefore, the usage of the PVDF gas sampling bag as large-volume reference seawater storage does not affect the random error of the measurements. For this reason we do not show any further precision evaluation here.

We can conclude that the quality of the A_T data achievable with our SOOP line installation is mostly affected by the reference seawater storage. The usage of a the PVDF gas sampling bag appears to introduce a small additional uncertainty by a slightly increasing drift while not affecting the short-term precision. Furthermore, on average, no systematic offset is introduced by the reference material storage. The entire data quality (accuracy and precision) provided by the installed analyzer fulfills the uncertainty criteria of ± 10 µmol kg^{-1} for ship-based A_T measurements on ICOS stations.

6.3.5.3 Comparison with A_T parameterization and its limits

In order to evaluate the consistency between the A_T data measured with the installed analyzer and the typical A_T range and variability in the monitored region, we compare the measured A_T values to A_T predicted from sea surface salinity (SSS) and sea surface temperature (SST) values using the parameterization of Lee et al. (2006). For the North Atlantic, the prediction follows the equation

$$\begin{aligned} A_{T,pred} = 2305 + 53.95 \times (SSS - 35) + 2.74 \times (SSS - 35)^2 - \\ 1.16 \times (SST - 20) - 0.040 \times (SST - 20)^2 \end{aligned} \quad (6.1)$$

which is valid between the latitudes 30 °N and 80 °N, for the SST range 0 °C to 20 °C, and for the SSS range 31 to 37. Hence, only A_T values measured within these ranges are compared with the respective predicted values.

The consistency is estimated by calculating the root mean square error (RMSE) following

$$RMSE = \sqrt{\frac{\sum_{i=1}^{n} (A_{T,corr,i} - A_{,pred,i})^2}{n}} \quad (6.2)$$

where n is the number of A_T measurements.

Figure 6.8 shows the results of the comparison by plotting the drift-corrected A_T values measured with the analyzer ($A_{T,corr}$) vs. the predicted A_T values ($AT_{,pred}$). The resulting linear correlations include the uncertainties of $A_{T,corr}$ and $A_{T,pred}$ using the MATLAB™ script provided by Thirumalai et al. (2011) based on the statistical method described by York et al. (2004).

Throughout all measuring campaigns, the correlation between $A_{T,corr}$ and $A_{T,pred}$ is not fully satisfactory with a slope of (0.981 ± 0.003) and an intercept of (41 ± 8). A perfect correlation would result in a slope of 1 and an intercept of 0 within their uncertainties. The four single campaigns show similar results (see Fig. 6.8). The average RMSE for all campaigns is estimated at ± 12.3 µmol kg^{-1}, and is therefore not satisfactory, too. However, the intercomparison with discrete samples confirms

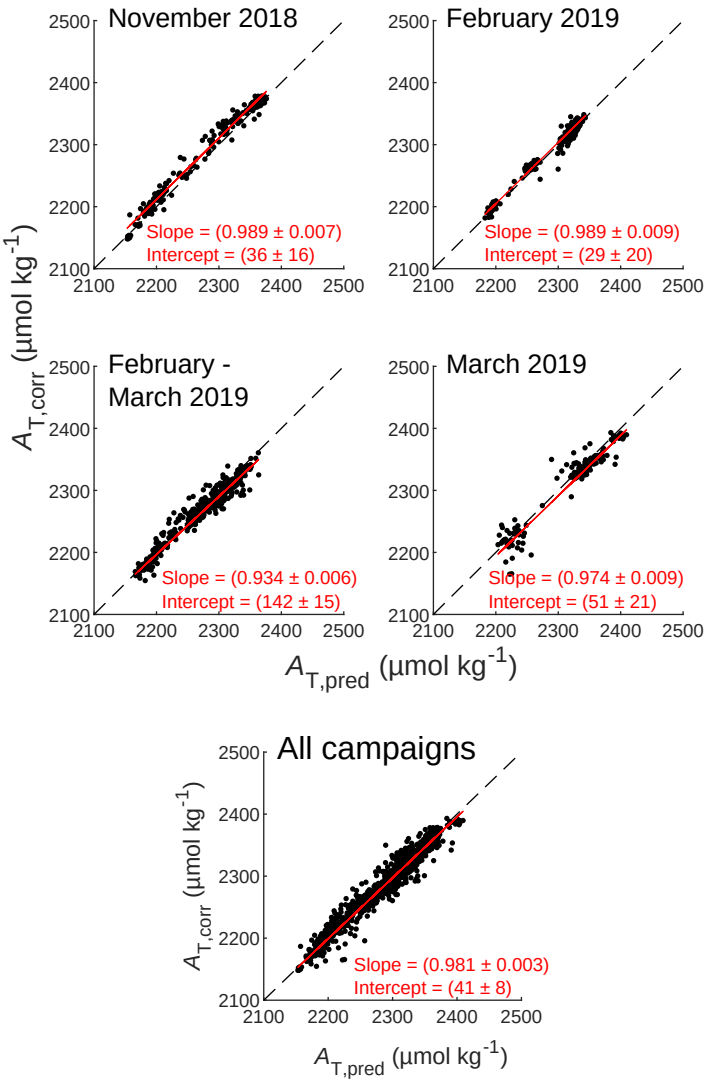

Figure 6.8: A_{T} values (after drift correction) measured by the analyzer ($A_{\mathrm{T,corr}}$) as a function of the predicted A_{T} values ($A_{\mathrm{T,pred}}$) using the established parameterization described by Lee et al. (2006) for each measuring campaign, and for all campaigns together. The black dashed lines indicate the 1-to-1 line of the plot. The red solid lines represent the linear correlation between $A_{\mathrm{T,corr}}$ and $A_{\mathrm{T,pred}}$ with their slopes and intercepts given in each plot.

the sufficient accuracy of the data, which means that these biases must be due to other reasons.

In order to discover these reasons, we compare our data set with the Global Data Analysis Project v1.1 (GLODAP) (Key et al. 2004) from 1990 to 1998, which was used by (Lee et al. 2006) for deriving their parameterization. Figure 6.9 shows this comparison, which reveals the fundamental limits of the used parameterization and, hence, possible reasons for the observed biases:

1. Spatial bias: The comparison of the spatial distribution of both data sets in the North Atlantic (see Fig. 6.9(a)) reveals that the GLODAP data set has an underrepresented area (38 °N – 50 °N, 35 °W – 65 °W), which includes about 60 % of our measured A_T values. Two major currents meet in this region: The warm and salty North Atlantic Current from the Southwest, and the cold and fresh Labrador Current from the North. Hence, this significant mixing area is not adequately represented in the parameterization by Lee et al. (2006), which may lead to biases. Another direct consequence is that values of $2100<A_T<2300$ µmol kg^{-1}, and 31<SSS<34.5 are also underrepresented in the parameterization due to the missing influence of the cold and fresh Labrador Current (see Fig. 6.9(b)), although Lee et al. (2006) confirmed a SSS validity from 31 to 37.

2. Temporal bias: Due to the fact that the parameterization is based on data from between 1990 and 1998, any changes in SSS and SST caused by e.g. global warming over the last decades are not considered. SSS and SST changes may influence the relationships between SSS, SST and A_T and therefore, the corresponding parameterization coefficients.

3. Seasonal bias: Figure 6.9(b) shows the comparison of the months, when the A_T values were measured. Clear most of the A_T data used by Lee et al. (2006) were acquired during spring and summer times, whereas our data were measured during fall and winter times. Throughout the year, different biogeochemical processes take place in the surface ocean affecting the A_T i.a. $CaCO_3$ formation during summer. As most of the parameterization data were acquired during summer, the influence of such processes may not apply to winter times, and vise versa, which may lead to biases.

Figure S6.2 in the Supplementary Material of this report shows the residuals between the measured A_T values ($A_{T,corr}$) and the predicted A_T values ($A_{T,pred}$) over the cruise tracks of the trans-Atlantic crossings, and as a function of SSS and SST. There, the spatial and seasonal biases are pointed out in particular. However, a detailed discussion of these residuals is not part of this report, as it only forms the explanation basis for the biased A_T comparison.

The not fully perfect agreement between our SOOP-based A_T observations and A_T predictions points at regional and seasonal limitations in the GLODAP database which can lead to biases in A_T predicted by parameterizations based

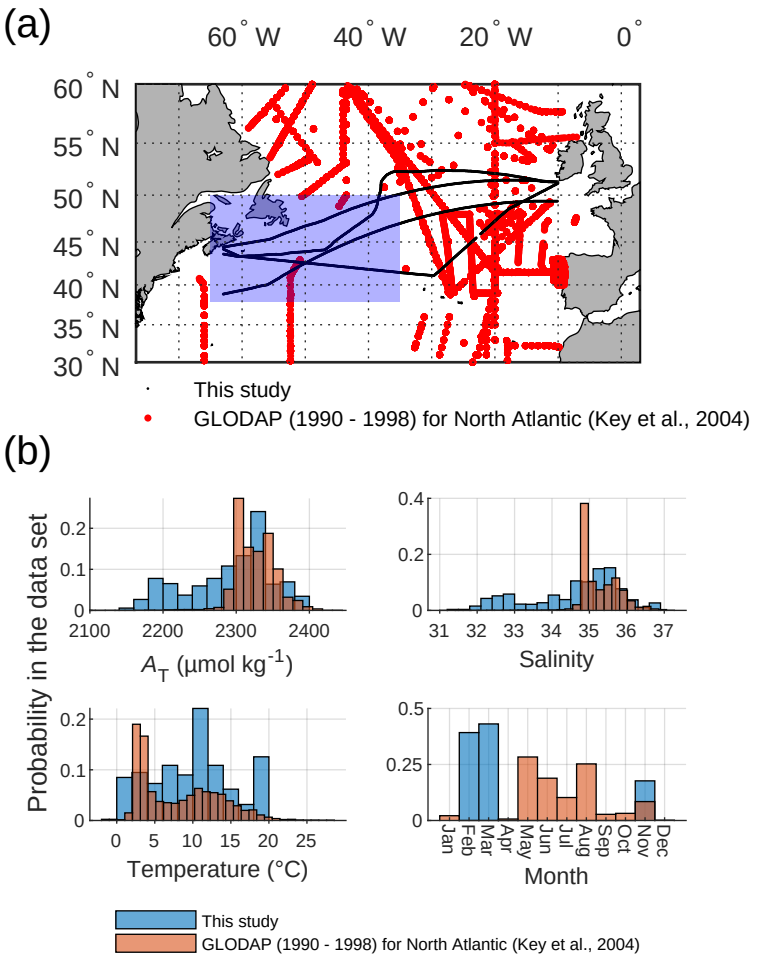

Figure 6.9: (a) Spatial distribution of our measured data (black) and the GLODAP data set between 1990 and 1998 (red) for the North Atlantic (30°N – 60°N). The blue patch represents the area, which is underrepresented in the parameterization by Lee et al. (2006). (b) Histograms of observations of A_T, salinity, temperature, and month of observation in the data set of this study (blue) and the GLODAP data set (orange).

on GLODAP such as that by Lee et al. (2006). This points at the need better spatiotemporal coverage of surface ocean A_T observations, which are now possible with the method described here. Future work will aim at a new regional SSS and SST based A_T prediction scheme based on the data sets provided by our North Atlantic SOOP line (see Sect. 6.5).

6.4 Summary

In this study, we present a ship-board installation scheme for autonomous underway A_T measurements using the novel CONTROS HydroFIA® TA analyzer on a Ship of Opportunity operating in the North Atlantic Ocean. The here described setup addresses the major issues arising from autonomous A_T measurements using this analyzer: 1) Regular reference measurements including the provision of sufficient CRM volume, 2) an automated DI-water flushing routine before idle times, 3) stabilization measurements at the beginning of a measuring campaign, and 4) separation of the waste water depending on underway or reference measurements.

Stability tests with different large-volume container types used as reference seawater storage revealed that the inner material of the container can strongly influence the long-term A_T stability. Synthetic materials like PE, PP or EVA were found not suitable as they reduce the A_T value by most likely contaminating the seawater with unknown chemical compounds. Borosilicate glass bottles, which are used as CRM bottles with a volume of 500 mL, seem to be a stable alternative, but due to their inflexible character, there could be problems with the increasing headspace in the bottle, especially with larger volumes over 5 L or more. The only promising container was a 5 L gas sampling bag made of PVDF. During a test period of 30 days, the seawater A_T on average only varied by (0.2 ± 1.3) µmol kg^{-1}. The bag therefore was deemed suitable as long-term reference seawater storage. Throughout all presented measurement campaigns on the SOOP, this bag was used for reference measurements.

The automated cleaning and waste separation procedures can be easily implemented by using electrically actuated 3/2-way pinch valves and a control software sending and receiving respective serial commands. The stabilization phase after idle times is set to 30 consecutive underway measurements and also implemented in the software. We conclude that all previously observed issues can be solved by our installation.

The success of the autonomous A_T measurement implementation on our SOOP line was verified by intercomparison with measurements performed by a reference open-cell titrator. During the first two campaigns, the overall agreement between the autonomous A_T measurements and the reference system was (-0.2 ± 4.7) µmol kg^{-1} (November 2018) and (-0.5 ± 4.3) µmol kg^{-1} (February 2019). Although the variation around the bias slightly deteriorates in comparison to the typical accuracy of (-0.3 ± 2.8) µmol kg^{-1} observed when using freshly opened CRM bottles, the analyzer still meet the uncertainty requirement of ± 10 µmol kg^{-1} for ship-based

ICOS stations. The deterioration of the systematic error variation was most likely due to the usage of the large-volume CRM storage instead of freshly opened CRM bottles. However, the random error of the analyzer was not affected by this and still featured the typical precision of $\pm$ 1.1 µmol kg^{-1}.

A comparison with predicted A_T values based on a established parameterization revealed biases between measured and predicted A_T values. These biases are mostly due to imperfect spatiotemporal coverage in the GLODAP data set used in establishing the parameterization. This points at the need better spatiotemporal coverage of surface ocean A_T observations like our installation on the North Atlantic SOOP line presented in this study.

Summing up, we can say that the implementation of the novel autonomous A_T analyzer CONTROS HydroFIA® TA on a commercial SOOP line was fully successful. The achieved A_T values are in full agreement with the ICOS quality requirements and therefore, in combination with $p(CO_2)$, perfectly usable for the characterization and long-term observation of the marine carbon system. This novel technology makes much improved spatiotemporal coverage of surface ocean A_T from the Carbon-SOOP network now possible.

6.5 Future work

As soon as we have collected enough data from our SOOP line (minimum one year of semi-continuous measurements), we want to evaluate the possibilities of establishing a A_T parameterization similar to the one described by Lee et al. (2006). Their SSS and SST fitting was based on 326 data points in the North Atlantic collected between 1990 and 1998 during spring and summer times. Our future parameterization would be based on about 12000 A_T data points from one full year with very good spatial coverage of the North Atlantic, and could be expanded by more data afterwards. Furthermore, there will be the possibility to include seasonal variability into the calculation scheme as we measure A_T throughout the year.

6.6 Acknowledgments

This research was supported by the European Horizon 2020 projects "AtlantOS" (#633211) and "RINGO" (#730944), the project "ICOS-D" (#01LK1224J) of German Federal Ministry of Education and Research, and the project “Digital Earth” of the Initiative and Networking Fund of the Helmholtz Association.

We thank the captains and crew of the M/V *Atlantic Sail* for their continuing support. Furthermore, we thank the shipping company "Atlantic Container Line" (ACL) for cooperation and the permission to install our scientific instruments on their ship and perform our measurements. We also thank the following companies for providing us free of charge test containers: "IMPROMEDIFORM GmbH" (Germany), "Meissner Filtration Products" (USA), "Olfasense GmbH" (Germany), "Restek Corporation" (USA), "Sense Trading" (Netherlands), and "SKC Ltd." (UK).

6.7 Appendix: Supplementary Material

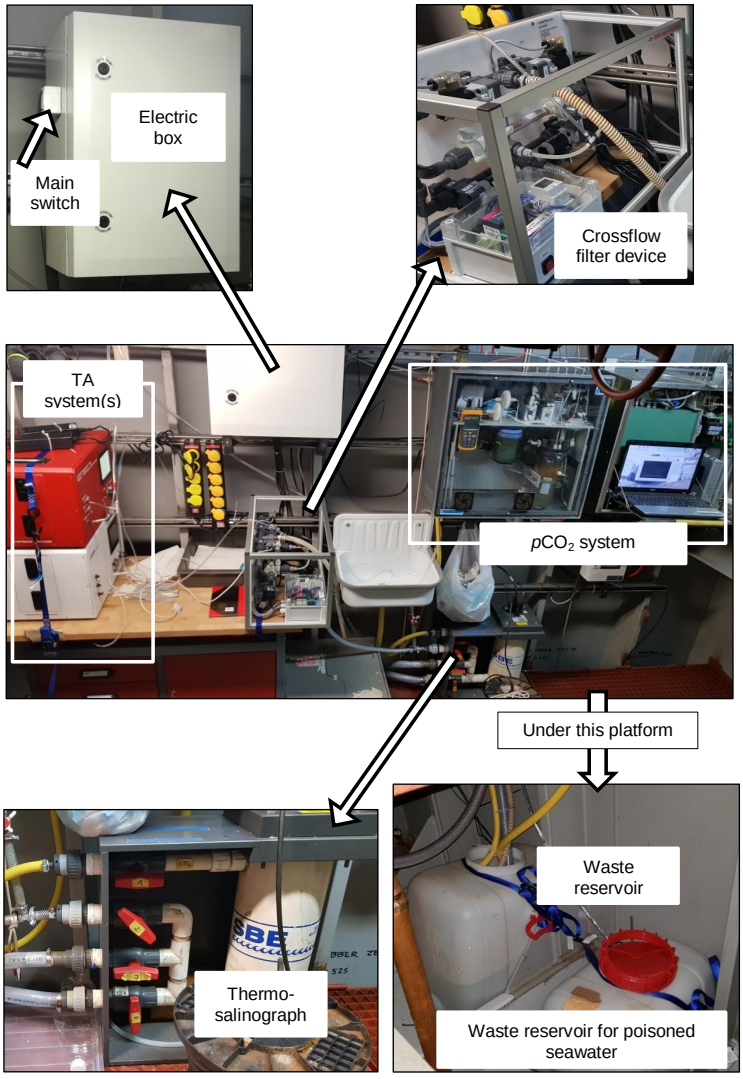

Figure S6.1: Photos of the onboard system

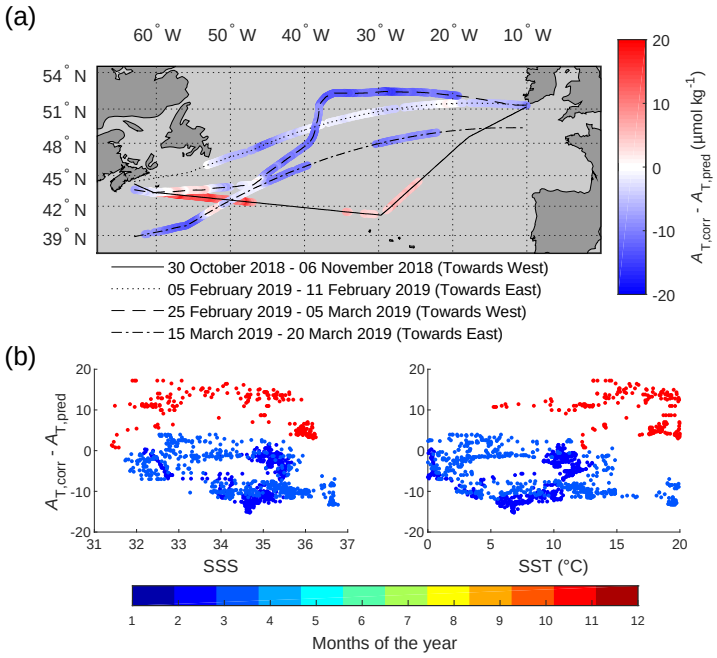

Figure S6.2: (a) Residuals between the measured A_{T} values ($A_{\mathrm{T,corr}}$) and the predicted A_{T}values ($A_{\mathrm{T,pred}}$) using the parameterization by Lee et al. (2006) over the cruise tracks of the campaigns of the North Atlantic SOOP line. (b) Residuals as a function of the SSS, and SST. The colors of the data points represent the month, when the measurements took place.

References

Bakker, D. C. E., B. Pfeil, C. S. Landa, N. Metzl, K. M. O'Brien, and others. **2016**. A multi-decade record of high-quality fCO_2 data in version 3 of the Surface Ocean CO_2 Atlas (SOCAT). Earth System Science Data. 8: 383–413, doi: 10.5194/essd-8-383-2016

Dickson, A. G., C. L. Sabine, and J. R. Christian. **2007**. Guide to best practices for ocean CO_2 measurements. PICES Special Publications 3.

Friedlingstein, P., M. W. Jones, M. O'Sullivan, R. M. Andrew, J. Hauck, and others. **2019**. Global Carbon Budget 2019. Earth System Science Data. 11: 1783–1838, doi: 10.5194/essd-11-1783-2019

Gruber, N., D. Clement, B. R. Carter, R. A. Feely, S. van Heuven, and others. **2019**. The oceanic sink for anthropogenic CO_2 from 1994 to 2007. Science. 363: 1193–1199, doi: 10.1126/science.aau5153

ICOS Ocean Thematic Centre. **2020**. ICOS Ocean Station Labelling Step 2. doi: 10.18160/8SDC-K4FR

Keeling, R. F., A. Körtzinger, and N. Gruber. **2010**. Ocean Deoxygenation in a Warming World. Annual Review of Marine Science. 2: 199–229, doi: 10.1146/annurev.marine.010908.163855

Key, R. M., A. Kozyr, C. L. Sabine, K. Lee, R. Wanninkhof, and others. **2004**. A global ocean carbon climatology: Results from Global Data Analysis Project (GLODAP). Global Biogeochemical Cycles. 18: GB4031, doi: 10.1029/2004GB002247

Lee, K., L. T. Tong, F. J. Millero, C. L. Sabine, A. G. Dickson, and others. **2006**. Global relationships of total alkalinity with salinity and temperature in surface waters of the world's oceans. Geophysical Research Letters. 33: L19605, doi: 10.1029/2006GL027207

Manning, A. and R. F. Keeling. **2006**. Global oceanic and land biotic carbon sinks from the Scripps atmospheric oxygen flask sampling network. Tellus B: Chemical and Physical Meteorology. 58: 95–116, doi: 10.1111/j.1600-0889.2006.00175.x

Millero, F. J., K. Lee, and M. Roche. **1998**. Distribution of alkalinity in the surface waters of the major oceans. Marine Chemistry. 60: 111–130, doi: 10.1016/S0304-4203(97)00084-4

Newton, J., R. Freely, P. Williamson, and J. Mathis. **2015**. Global Ocean Acidification Observing Network: Requirements and Governance Plan, 2nd Ed. GOA-ON.

Pfeil, B., A. Olsen, D. C. E. Bakker, S. Hankin, H. Koyuk, and others. **2013**. A uniform, quality controlled Surface Ocean CO_2 Atlas (SOCAT). Earth System Science Data. 5: 125–143, doi: 10.5194/essd-5-125-2013

Pierrot, D., C. Neill, K. Sullivan, R. Castle, R. Wanninkhof, and others. **2009**. Recommendations for autonomous underway pCO_2 measuring systems and data-reduction routines. Deep Sea Research Part II: Topical Studies in Oceanography. 56: 512–522, doi: 10.1016/j.dsr2.2008.12.005

Riebesell, U., A. Kortzinger, and A. Oschlies. **2009**. Sensitivities of marine carbon fluxes to ocean change. Proceedings of the National Academy of Sciences. 106: 20602–20609, doi: 10.1073/pnas.0813291106

Seelmann, K., S. Aßmann, and A. Körtzinger. **2019**. Characterization of a novel autonomous analyzer for seawater total alkalinity: Results from laboratory and field tests. Limnology and Oceanography: Methods. 17: 515–532, doi: 10.1002/lom3.10329

Steinhoff, T., T. Gkritzalis, S. K. Lauvset, S. Jones, U. Schuster, and others. **2019**. Constraining the Oceanic Uptake and Fluxes of Greenhouse Gases by Building an Ocean Network of Certified Stations: The Ocean Component of the Integrated Carbon Observation System, ICOS-Oceans. Frontiers in Marine Science. 6: 544, doi: 10.3389/fmars.2019.00544

Takahashi, T., S. C. Sutherland, R. Wanninkhof, C. Sweeney, R. A. Feely, and others. **2009**. Climatological mean and decadal change in surface ocean pCO_2, and net sea–air CO_2 flux over the global oceans. Deep Sea Research Part II: Topical Studies in Oceanography. 56: 554–577, doi: 10.1016/j.dsr2.2008.12.009

Thirumalai, K., A. Singh, and R. Ramesh. **2011**. A MATLAB™ code to perform weighted linear regression with (correlated or uncorrelated) errors in bivariate data. Journal of the Geological Society of India. 77: 377–380, doi: 10.1007/s12594-011-0044-1

Voynova, Y. G., W. Petersen, M. Gehrung, S. Aßmann, and A. L. King. **2019**. Intertidal regions changing coastal alkalinity: The Wadden Sea-North Sea tidally coupled bioreactor. Limnology and Oceanography. 64: 1135–1149, doi: 10.1002/lno.11103

Wanninkhof, R., P. A. Pickers, A. M. Omar, A. Sutton, A. Murata, and others. **2019**. A Surface Ocean CO_2 Reference Network, SOCONET and Associated

Marine Boundary Layer CO_2 Measurements. Frontiers in Marine Science. 6: doi: 10.3389/fmars.2019.00400

York, D., N. M. Evensen, M. L. Martínez, and J. De Basabe Delgado. **2004**. Unified equations for the slope, intercept, and standard errors of the best straight line. American Journal of Physics. 72: 367–375, doi: 10.1119/1.1632486

Chapter 7

Conclusions and outlook

7.1 Conclusions

The goal of this thesis was to successfully implement a novel autonomous analyzer for seawater total alkalinity (A_T) on a Ship of Opportunity (SOOP) station, which provides high-spatiotemporal A_T data of required quality in unattended mode. This goal is motivated by the necessity to better understand the responses of the natural marine carbon cycle to ongoing and future global changes like warming, acidification or deoxygenation, for which two out of the four measurable carbonate variables are necessary. As unattended CO_2 partial pressure ($p(CO_2)$) measurements on SOOP stations are well established and often conducted, the second measurable variable has to be one of the remaining three: dissolved inorganic carbon (C_T), A_T or pH. There were three major reasons for choosing A_T and the CONTROS HydroFIA® TA analyzer: 1) There is no autonomous analyzer for C_T available (to our knowledge), 2) the measured variable combination $p(CO_2)$-pH leads to higher uncertainties in the marine carbonate chemistry calculation then $p(CO_2)$-A_T, and 3) the CONTROS HydroFIA® TA was (and still is) the only available underway analyzer for A_T. Furthermore, its design and development is based on a previous dissertation carried out in our working group (Aßmann 2012).

Based on the results of this thesis, the main research questions raised in Chapter 2 can be answered as follows:

1. **Can the CONTROS HydroFIA® TA provide high-quality A_T data under laboratory and field conditions, which meet fundamental quality requirements?**

   In order to evaluate the performance of the CONTROS HydroFIA® TA analyzer, both laboratory and field measurements were carried out. For the field experiments, we participated in two major research cruises across the South Atlantic, and from the eastern North Atlantic to the eastern subtropical Atlantic, where the A_T measurements were fully supervised and attended by us. In order to evaluate, whether the measurement quality of the analyzer is suitable for underway A_T measurements in the open ocean, we compared the results with fundamental quality targets: 1) The "Guide to best practices for Ocean CO_2 measurements" by Dickson et al. (2007), which requires a precision of ± 1 µmol kg^{-1} and an overall bias of ± 2.0 µmol kg^{-1}

for standard open-cell titrators, and 2) The "Global Ocean Acidification Observing Network: Requirements and Governance Plan" by Newton et al. (2015), which requires an uncertainty of ± 10 µmol kg^{-1} as "weather" goal (to identify relative spatial patterns and short-term variations) and ± 2 µmol kg^{-1} as "climate" goal (to assess long-term trends with a defined level of confidence), respectively.

The performance under laboratory conditions was evaluated by using a standard addition experiment. This experiment revealed a precision (standard deviation, σ) of ± 1.5 µmol kg^{-1}, a bias (root mean square error) of ± 1.0 µmol kg^{-1} and an uncertainty of (1.6 – 2.0) µmol kg^{-1} (working range of 2000 – 2450 µmol kg^{-1}).

The performance under field conditions was evaluated by regular measurements of Certified Reference Material (CRM) and the intercomparison with discrete samples, which were measured with a potentiometric A_T titrator (VINDTA 3S, Marianda, Germany) in the home laboratory. This experiments revealed a precision (standard deviation, σ) of ± 1.1 µmol kg^{-1}, a bias (ΔA_T) of (-0.3 ± 2.8) µmol kg^{-1} and an uncertainty of (2.0 – 2.5) µmol kg^{-1} (working range of 2000 – 2450 µmol kg^{-1}).

While the CONTROS HydroFIA® TA analyzer reached the bias requirement for standard open-cell titrators provided by Dickson et al. (2007) both in the laboratory and in field, the precision requirement could not be completely met, but the analyzers precision was still in favorable comparison to the standard A_T titration methods. Furthermore, uncertainty approximations both in the laboratory and in field were in full agreement with the "weather" goal required by Newton et al. (2015) for ocean acidification observations. The very high requirement of the "climate" goal was achieved in the laboratory and almost be achieved in the field by being only 0.5 µmol kg^{-1} higher than the target of 2 µmol kg^{-1}.

A very important outcome of the performance characterization was that the analyzer appears to show a linear offset drift to higher A_T values caused by unavoidable colored deposits in the optical pathway of the system. This drift must be accepted as typical behavior of the CONTROS HydroFIA® TA, but can be easily corrected for by regular CRM or other standard measurements due to its linear character to achieve the required accuracy.

In conclusion, the raised research question stated above can be answered as follows: Yes, the CONTROS HydroFIA® TA provides high-quality A_T data both under laboratory and field conditions, which meet fundamental quality requirements, provided that regular reference measurements are carried out for subsequent drift correction in order to achieve the accuracy requirements.

Other important outcomes of this thesis part were:

1) An Overlapping Allan experiment revealed, that regular CRM measurements must consist of 3 – 6 repetitive measurements in order to avoid statistical noises or long-term drift effects.

2) Regular reference measurements enabled malfunction detection without the need to perform manual functionality checkups of single components.

3) The very good performance of the analyzer was still maintained at higher pH ranges (4.0 – 4.5) of the acidified sample. There, the measurements became more precise, but less accurate, which may be useful for regions, where small A_T changes needs to be detected. However, it is not recommended to measure at pH values higher than 4.5 due to the detection limit of the spectrophotometer.

4) DI-water flushes, which are recommended before idle times of the analyzer, did not affect the stability of the measurements after this idle time as long as it is not longer than 48 hours.

5) A long-term precision experiment revealed that 6.2 % of the measurements were outliers showing always clearly higher A_T values than the regular data, which could be useful for outlier removal algorithms.

Based on the outcomes of this part, we provided recommendations for automated long-term deployments of the CONTROS HydroFIA® TA analyzer (see Sect. 4.7) in order to gain the optimal performance characteristics.

2. **Do impurities in the used indicator dye bromocresol green (BCG) affect the measurements with the CONTROS HydroFIA® TA? Will the usage of purified BCG improve the measurement quality?**

   In order to evaluate the influences of impurities in the indicator dye BCG, we developed an high-performance liquid chromatography (HPLC) method for analyzing and purifying the dye. An analytical HPLC of BCG from four different vendors revealed different impurity types and quantities. The purity grades of the unpurified dyes ranged from 85.4 % up to 98.1 % (gained with the showed method). A purification increased the purity grade up to 99.6 % by removing mostly all of the impurities, which demonstrated the success of the purification method development.

   Laboratory long-term A_T measurements with the CONTROS HydroFIA® TA using both unpurified and purified BCG dyes revealed a direct influence of the impurity types and quantities on the drift behavior of the analyzer. The purer the BCG, the smaller was the A_T increment per measurement, but the drifting could not be fully overcome. Hence, BCG purification appeared to significantly reduce but not completely eliminate the observed system drift. Another important outcome of these experiments was that BCG dyes containing a certain impurity (retention time $\approx$ 58 :min) showed a nonlinear drift pattern,

which can impair long-term deployments of the analyzer. Consequently, such indicator dyes are impractical for the CONTROS HydroFIA® TA.

Laboratory standard addition experiments for performance characteristics revealed no significant improvement of the measurement quality by using purified BCG in comparison to unpurified BCG with an impurity quantity of not more than 2 %. However, BCG dyes with impurity quantities of more than 6 % provided A_T measurements which failed fundamental quality requirements.

In conclusion, the raised research questions stated above can be answered as follows: Yes, impurities in the indicator dye BCG affect the measurements with the CONTROS HydroFIA® TA, especially its drift behavior. The effects depend on the types and quantities of the containing impurities. However, high-quality A_T measurements do not require purified BCG but the purest BCG dye (purity grade $\geq$ 98 %) that is purchasable.

Users of the CONTROS HydroFIA® TA should take these facts into account by purchasing the indicator dye for their BCG solution. If applicable, an HPLC analysis of the purchased dye following the developed methodology described in Sect. 5.2.1.2 would be the preferred approach to the test the BCG purity and avoid a possible loss of analytical performance. If an HPLC analysis is not possible, the compatibility of the purchased dye can be easily tested by applying the laboratory long-term experiment explained in Sect. 5.2.2.2. By following the recommendations provided in this study, the CONTROS HydroFIA® TA can provide high-quality A_T data meeting fundamental quality requirements even by using unpurified BCG dye.

3. **What needs to be considered for a successful implementation of the CONTROS HydroFIA® TA analyzer on a Ship of Opportunity in unattended measurement mode? Can the installed system provide high-quality A_T data meeting fundamental quality requirements?**

   The last part of this thesis dealt with the installation of the CONTROS HydroFIA® TA analyzer on a Ship of Opportunity (SOOP) line operating in the North Atlantic. In order to gain high-quality A_T measurements in unattended measurement mode, several issues had to be addressed. Finally, the success of the implementation was verified by an intercomparison with discrete samples. Furthermore, a comparison with predicted A_T values using an often used and established parameterization (Lee et al. 2006), which represents the so far common way of providing a second carbonate variable for the characterization of the oceanic carbon chemistry, was conducted. This should verify, if there is a real need of autonomous A_T measurements or if the predicted A_T values are still sufficient.

The most important conclusion of the first part of this thesis was that the analyzer needs regular (ideally daily) reference measurements in order to correct its drift and, therefore, achieve fundamental quality requirements. During long-term deployments, this procedure needs large volumes of reference seawater, which cannot be provided by the standard 500 mL CRM bottles. We tested several large volume ($\geq$ 5 L) container types on their suitability to store seawater over a long time period (min. 30 days) without significant changes in A_T. Only a 5 L gas sampling bag made of polyvinylidene fluoride (PVDF) satisfied the stability requirements with an averaged A_T variation of (0.2 $\pm$ 1.3) µmol kg^{-1} after 30 days.

Other issues, which needs to be considered during unattended long-term deployments, were the cleaning of the system before idle times, stabilization measurements after idle times (longer than 48 hours) and the waste separation between the measured reference seawater and the measured underway seawater. The cleaning procedure and the waste handling could be easily solved by installing electrically actuated 3/2-way pinch valves before the inlet and downstream the outlet of the analyzer, respectively. A permanently running script written in Python controlled these valves. Furthermore, it conducted the stabilization measurements after idle times. The whole A_T measurement workflow controlled by the script is illustrated in Fig. 6.4 (page 112).

Afterwards the system was installed on the ship with all named issues considered, discrete samples were taken during the first two unattended campaigns (November 2018 and February 2019) and measured in the home laboratory. The comparison of the fully post-processed A_T data measured in unattended mode with the A_T values of the discrete samples revealed averaged residuals of (-0.2 $\pm$ 4.7) µmol kg^{-1} for November 2018, and (-0.5 $\pm$ 4.3) µmol kg^{-1} for February 2019. Compared to the results from the first part of this thesis, the measurement accuracy in unattended mode slightly deteriorated, which was due to the usage of the large-volume reference seawater container. During the first performance characterization, freshly opened CRM bottles were used for reference measurements, which represented a best-case-scenario. Hence, a slight deterioration of the measurement quality was expectable when using the large-volume container. However, the uncertainty of the system fulfilled the requirements for A_T measurements on SOOP stations provided by the European research infrastructure "Integrated Carbon Observation System" (ICOS) (ICOS Ocean Thematic Centre 2020), which is based on the "weather" goal of $\pm$ 10 µmol kg^{-1}described by Newton et al. (2015).

In conclusion, the raised research questions stated above can be answered as follows: For a successful implementation of the CONTROS HydroFIA® TA on a SOOP line, four major issues must be considered: 1) Provision of enough (min. 5 L) reference seawater volume for regular reference measurements, 2) automated cleaning procedure before idle times, 3) stabilization mea-

surements after idle times longer than 48 hours, and 4) automated waste separation between reference and underway seawater. These implementations are explained in detail in the last part of this thesis. By following these recommendations, the installed system can provide high-quality A_T data in unattended mode, which meet fundamental uncertainty requirements for SOOP lines.

Another important conclusion of the last part of this thesis resulted from the comparison with predicted A_T values (Lee et al. 2006). We encountered a not fully perfect agreement between our SOOP-based A_T observations and the predicted A_T (root mean square error = $\pm$ 12.3 µmol kg^{-1}). A comparison of our data set and the Global Data Analysis Project v1.1 (GLODAP) (Key et al. 2004) from 1990 to 1998, which was used by Lee et al. (2006) for deriving their parameterization, revealed the fundamental limitations of such A_T predictions due to spatial, temporal and seasonal biases. This result particularly points out that surface ocean A_T observations of better spatiotemporal coverage as it is provided by our SOOP-based installation are of utmost need.

The overall results of this thesis has shown that high-quality A_T measurements with the novel autonomous analyzer CONTROS HydroFIA® TA are totally possible. This study provides recommendations for its general usage in the laboratory and in field, for the right handling with the indicator dye BCG, and, finally, for its implementation on a Carbon-SOOP station in order to fulfill fundamental quality requirements. But these results themselves are not a fully answer to the overarching research question. As a reminder, the overarching research question of this thesis was:

Are autonomous, high-quality A_T measurements on a Carbon-SOOP station an enhancement of ocean carbon observations?

The answer was already given by the comparison of the SOOP-based A_T data with predicted A_T values using the established parameterization provided by Lee et al. (2006). This parameterization is often used by the oceanographic community to predict A_T values from sea surface salinity (SSS) and sea surface temperature (SST) data as a second carbonate variable. In the last part of this thesis, we could show that this A_T prediction is prone to spatial, temporal and seasonal biases due to the usage of the GLODAPv1.1 data set. Consequently, by using this A_T prediction as second carbonate variable, there could be the risk of misinterpretations of the resulting oceanic carbon chemistry due to these biases, e.g. because of the missing SSS and SST changes since 1998. Furthermore, the significant mixing area of the warm and salty North Atlantic Current from the Southwest, and the cold and fresh Labrador Current from the North ($\approx$ 38 °N – 50 °N, $\approx$ 35 °W – 65 °W) was not adequately represented in the data set, which was used for deriving the parameterization (see Fig. 6.9(a), page 123). This could lead to biased ocean carbon

chemistry calculations in this certain area and, therefore, misinterpretations. In contrast, our SOOP-based measurements provide high-quality A_T data with highly spatial coverage of the subpolar North Atlantic (between ≈ 38 °N and 54 °N, and between ≈ 10 °W and 65 °W) over the entire year. Consequently, seasonal variations in surface ocean A_T are detectable. Every month, approximately 1000 A_T data points are collected.

In conclusion, compared with the so far common way to provide a second carbonate variable for oceanic carbon chemistry calculations, the overarching research question of this thesis can be answered as follows: Yes, autonomous, high-quality A_T measurements on a Carbon-SOOP station are a great enhancement of ocean carbon observations.

Of course, it is unquestionable that the shown results and conclusions of this thesis are only valid for a very restricted area in the North Atlantic Ocean. However, it is also unquestionable that the observed fundamental limitations of the A_T predictions are a global issue and not restricted to the certain area shown in this study. Consequently, this thesis aims to be a blueprint for other Carbon-SOOP operators in order to better statiotemporally cover the surface ocean A_T worldwide. In the hopefully near future, this would be the real enhancement of ocean carbon observations.

7.2 Outlook

Future work will certainly aim at the continuation of the SOOP-based A_T measurements together with $p(CO_2)$ observations. With these two sets of carbonate variable data we will be able to both calculate the CO_2 flux and fully characterize the marine carbonate chemistry in surface waters of the monitored region. This will lead to fundamental knowledge about how the natural oceanic carbon cycle will response to anthropogenic CO_2 emissions.

Secondly, as soon as we have collected enough data from the SOOP line (minimum one year of semi-continuous A_T measurements), the possibility of establishing an improved A_T parameterization for the North Atlantic similar to the one described by Lee et al. (2006) will be evaluated. This future parameterization will then be based on about 12000 quality controlled A_T measurements from one full year of observations with very good spatial coverage of the subpolar North Atlantic. One important advantage will be that it could be expanded by more data afterwards as the SOOP line will continue the A_T measurements. Another advantage will be the possibility to include seasonal variability into the prediction scheme.

One severe shortcoming of ocean carbon observations provided by SOOP stations are their limitation to surface measurements, i.e. the missing vertical dimension in the marine carbon system. At the moment, the emerging Biogeochemical-Argo (BGC-Argo) program wants to fill this observational gap by equipping their BGC-Argo floats with pH sensors as sole carbonate variable. There are currently about

156 floats equipped with pH sensors, which produce more than five times as many pH profiles annually as ship-based measurements (Claustre et al. 2020). However, the used pH sensors are prone to drift over time, and must be therefore calibrated on regular basis. Currently, this calibration is done at the sea surface by a comparison with calculated pH data from $p(CO_2)$ provided from the Carbon-SOOP network and predicted A_T data. As pointed out before in this thesis, these A_T predictions show spatiotemporal biases, which leads to biased pH sensor calibrations. This can be overcome by the A_T measurement implementation on Carbon-SOOP stations described in this study. Alternatively, as soon as the improved A_T parameterization for the North Atlantic Ocean is available, the calibration could be done by using A_T predicted from this parameterization. In conclusion, the autonomous A_T measurements on the North Atlantic SOOP line will be a vital link between the Carbon-SOOP network and the BGC-Argo program.

Finally, in cooperation with BGC-Argo, it is planned to implement high-quality pH measurements on the North Atlantic SOOP line similar to the A_T measurement implementation described here in this thesis. The pH measurements will be conducted by the autonomous underway analyzer CONTROS HydroFIA® pH (-4H-JENA engineering GmbH, Germany). As this analyzer is closely related to the CONTROS HydroFIA® TA, we can fully use our expertise gained during the A_T implementation. After the successful installation, the BGC-Argo floats will be able to directly calibrate their pH sensors with measured pH data from the SOOP line as soon as they pass the track of the ship.

References

Aßmann, S. **2012**. Entwicklung und Qualifizierung autonomer Messsysteme für den pH-Wert und die Gesamtalkalinität von Meerwasser. Doctoral thesis. Available at: `https://macau.uni-kiel.de/receive/diss_mods_00010645`.

Claustre, H., K. S. Johnson, and Y. Takeshita. **2020**. Observing the Global Ocean with Biogeochemical-Argo. Annual Review of Marine Science. 12: 23–48, doi: 10.1146/annurev-marine-010419-010956

Dickson, A. G., C. L. Sabine, and J. R. Christian. **2007**. Guide to best practices for ocean CO_2 measurements. PICES Special Publications 3.

ICOS Ocean Thematic Centre. **2020**. ICOS Ocean Station Labelling Step 2. doi: 10.18160/8SDC-K4FR

Key, R. M., A. Kozyr, C. L. Sabine, K. Lee, R. Wanninkhof, and others. **2004**. A global ocean carbon climatology: Results from Global Data Analysis Project (GLODAP). Global Biogeochemical Cycles. 18: GB4031, doi: 10.1029/2004GB002247

Lee, K., L. T. Tong, F. J. Millero, C. L. Sabine, A. G. Dickson, and others. **2006**. Global relationships of total alkalinity with salinity and temperature in surface waters of the world's oceans. Geophysical Research Letters. 33: L19605, doi: 10.1029/2006GL027207

Newton, J., R. Freely, P. Williamson, and J. Mathis. **2015**. Global Ocean Acidification Observing Network: Requirements and Governance Plan, 2nd Ed. GOA-ON.